

REPORT NO.
UCB/EERC-97/13
DECEMBER 1997
59A131

EARTHQUAKE ENGINEERING RESEARCH CENTER

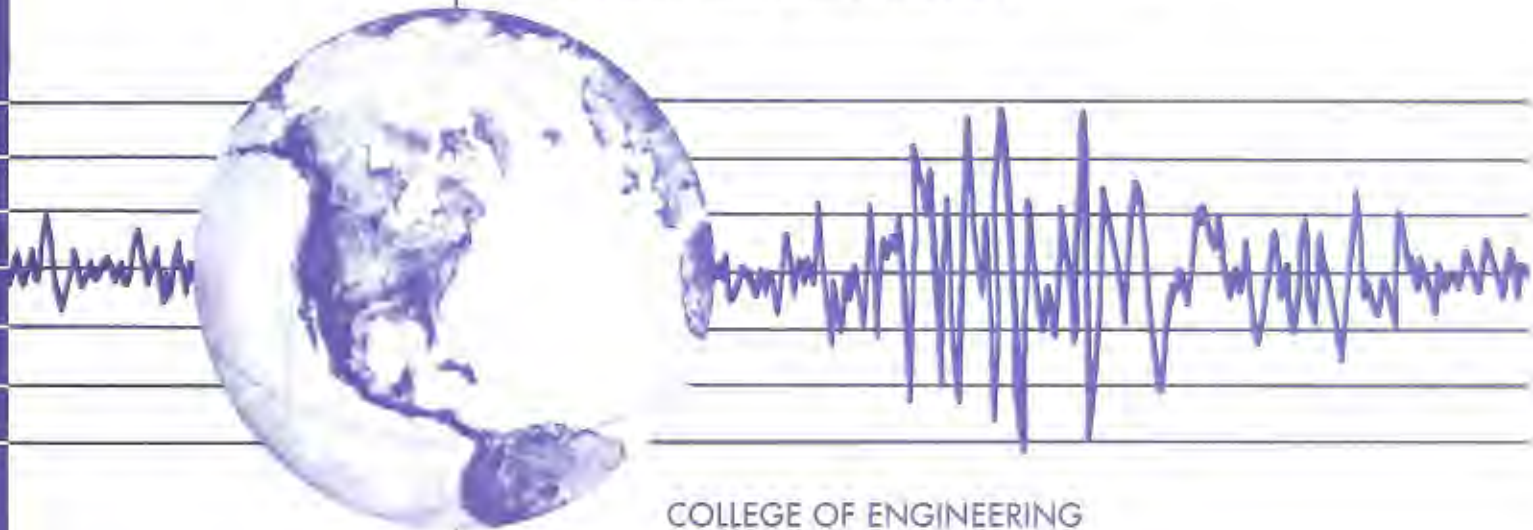
FATIGUE LIFE EVALUATION OF CHANGEABLE MESSAGE SIGN STRUCTURES

VOLUME 2: RETROFITTED SPECIMENS

by

JUAN W. CHAVEZ
AMIR S. GILANI
ANDREW S. WHITTAKER

Report to the California Department of Transportation
for Research under Contract RTA-59A131



COLLEGE OF ENGINEERING
UNIVERSITY OF CALIFORNIA AT BERKELEY

For sale by the National Technical Information Service, U.S. Department of Commerce, Springfield, Virginia 22161

See back of report for up to date listing of EERC reports.

DISCLAIMER

Any opinions, findings, and conclusions or recommendations expressed in this publication are those of the authors and do not necessarily reflect the views of the Sponsor or the Earthquake Engineering Research Center, University of California at Berkeley.

**FATIGUE LIFE EVALUATION OF
CHANGEABLE MESSAGE SIGN STRUCTURES**

VOLUME 2: Retrofitted Specimens

by

Juan W. Chavez

Amir S. Gilani

Andrew S. Whittaker

Report No. UCB/EERC-97/13
Earthquake Engineering Research Center
College of Engineering
University of California at Berkeley

December 1997

1. Report No. UCB/EERC-97/13	2. Government Accession No. _____	3. Recipients's Catalog No. _____	
4. Title and Subtitle Fatigue Life Evaluation of Changeable Message Sign Structures Volume 2: Retrofitted Specimens		5. Report Date December 1997	6. Performing Organization Code UCB ENG-8789
7. Authors Juan W. Chavez, Amir S. Gilani, and Andrew S. Whitaker		8. Performing Organization Report No. UCB/EERC-97/13	
9. Performing Organization Name and Address Earthquake Engineering Research Center University of California, Berkeley 1301 S. 46th Street, Richmond, California 94804		10. Work Unit No. (TRAIS) _____	11. Contract or Grant No. RTA 59A131
12. Sponsoring Agency Name and Address California Department of Transportation Division of Structures 1801 30th Street, Sacramento, California 95814		13. Type of Report and Period Covered Final, 9/1/96-12/31/97	
15. Supplementary Notes 		14. Sponsoring Agency Code RTA 59A131	
16. Abstract <p>This report outlines the research program undertaken at the Earthquake Engineering Research Center (EERC) to investigate the fatigue life of retrofitted Changeable Message Sign (CMS) structure posts. This type of sign structure is an inverted "L" shaped structure, fabricated from steel pipe sections, and composed of a vertical (post) section that is connected to a horizontal (mast arm) section by a flanged connection. These steel structures are inherently flexible and have low structural damping. Following the failure of one CMS structure in Southern California, field studies were undertaken that indicated that the groove-welded post-to-base plate connections were susceptible to wind-induced fatigue cracking. Laboratory studies on CMS posts indicated that the post cross-section adjacent to the electrical conduit hole was also susceptible to fatigue-induced cracking. To increase the fatigue life of CMS structures, Caltrans engineers identified the following retrofit strategies: 1) increase the section modulus of the post near the post-to-base plate connection and the conduit hole to reduce the cyclic stress ranges at the critical cross-sections; and 2) increase the mechanical damping of the sign structure.</p> <p>Two retrofit schemes corresponding to the first retrofit strategy were developed and tested: a steel gusset-retrofit (GR1), and a cast-in-place concrete-jacket retrofit (CIP1). Both retrofit schemes were designed and detailed by Caltrans. The steel gusset retrofit consisted of welding eight gusset plates to the post-to-base plate connection. The concrete-jacket retrofit consisted of adding a reinforced concrete shell to the steel post. Specimen GR1 was tested to approximately one million cycles before significant cracking developed. Specimen CIP1 was subjected to 4,500,000 cycles of loading without failing.</p>			
17. Key Words Changeable sign structures, Fatigue life, Steel-gusset retrofit, Concrete-jacket retrofit, Conduit hole cracks, Gusset cracks, Increased damping, Increased stiffness.		18. Distribution Statement Unlimited	
19. Security Classif. (of this report) Unclassified	20. Security Classif. (of this page) Unclassified	21. No. of Pages 94	22. Price _____

ABSTRACT

This report outlines the research program undertaken at the Earthquake Engineering Research Center (EERC) to investigate the fatigue life of retrofitted Changeable Message Sign (CMS) structure posts. This type of sign structure is an inverted "L" shaped structure, fabricated from steel pipe sections, and composed of a vertical (post) section that is connected to a horizontal (mast arm) section by a flanged connection. These steel structures are inherently flexible and have low structural damping. Following the failure of one CMS structure in Southern California, field studies were undertaken that indicated that the groove-welded post-to-base plate connections were susceptible to wind-induced fatigue cracking. Laboratory studies on CMS posts indicated that the post cross-section adjacent to the electrical conduit hole was also susceptible to fatigue-induced cracking. To increase the fatigue life of CMS structures, Caltrans engineers identified the following retrofit strategies: 1) increase the section modulus of the post near the post-to-base plate connection and the conduit hole to reduce the cyclic stress ranges at the critical cross-sections; and 2) increase the mechanical damping of the sign structure.

Two retrofit schemes corresponding to the first retrofit strategy were developed and tested: a steel gusset-retrofit (GR1), and a cast-in-place concrete-jacket retrofit (CIP1). Both retrofit schemes were designed and detailed by Caltrans. The steel-gusset retrofit consisted of welding eight gusset plates to the post-to-base plate connection. The concrete-jacket retrofit consisted of adding a reinforced concrete shell to the steel post. Specimen GR1 was tested to approximately one million cycles before significant cracking developed. Specimen CIP1 was subjected to 4,500,000 cycles of loading without failing.

ACKNOWLEDGEMENTS

The work described in this report was funded by the California Department of Transportation (Caltrans) under Grant No. RTA 59A131. The authors thank Caltrans engineers, Messrs. Anthony Gugino (the Caltrans Technical Monitor for this project), George Amaro, John Dusel, Tim Leahy, James Roberts, Richard Shepard, Walt Winter, and Jeff Woody for their contributions to this project.

The significant efforts of the staff at the Earthquake Engineering Research Center especially Messrs. Don Clyde, Wesley Neighbor, Changrui Yin, and Ms. Carol Cameron made possible the timely completion of the work described herein. These efforts are gratefully acknowledged.

The findings, conclusions, opinions, and recommendations expressed in this report are solely those of the authors and do not necessarily represent the views of the sponsor.

TABLE OF CONTENTS

Chapter 1. INTRODUCTION	1
1.1. General	1
1.2. Changeable Message Signs	1
1.3. Objectives and Scope	2
1.4. Organization of the Report	3
Chapter 2. BACKGROUND INFORMATION	3
2.1. General	7
2.2. Wind Loading	7
2.3. Fatigue	8
2.4. Design against Fatigue Failure	9
2.5. Retrofit Strategies	9
2.5.1. Fatigue Response of Gusseted Connections	10
2.5.2. Fatigue Response of Reinforced Concrete	10
Chapter 3. EXPERIMENTAL PROGRAM	13
3.1. General	13
3.2. Fabrication Procedure	13
3.2.1. Fabrication	13
3.2.2. Material Properties	13
3.2.3. Welding Procedure and Inspection	13
3.3. Experimental Program	14
3.3.1. Test Setup	14
3.3.2. Test Parameters	14
3.3.3. Instrumentation	15
3.3.4. Data Acquisition	15
Chapter 4. RESPONSE OF SPECIMEN GR1	21
4.1. General	21
4.2. Retrofit Strategy	21

4.3. Test Configuration	21
4.4. Material Properties, Welding Procedures, and Inspection	22
4.5. Specimen Testing	22
4.6. Crack Detection and Propagation	23
4.7. Instrumentation	23
4.8. Experimental Results	23
4.8.1. General	23
4.8.2. Data Analysis Procedures	24
4.8.3. Cracks in the Test Specimen	24
4.8.4. Typical Test Data	25
4.8.5. Response Maxima	25
4.8.6. Strain Gage Histories	25
4.8.7. Stress Profiles	25
4.9. Analysis of Test Specimen	26
4.9.1. General	26
4.9.2. Modeling	26
4.9.3. Stiffness of Specimen GRI	26
4.9.4. Stress Distribution	27
4.10. Summary	27
Chapter 5. RESPONSE OF SPECIMEN CIP1	45
5.1. General	45
5.2. Retrofit Strategy	45
5.3. Test Configuration	45
5.4. Material Properties, Welding Procedures, and Inspection	46
5.5. Specimen Testing	46
5.5.1. Cyclic Tests	46
5.5.2. Pull-back Tests	47
5.5.3. Push-over Test	47
5.6. Crack Detection and Propagation	47
5.7. Instrumentation	47

5.8. Experimental Results: Cyclic Tests	48
5.8.1. General	48
5.8.2. Data Analysis Procedures	48
5.8.3. Cracks in the Test Specimen	48
5.8.4. Typical Test Data	48
5.8.5. Response Maxima	49
5.8.6. Strain Gage Histories	49
5.8.7. Stress Profiles	49
5.9. Experimental Results: Pull-back Tests	50
5.9.1. General	50
5.9.2. Analysis of Experimental Data	50
5.9.3. Modal Properties	50
5.10. Experimental Results: Push-over Tests	51
5.11. Summary	51
Chapter 6. SUMMARY, CONCLUSIONS, AND RECOMMENDATIONS	77
6.1. Summary	77
6.1.1. Introduction	77
6.1.2. Retrofit Schemes	78
6.1.3. Summary of Laboratory Experimental Data	78
6.1.4. Modeling of CMS Structures	79
6.2. Conclusions and Recommendations	79
6.2.1. Fatigue Life of Retrofitted CMS Posts	79
6.2.2. Recommendations for Improving the Fatigue Life of New CMS Structures	80
6.3. Recommendations for Future Studies	81
Chapter 7. REFERENCES	83

LIST OF TABLES

Table 3.1. Retrofit test specimen data	16
Table 3.2. Material properties of retrofit test specimens	16
Table 4.1. Instrumentation for Specimen GR1	28
Table 4.2. Test summary for Specimen GR1	30
Table 5.1. Stress range for the cyclic tests of Specimen CIP1	52
Table 5.2. Sequence of pull-back tests	52
Table 5.3. Instrumentation for Specimen CIP1	53
Table 5.4. Test summary for Specimen CIP1	55
Table 5.5. Modal properties of the test specimen	55
Table 6.1. Summary data for retrofitted specimens	78

LIST OF FIGURES

Figure 1.1. Photograph of gusset retrofitted CMS structure on Interstate 80	4
Figure 1.2. Gusset-retrofitted Model 500 CMS structure	5
Figure 1.3. Concrete-jacket retrofitted Model 500 CMS structure	6
Figure 2.1. Gusset welded connection details (adapted from Daniels and Herbein, 1980)	11
Figure 2.2. S-N curve for a gusseted connection (adapted from Daniels and Herbein, 1980)	11
Figure 2.3. S-N curve for plain concrete (adapted from Bury and Domone, 1974)	12
Figure 2.4. S-N curve for various reinforcing bars (adapted from Bury and Domone, 1974)	12
Figure 3.1. Foundation details for Specimen CIP1	17
Figure 3.2. Test setup for Specimen GR1	17
Figure 3.3. Main components of the test setup for Specimen GR1	18
Figure 3.4. Main components of the test setup for Specimen CIP1	19
Figure 3.5. Instrumentation of Specimen CIP1	20
Figure 3.6. View of the data acquisition system	20
Figure 4.1. Dimensions and connection details for gusset-retrofit Specimen GR1	31
Figure 4.2. Schematics of setup for Specimen GR1	32
Figure 4.3. Instrumentation for Specimen GR1	33
Figure 4.4. Cracking of gusset-to-base plate weld for Specimen GR1	34
Figure 4.5. Crack propagation at the conduit hole for Specimen GR1	34
Figure 4.6. Crack pattern around the conduit hole for Specimen GR1	35
Figure 4.7. Cracking (solid heavy line) in the gusset plates (shown in exploded view) of Specimen GR1	36
Figure 4.8. Typical response histories for Specimen GR1	37
Figure 4.9. Response maxima for Specimen GR1	38
Figure 4.10. Response history (mean value removed) at the bottom left corner of conduit hole for Specimen GR1	39
Figure 4.11. Stress distribution (mean value removed) along the post for Specimen GR1	40
Figure 4.12. Analytical model of Specimen GR1	41
Figure 4.13. Deformed configuration due to a unit load applied at the top of Specimen GR1	42
Figure 4.14. Computed stresses for Specimen GR1	43

Figure 5.1.	Connection details for the steel post of Specimen CIP1	56
Figure 5.2.	Retrofit details for Specimen CIP1	57
Figure 5.3.	Removing the cover concrete and exposing top reinforcement	58
Figure 5.4.	Drilling the existing foundation	58
Figure 5.5.	Grouting the longitudinal reinforcement	59
Figure 5.6.	Placing the transverse hoops	59
Figure 5.7.	Placing the steel formwork	60
Figure 5.8.	Casting the concrete jacket	60
Figure 5.9.	Test setup for Specimen CIP1	61
Figure 5.10.	Location of flaws on the tension side of the post detected by ultrasonic testing	61
Figure 5.11.	Test setup for the pull-back tests	62
Figure 5.12.	Machined bolt used for the sudden release of applied load	62
Figure 5.13.	Schematic view of longitudinal strain gages on the post and jacket reinforcement	63
Figure 5.14.	Photograph of Specimen CIP1 prior to cyclic testing	64
Figure 5.15.	Photograph of Specimen CIP1 at the conclusion of the cyclic testing	64
Figure 5.16.	Typical response histories for Specimen CIP1	65
Figure 5.17.	Lateral stiffness history for Specimen CIP1	66
Figure 5.18.	Response maxima for Specimen CIP1	67
Figure 5.19.	Post stress history at 3 in. above the base plate (sg5) for Specimen CIP1	68
Figure 5.20.	Reinforcement stress history at 3 in. above the base plate (sg33) for Specimen CIP1	69
Figure 5.21.	Stress profiles for Specimen CIP1	70
Figure 5.22.	Free vibration acceleration response for Specimen CIP1	71
Figure 5.23.	Acceleration frequency response for Specimen CIP1	72
Figure 5.24.	Analytical acceleration curve fit for Specimen CIP1	73
Figure 5.25.	Push-over response for Specimen CIP1	74
Figure 5.26.	Photos of Specimen CIP1 at the conclusion of the push-over tests	75

CHAPTER 1: INTRODUCTION

1.1 General

Changeable Message Sign (CMS) structures are widely used in California by the California Department of Transportation (Caltrans) for communicating information on road conditions to the driving public. Figure 1.1 shows a newly installed gusset-retrofitted CMS structure on Interstate 80, near Rodeo California. In the field, the CMS structures are subjected to variable environmental and wind-vibration conditions. They are designed by Caltrans using the AASHTO Standard Specifications for Structural Supports for Highway Signs, Luminaries, and Traffic Signals (AASHTO, 1994).

Following the failure of a CMS structure in 1995, Caltrans investigators inspected the more than 200 CMS structures in use in California. Several CMS structures were instrumented to characterize their dynamic response. The field data indicated that: a) the welded connections in the CMS structures are subjected to stress levels that substantially exceeded the allowable stress levels recommended by the AASHTO specifications (AASHTO, 1994), and b) CMS structures are relatively flexible with little structural damping (Winter, 1996).

As a result of these findings, Caltrans identified three topical areas for immediate investigation: 1) evaluation of the response of existing CMS structures; 2) development and testing of retrofit details for vulnerable groove-welded post-to-base plate connection; and 3) the use of energy dissipation devices to mitigate the wind-induced response of CMS structures.

1.2 Changeable Message Signs

CMSs are composed of an electronic message sign hung from a mast arm, which is supported in turn by a vertical cantilever post. The approximate weight of the sign is 2.5 kips (11 kN). The mounting brackets, shelf angles, and walkway weigh approximately 2.1 kips (9.2 kN).

The structural framing is composed of a 25 ft (7.6 m) long mast arm with an outside diameter of 18 in. (457 mm) and a wall thickness of 3/8 in. (9.5 mm), which is connected to a vertical cantilever post with a maximum height of 29 ft 5 in. (7.3 m), an outside diameter of 18 in. (457 mm), and a wall thickness of 1/2 in. (12.7 mm). The mast arm and the post are connected via annular flange plates. The annular flange plates, which have an outside diameter of 24 in. (610 mm), an inside diameter of 16 in. (406 mm), and a thickness of 1-3/8 in. (35 mm), are groove welded to the ends of the mast arm and the post; 26 No. 3/4 in. (19 mm) bolts are used to connect these plates.

The post in a CMS structure is welded at its base to an octagonal 2-3/4 in. (70 mm) thick base plate (hereafter termed the post-to-base plate connection), which, in turn, is attached to a reinforced concrete foundation using eight high-strength, 2-1/4 in. (57 mm) diameter anchor bolts. Two welded details are used for the post-to-base plate connection: a full-penetration detail, and a socket detail. A rectangular steel-reinforced conduit hole measuring 4 by 6 in. (102 x 152 mm) is typically flame cut in the post approximately 18 in. (457 mm) above the base plate on the face of the post opposite to the mast arm (hereafter termed the tension side of the post). Two retrofit schemes for the post-to-base plate connection were studied by the authors: a steel-gusset retrofit, and a concrete-jacket retrofit. Both retrofit details were designed and detailed by Caltrans.

The gusset-retrofit detail consisted of welding eight gusset plates of 9/16 in. (14 mm) thick A36 steel to the post-to-base plate connection. The triangular gusset plates were welded to the post and the base plate using full-penetration groove welds. The radial gussets were centered between the base plate anchor bolts. The gusset coinciding with the conduit hole on the tension face of the post was 17 in. (432 mm) tall and was terminated approximately 1 in. (25 mm) below the underside of the conduit hole. The other seven gussets were 24 in. (610 mm) tall and terminated at the level of the top of the conduit hole. All eight gussets were 6.5 in. (165 mm) wide at their base. Figure 1.2 shows the dimensions of a gusset-retrofitted Model 500 CMS structure. The lower 15 ft (4.6 m) of a gusset-retrofitted CMS was tested at EERC; refer to Chapter 4 for details.

The concrete jacket retrofit detail consisted of adding a reinforced concrete shell to the steel post. The jacket had a outside diameter of 42 in. (1.1 m) and was 6 ft (1.8 m) tall. The jacket was attached to the existing foundation by drilling and bonding a total of 16 #7 vertical reinforcement bars. The transverse reinforcement in the jacket consisted of #4 hoops with a 15 in. (381 mm) lap placed at 4 in. (102 mm) spacing. Trim reinforcement was added around the conduit hole. Figure 1.3 shows the dimensions of a concrete jacket retrofitted Model 500 CMS structure. The lower 15 ft (4.6 m) of a concrete jacket retrofitted CMS was tested at EERC; refer to Chapter 5 for details.

1.3 Objectives and Scope

Caltrans contracted with the Earthquake Engineering Research Center (EERC) to study the first two topical areas identified in Section 1.1. This report addresses the second topic, namely, the response of retrofitted CMS structures. The reader is referred to Gilani, et al. (1997) for results of the studies on the response of components of existing CMS structures.

1.4 Organization of the Report

Chapter 2 provides limited background information on the subjects of wind loading and fatigue. Chapter 3 describes the experimental program for the retrofit work, and Chapters 4 and 5 detail the experimental results for the gusset-retrofit and concrete-retrofit post specimens, respectively. Conclusions and recommendations are presented in Chapter 6. For additional information on wind loading and fatigue failure of steel structures and weldments, refer to the appendices of Gilani, et al. (1997).



Figure 1.1: Photograph of gusset retrofitted CMS structure on Interstate 80

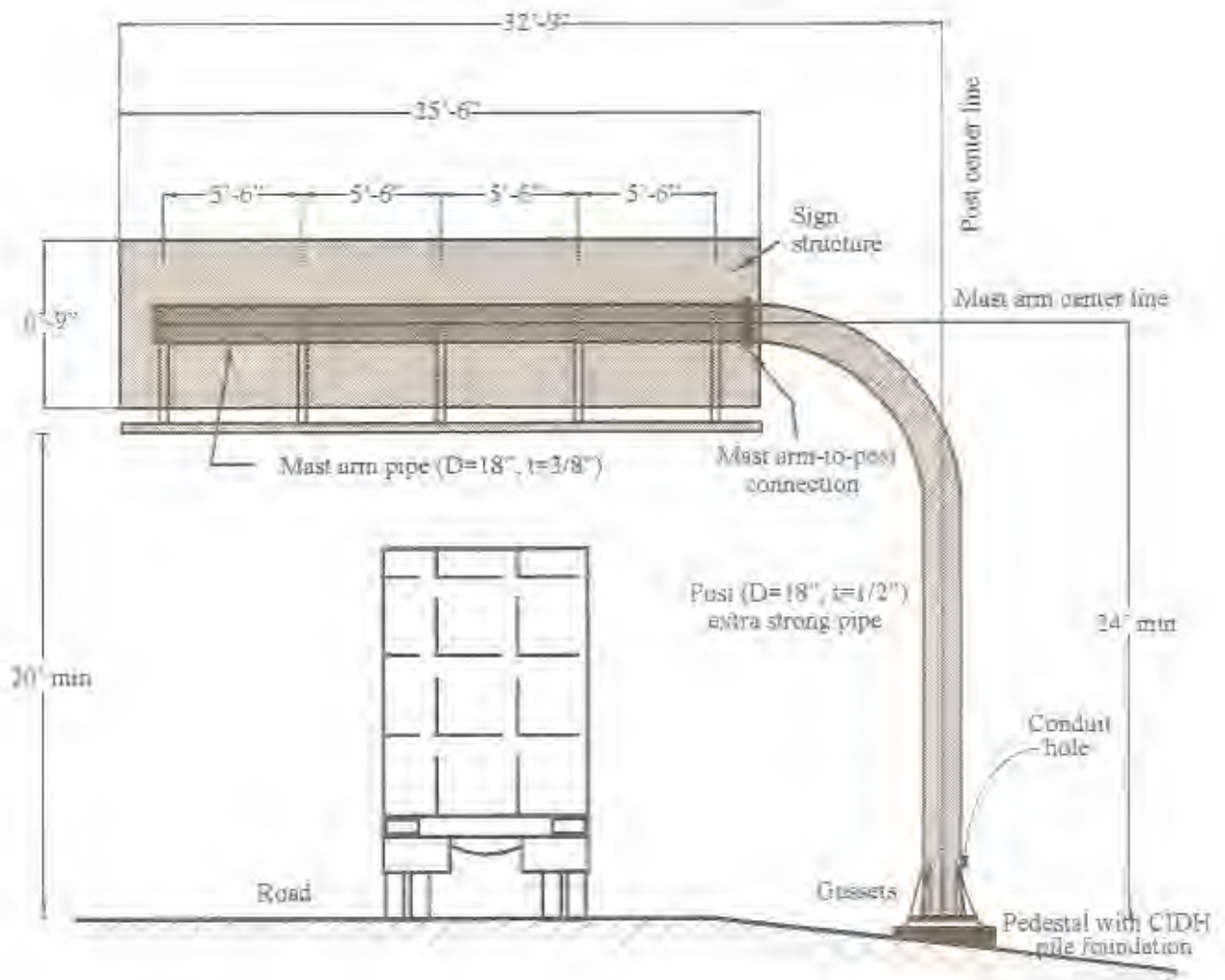


Figure 1.2: Steel-gusset retrofitted Model 500 CMS structure

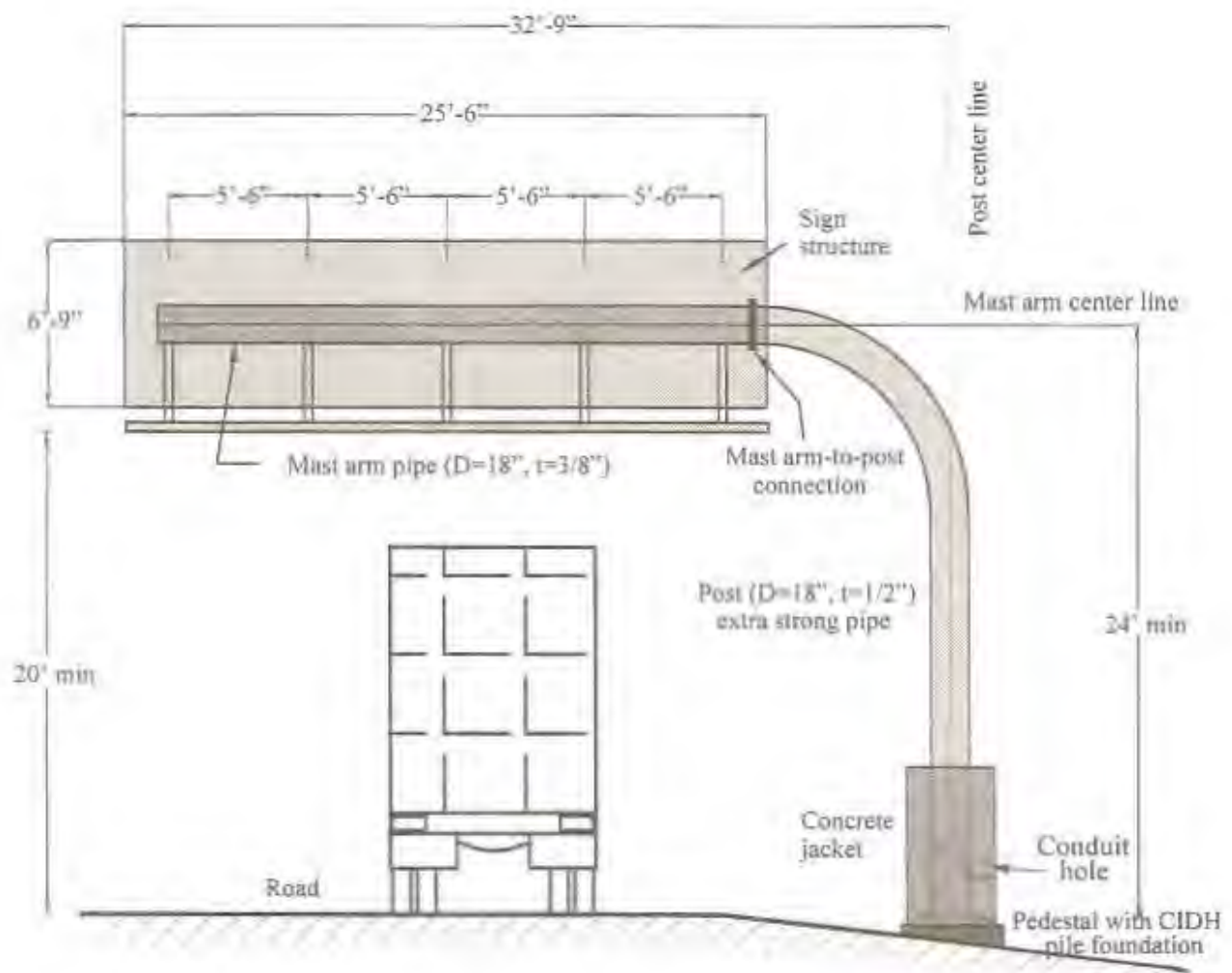


Figure 1.3: Concrete-jacket retrofitted Model 500 CMS structure

CHAPTER 2: BACKGROUND INFORMATION

2.1 General

The study described in this report was funded by Caltrans with the purpose of developing procedures and details for retrofit CMS construction. Prior to discussing the result of the research program, brief background information on wind effects on structures, fatigue, and current AASHTO design procedures to avoid fatigue failure are presented. A more comprehensive treatment of this material is presented in the companion report by Gilani, et al. (1997). The last section in this chapter provides a brief outline of possible retrofit strategies for CMS structures including information on fatigue.

2.2 Wind Loading

Wind effects on CMS structures can be classified as either aerodynamic (due solely to external loading) or aeroelastic (due to the interaction of aerodynamic forces and structural motion). Two aerodynamic effects, natural and truck-induced wind gusts, and two aeroelastic effects, vortex shedding and galloping, can influence the response of CMS structures.

Wind gusts occur naturally from a change in the flow direction and/or amplitude of wind. The wind turbulence will cause a structure to vibrate, and the resulting variable stresses introduced in a structure and its connections can contribute to fatigue-induced cracking.

The passage of trucks underneath a CMS structure induces wind pressure (horizontal and vertical) gradients on the CMS sign and its attachments to the mast arm. The horizontal pressure acting on the faces of the sign introduce torsion and bending moment in the vertical post. The vertical gust pressures acting on the underside of the sign introduce bending moment in the vertical post. The resulting stresses must be considered in the design of CMS structures.

Regular vortex shedding occurs when alternating regular vortices are shed in the wake of a structure. The frequency of these vortices is given by the Strouhal equation:

$$f_s = \frac{VS}{D} \quad (2.1)$$

where D is the dimension of the structure perpendicular to the flow, V is the mean wind velocity, and S is the Strouhal number. The value of S depends on the geometry of the structure and the Reynolds number (which is used to characterize the nature of wind flow as either laminar or turbulent). When the frequency expressed by Equation 2.1 approaches one of the natural frequencies of a flexible and lightly damped

structure, large oscillatory motions may occur.

Galloping corresponds to large-amplitude motions in the direction normal to the wind flow, at frequencies smaller than f_n in Equation 2.1. If a structure experiences motion in the across-wind direction, the flow around the structure can become unsymmetrical, generating a lift force. This force will increase the motion of the structure in the across-wind direction, and large amplitude motions may result.

For a prismatic, single-degree-of-freedom oscillator in a smooth wind flow and oscillating in the across-wind direction, the total system damping (ξ_{total}) may be expressed as:

$$\xi_{total} = \xi_{mech} + \xi_{aero} \quad (2.2)$$

where ξ_{mech} is the mechanical or equivalent viscous damping of the oscillator (always positive), and ξ_{aero} is the aerodynamic damping (often negative). Galloping instability (the Glauert-Den Hartog criterion) will occur when the total system damping is negative, that is, when the value of the aerodynamic damping, if negative, is larger than the mechanical damping. Steel CMS structures possess small mechanical damping and are susceptible to galloping instability (Gugino and Woody, 1996).

2.3 Fatigue

Fatigue, which is often classified as either low-cycle or high-cycle, is a problem that occurs in many types of structures utilizing welded connections, such as bridges, off-shore platforms, and sign support structures. The fatigue failure of a CMS structure is related to high-cycle fatigue, which is associated with a large number of loading cycles at strain levels less than the yield strain.

Geometry, the metallurgical characteristics of the steel and the weld filler metal, and the presence of defects all affect the fatigue life of a connection. Material strength alone is not a significant factor in the fatigue life of a structure. However, the ratio of the applied stress to the yield stress has a significant effect on fatigue life.

Although structures are typically subjected to complex loadings, constant amplitude sinusoidal loading is usually used to characterize the fatigue life of components and connections. The applied stress range is defined as the total stress amplitude in a given cycle. Using this definition, the fatigue life of a specimen at different stress ranges can be represented by an S-N curve (where S is the stress range and N is the number of loading cycles to failure). A point on the S-N plot indicates the number of cycles a component or connection can sustain at a given stress range prior to failure. The S-N curve is typically plotted in logarithmic form, that is, the logarithm of the stress range is plotted versus the logarithm of the number of loading cycles to failure. The cycle count in the plot is the sum of the number of cycles required to initiate a crack and the number of cycles needed to propagate the crack to failure. Typical S-N curves

consist of a descending branch and a constant value branch. In the descending branch, fatigue life is reduced as the stress range is increased. The fatigue limit is the stress level at which the number of cycles to failure is infinite. Theoretically, a component or connection loaded to stress ranges below the fatigue limit will have infinite fatigue life. For design, an S-N relation two standard deviations below the mean relation is typically used.

For structures subjected to a variable loading history, the fatigue damage caused by each loading cycle can be accumulated to determine the total fatigue life. A damage model known as the Palmgren-Miner rule (Miner, 1945) is typically used to sum damage ratios for each loading cycle.

2.4 Design against Fatigue Failure

The AASHTO specifications (AASHTO, 1994) for the design of cantilever sign post structures use equivalent static methods of analysis, and combine stresses due to different sources of loading. Wind and vortex shedding effects are included in the stress check. New guidelines, based on the recommendations of Kaczinski, et al. (1996), will likely include provisions for galloping, natural wind gusts, and truck-induced gusts.

The design of sign structures for fatigue resistance is routinely based on criteria outlined in the AASHTO Guidelines for Design of Highway Bridges (AASHTO, 1992). Welded connections are classified into eight categories ranging from A (longest fatigue life) through E' (shortest fatigue life). The full-penetration or the socket welded connections at the post-to-base plate connection of a CMS structure are categorized as class E'. As such, they have a theoretically infinite fatigue life for stress ranges below 2.6 ksi (17.9 MPa). The E' classification is based on the difficulty associated with inspecting these welds due to the presence of the back-up ring inside the post immediately above the base plate.

2.5 Retrofit Strategies

To improve the fatigue life of the CMS structures, Caltrans investigated several retrofit strategies. Galloping was identified (Gugino and Woody, 1996) as the primary loading condition that gave rise to large dynamic stresses (exceeding the AASHTO design stresses) in the post-to-base plate welded connections. The retrofit schemes concentrated on the following areas: 1) increasing the overall stiffness of the system; 2) increasing the structural damping; and 3) moving the critical region away from the post-to-base plate welded connection by increasing the section modulus at the base.

One of the two retrofit specimens tested at EERC incorporated radial steel gussets groove-welded to the post and the base plate. A reinforced concrete jacket was cast in place around the steel post to retrofit the second specimen. A brief review of the fatigue response of gusseted connections and reinforced

concrete members is presented below for additional information.

2.5.1 *Fatigue Response of Gusseted Connections*

Gusset and stiffener plates are commonly used in steel bridge members. Fatigue problems are likely to occur at the welded connections between the gusset plates and the main bridge members in the tensile stress regions (Fisher, et al., 1974). AASHTO recognizes various weld categories depending on the type of the connection. An experimental study conducted by Daniels and Herbein (1980) for curved girder assemblies indicated that gusset connections of the type shown in Figure 2.1 (similar to those used in the retrofit of CMS structures) are most likely classified as Category C (see Figure 2.2), with nominal stress range of 13 ksi (89 MPa). For this case, cracks are expected in the weld at the base of the stiffener plate.

2.5.2 *Fatigue Response of Reinforced Concrete*

Investigations into the fatigue properties of plain concrete in compression (e.g., ACI, 1974; and Bennet, et al., 1967) have been carried out. The findings indicate that the fatigue life of the plain concrete depends on the range of loading, rate of loading, eccentricity of loading, load history, material properties, and environmental conditions. In the S-N plots for plain concrete, the ordinate S corresponds to the stress level as a percentage of the static strength. A typical S-N curve for plain concrete is shown in Figure 2.3. For concrete tested up to 10 million cycles, it was found that the fatigue strength was approximately 60 percent of the static strength, and the fatigue strength did not vary considerably for concrete strengths of up to 8.7 ksi (60 MPa). For samples subjected to variable loading, the Palmgren-Miner equation takes the following form:

$$\sum \frac{n_i}{N_i} \leq 1 \quad (2.3)$$

where n_i designates the number of cycles at a particular stress range, and N_i denotes the number of cycles causing fatigue failure at the same stress condition. The total sum depends on the sequence of loading and the relative stress level, and may be as low as 0.2.

The fatigue strength of reinforcing bars under either uniaxial loading or flexural loading in reinforced concrete beams has been studied by several authors (e.g., Bury and Domone, 1974). The findings indicate that the fatigue life of reinforcing bars depends on minimum stress level, bar size, geometry of deformation, yield strength, prior bending of the bar, and welding. As is typical for metals, the fatigue life of reinforcing steel is determined by the stress range and not the absolute values of minimum and maximum applied stresses. Figure 2.4 shows a typical S-N curve of reinforcing steel bars.

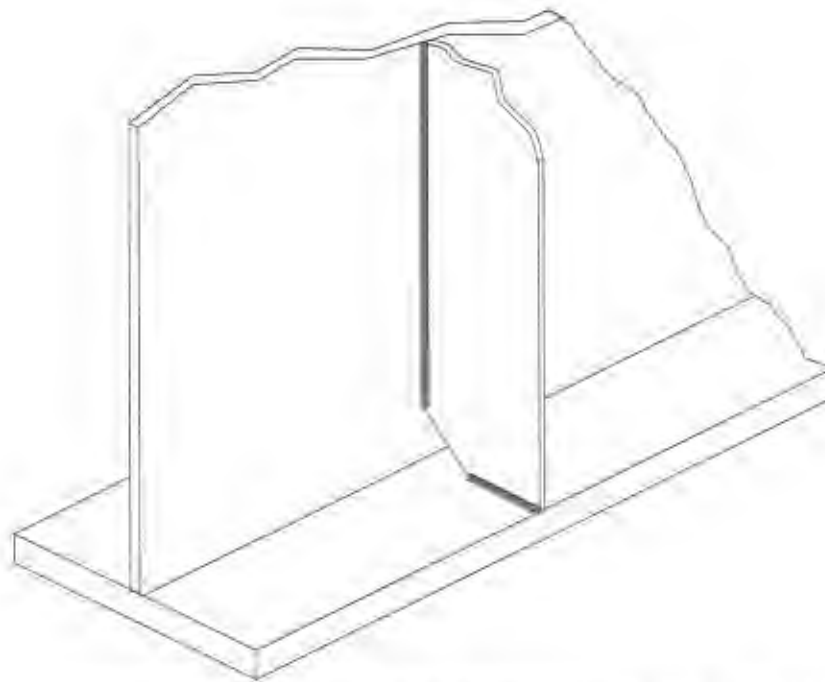


Figure 2.1: Gusset welded connection details (adapted from Daniels and Herbein, 1980)

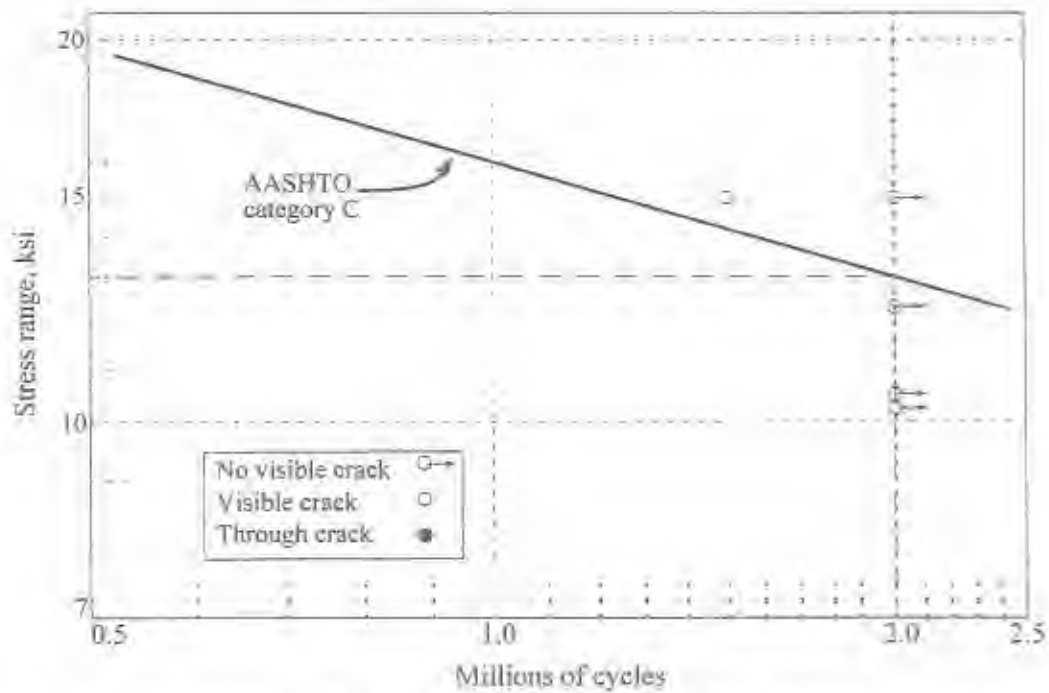


Figure 2.2: S-N curve for a gusseted connection (adapted from Daniels and Herbein, 1980)

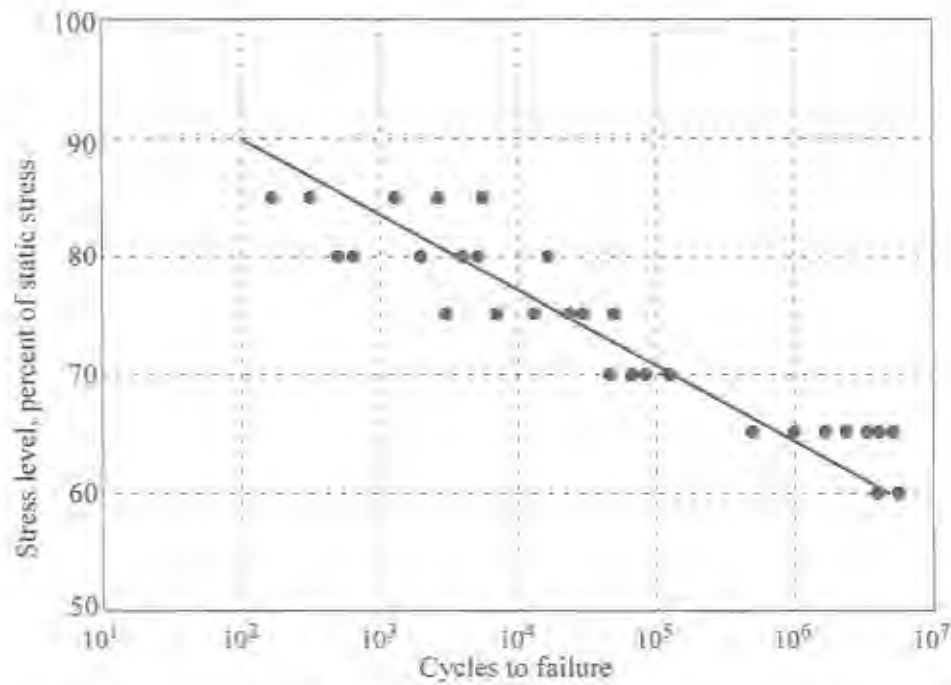


Figure 2.3: S-N curve for plain concrete (adapted from Bury and Domone, 1974)

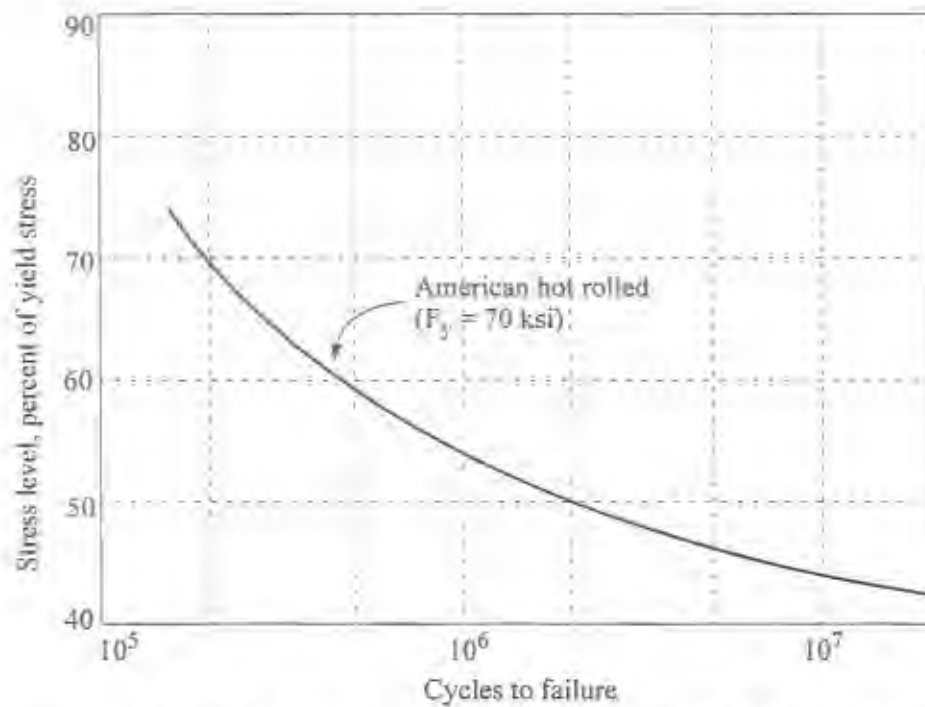


Figure 2.4: S-N curve for various reinforcing bars (adapted from Bury and Domone, 1974)

CHAPTER 3: EXPERIMENTAL PROGRAM

3.1 General

The experimental program for the retrofit specimens involved the full-scale testing of two CMS cantilever posts; one post was retrofitted using welded radial gusset plates at the post-to-base plate connection (hereafter referred to as Specimen GR1); the second post was retrofitted by casting a reinforced concrete jacket around the steel post (hereafter referred to as Specimen CIP1). Table 3.1 summarizes the key information on the two retrofitted specimens.

This chapter describes the two test specimens (fabrication, material properties, welding procedure, and inspection) and the associated experimental program (test setup, test parameters, instrumentation, and data acquisition system).

3.2 Fabrication Procedure

3.2.1 Fabrication

The cantilever post structure for the gusset-retrofit Specimen GR1 was fabricated by Sierra Nevada Steel Corp. of San Fernando, California (a Caltrans-approved vendor) specifically for testing at the Earthquake Engineering Research Center. The vertical steel post for the cast-in-place concrete-jacket retrofit Specimen CIP1 was also fabricated by Sierra Nevada Steel Corp. as part of three CMS structures designated for field installation. East Bay Steel Products, Inc. of Oakland, California (a local Caltrans-approved vendor) modified the cantilever tip of the steel post for connection to the testing hardware at EERC. DOT Constructors of Berkeley, California, was responsible for the placement of the reinforced concrete jacket.

3.2.2 Material Properties

Coupon testing of the anchor bolts and the post material was undertaken to determine the mechanical properties of the test specimens. Good agreement between the mill certificate and coupon test data was obtained. For Specimen CIP1, compressive cylinder tests of the foundation and jacket concrete, tensile tests of reinforcement bars, and pull-out tests of the bonding agent were conducted. Material properties for both specimens are summarized in Table 3.2.

3.2.3 Welding Procedure and Inspection

Prior to the failure reported in Chapter 1, Caltrans inspection of CMS weldments consisted solely

of visual inspection of a completed CMS structure immediately prior to its shipment to the field. Based on experience gained during the SAC testing program at EERC (Whittaker, et al., 1997), ultrasonic testing (UT) was utilized by the authors to detect weld imperfections in both retrofit specimens. Although no ultrasonic test data was available for Specimen GR1 prior to cyclic testing, the ultrasonic tests conducted at the conclusion of the cyclic testing of GR1 detected flaws in the groove-welded gusset-to-post and gusset-to-base plate connection at 90° to the direction of cyclic loading. Ultrasonic tests conducted prior to the placement of the concrete jacket in Specimen CIP1 likewise revealed a number of rejectable flaws in the groove-welded post-to-base plate connection.

3.3 Experimental Program

3.3.1 Test Setup

A reinforced concrete foundation blocks were cast and anchored to the strong floor in the Structures Research Laboratory at EERC. The concrete foundation simulated the CIDH pile typically used as the foundation for 18 in. (46 mm) diameter CMS structures. As shown in Figure 3.1, specially fabricated anchor bolts, identical to bolts used in the field, were embedded in the foundation. The test specimens were attached to the foundation using these anchor bolts. Each specimen was leveled using nuts placed underneath the base plate. The anchor bolts at the base plate were initially snug tightened and then tightened further using the turn-of-the-nut method (AISC, 1995). The gap between the base plate and the foundation was then grouted with mortar cement.

A support frame was designed for the dynamic servo-actuator and attached to an existing reaction frame. Two catwalks and a supporting framework were built to provide access to the top of the test specimen at its connection to the actuator (see Figure 3.2). Figures 3.3 and 3.4 show the test setup for Specimens GR1 and CIP1, respectively.

The specimens were loaded at their tips using a servo-hydraulic actuator attached to the reaction frame. The actuator consisted of a double acting ram with a capacity of 100 kips, a stroke of 20 in. (508 mm), and a servo-valve with a maximum flow rate of 200 gpm (757 lpm).

3.3.2 Test Parameters

The specimens were tested vertically. A unidirectional constant amplitude cyclic displacement history was imposed at the top of the post. Axial load, to simulate the weight of the mast arm and the sign, was not imposed on any of the specimens. Other post deformations observed in the field, such as those due to torsion and bidirectional displacements, were not accounted for.

A testing frequency of 5 Hz was selected for the test. This frequency is within the range of 1 to 13

Hz used in other studies (Fisher, et al., 1974; Schilling, et al., 1978; Fisher, et al., 1979), and is smaller than the specimen frequency (approximately 10 Hz for the steel cantilever post) and the oil-column frequency of the servo-actuator. The tests were conducted at this frequency, and dynamic resonance effects were not observed. All tests were performed at room temperature.

The mean stress for Specimen CIP1 was zero. Static dead-load stresses varying across the pipe diameter were imposed on Specimen GR1 to simulate the bending moment induced in the specimen by the dead weight of the sign.

3.3.3 Instrumentation

The instrumentation for the two specimens consisted of: an LVDT on the actuator center-line measuring the imposed displacement; a load cell in-line with the actuator measuring the axial force in the actuator; and strain gages placed at strategic locations along the height of the specimens measuring local stresses. Chapters 4 and 5 detail the instrumentation used for each specimen. Figure 3.5 shows part of Specimen CIP1 instrumented with strain gages.

3.3.4 Data Acquisition

The test machine and data acquisition system are run by a PC Windows-based control and acquisition program, known as the Automated Testing System (ATS), developed by SHRP Equipment Corporation of Walnut Creek, California. This program is capable of signal generation, four channel servo-actuator command, and sixteen-channel data acquisition. For the tests reported on herein, the ATS system was used to monitor and control the displacement and force-feedback signals.

Other data was monitored and recorded using an AutoNet data acquisition system with a capacity of 64 channels. Pacific signal conditioners were used to amplify the transducer signals and to remove frequencies above 100 Hz from the analog signal.

In order to limit the size of the data files, data was recorded for two seconds for every 16 minutes. Each two-second data file records 10 cycles, which represents 200 sample points for each recorded channel. The data was constantly monitored during the test. Part of the data acquisition system is shown in Figure 3.6.

Table 3.1: Retrofit test specimen data

Specimen ID	Connection details			
	Retrofit	Post-to-base plate weld	Drainage hole ¹	Conduit hole
GR1	steel gussets	socket fillet	no	rectangular, tension side
CIP1	concrete jacket	full-penetration	yes	rectangular, tension side

1). Small hole for discharge of galvanizing material flame-cut into the groove weld on the tension side.

Table 3.2: Material properties of retrofit test specimens

Member	Size	Grade	Yield stress (ksi)		Ultimate stress (ksi)	
			mill certificate	coupon test	mill certificate	coupon test
GR1						
Post	18" OD, t = 1/2"	B/X42/A53	61	64	71	71
Base plate	t = 2-3/4"	A36	42	NT ¹	70	NT
Anchor bolts	d = 2-1/4", l = 39-3/4"	A36	46	41	70	69
Gussets	t = 5/8"	A36	42.2	NT	65.2	NT
CIP1 ²						
Post	18" OD, t = 1/2"	B/X42/A53	67	NT	75	NT
Anchor bolts	d = 2-1/4", l = 39-3/4"	A36	46	41	70	69
Base plate	t = 2-3/4"	A36	42	NT	70	NT
Reinforcement	#7	Gr. 60	66	59	107	99
Reinforcement	#4	Gr. 60	65	NT	102	NT
Reinforcement	#3	Gr. 60	72	NT	110	NT

1. NT denotes Not Tested.

2. Foundation: 4,000 psi in 28 days; concrete jacket: 5,600 psi in 28 days; bond strength >20 kips.



Figure 3.1: Foundation details for Specimen CIP1



Figure 3.2: Test setup for Specimen GR1

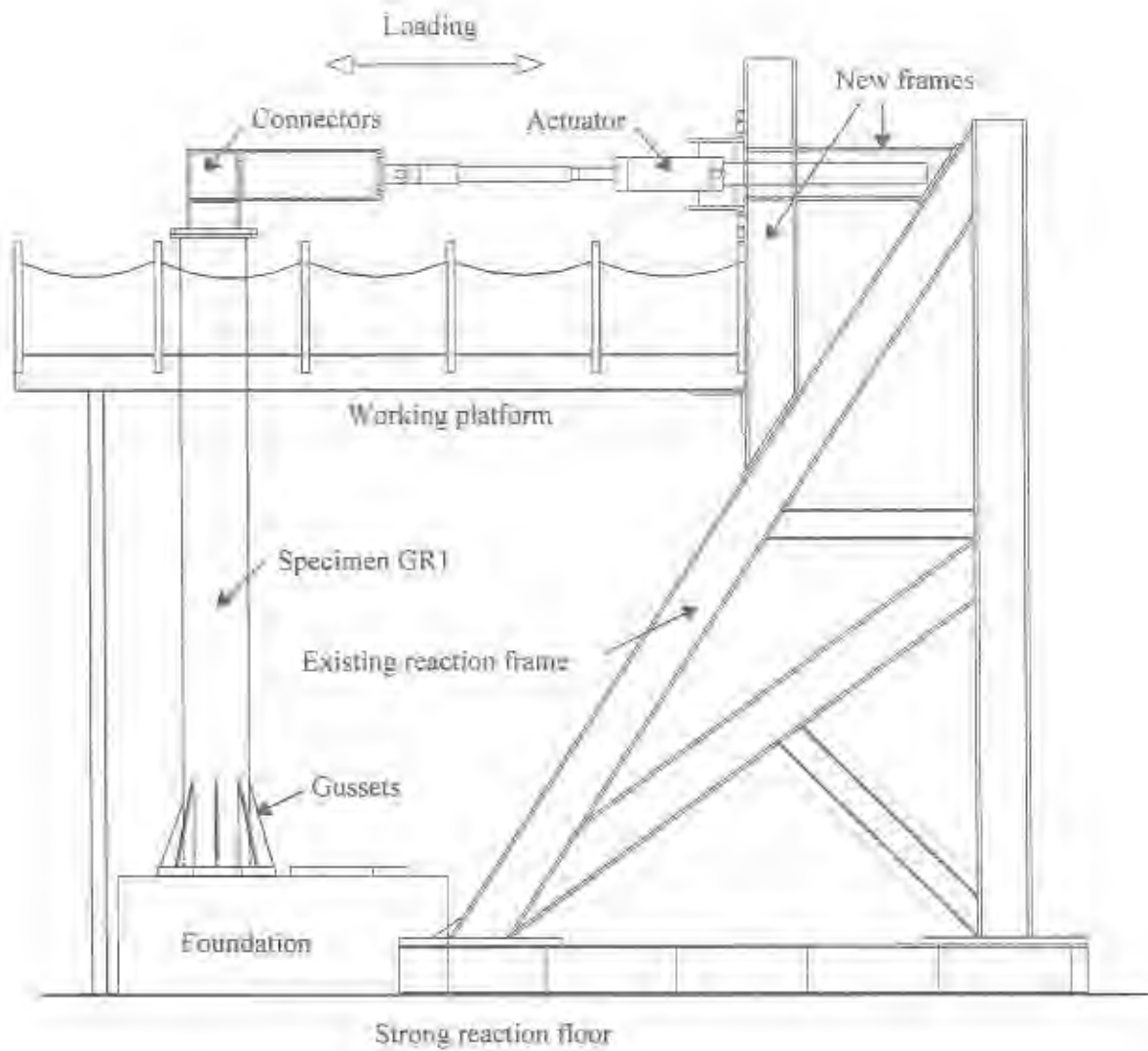


Figure 3.3: Main components of the test setup for Specimen GR1

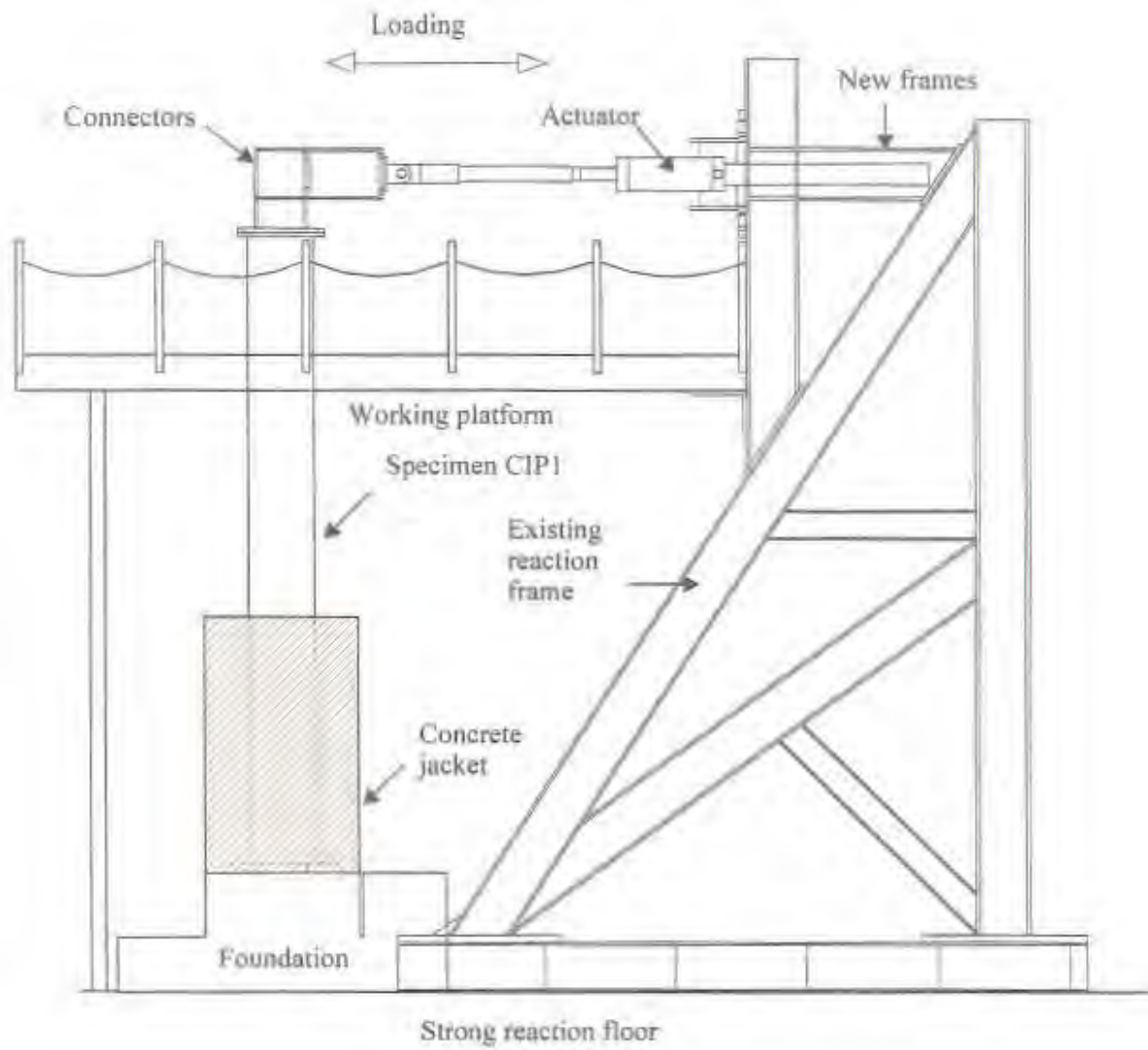


Figure 3.4: Main components of the test setup for Specimen CIP1



Figure 3.5. Instrumentation of Specimen (CFI)

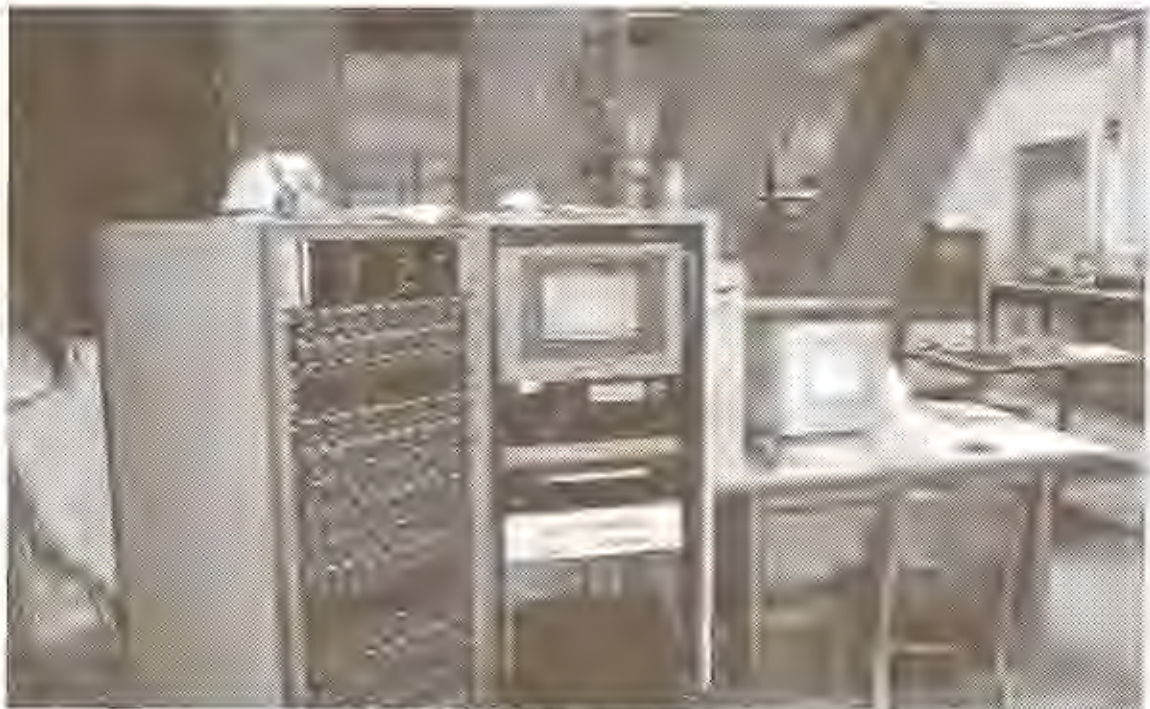


Figure 3.6. View of the data acquisition system

CHAPTER 4 : RESPONSE OF SPECIMEN GR1

4.1 General

Specimen GR1 was a cantilever steel post from a CMS structure incorporating a socket post-to-base plate connection that was retrofitted with eight triangular gusset plates welded both to the post and the base plate. The objective of this retrofit scheme was to increase the section modulus of the post near its base and to decrease the stresses at the post-to-base plate connection. The gusset plates were 24 in. (610 mm) tall. To accommodate the 4 in. by 6 in. (102 mm by 152 mm) conduit hole located 18 in. (457 mm) above the base plate, one of the gusset plates was cut short. The specimen was fabricated by a Caltrans-approved vendor per Caltrans guidelines for CMS structures. The specimen was inspected and approved by Caltrans prior to shipment to EERC.

Figure 4.1 shows the details of the gusset-retrofitted post designed by Caltrans (Guginó and Woody, 1996). Shown in the figure are the plan view, elevation of the gusset-retrofitted post, details of the post-to-base plate socket-welded connection, dimensions of the gusset plates, and details of the conduit hole. The conduit hole is typically flame cut; its edges are neither ground smooth nor its corners cut to a radius to minimize stress concentrations. A stiffening tube is fillet welded to the steel post inside the flame-cut hole.

4.2 Retrofit Strategy

Examination by Gilani, et al. (1997) of results from the laboratory testing of components of CMS specimens identified two locations in a steel CMS post that are susceptible to fatigue failure: the post-to-base plate connection, and the region around the conduit hole. The gusset-retrofit scheme increased the section modulus near the post-to-base plate connection and reduced the cyclic stress range at the base of the post.

4.3 Test Configuration

The test specimen was fabricated by cutting a CMS post with an outside diameter of 18 in. (457 mm) and a wall thickness of 1/2 in. (13 mm) to a length of 14 ft. 4 in. (4.4 m) to accommodate the framing built for testing of other CMS components (Gilani, et al., 1997). The post was socket fillet welded at its base (see Figure 4.1) to a 2-3/4 in. (70 mm) thick octagonal steel plate. The specimen was connected to the foundation using eight 2-1/4 in. (57 mm) diameter anchor bolts following Caltrans guidelines. The upper nuts were first snug tightened, then further tightened by the turn-of-the-nut method (AISC, 1995). A

rectangular plate was welded to the top of the post to facilitate its connection to the servo-actuator.

The retrofit work involved groove welding eight triangular 9/16 in. (14 mm) thick steel gusset plates connected to the post and the base plate. The gusset plates had a base length of 6.5 in. (165 mm) and a height of 24 in. (610 mm) except for the gusset located below the conduit hole, which had a height of 17 in. (432 mm).

The post was positioned such that the direction of loading, as shown in Figure 4.2, was normal to the vertical face of the conduit hole (side CD or North side). The bolt designation in the figure identifies the direction of loading and the gusset plates.

4.4 Material Properties, Welding Procedures, and Inspection

Table 4.2 summarizes material properties for Specimen GR1. The steel post was fabricated from Grade A53 steel (API, 1995; ASTM, 1991) extra strong pipe. The gusset plates and the base plate were fabricated using A36 steel. The foundation anchor bolts were A307 steel. The test specimen was fabricated by a Caltrans-approved vendor and inspected by Caltrans prior to shipment to EERC.

At the conclusion of the cyclic testing of Specimen GR1, ultrasonic testing (UT) was used to evaluate the integrity of the welds in the post-to-base plate, gusset-to-post, and gusset-to-base plate connections. Defects were observed in all of these welds, and the ultrasonic testing verified the presence of those cracks identified by other means during the testing program. In addition, flaws were detected in the groove-welded gusset-to-post and gusset-to-base plate connection of gusset AB, which was oriented 90° to the direction of the cyclic loading. It is not known whether these flaws existed prior to the testing program.

4.5 Specimen Testing

Specimen GR1 was tested under displacement control, with displacements applied at the top of the post (see Figure 4.2). The unidirectional cyclic loading was applied at a frequency of 5 Hz. To simulate the dead-load effects, Specimen GR1 was tested with an initial mean (static) stress. The cyclic tests were carried out symmetrically with respect to this mean stress value. The target stress range for Specimen GR1 was 10.5 ksi (72 MPa) at 27 in. (610 mm) above the base plate (Gugino and Woody, 1996). The mean (static) stress range at the base of the post was set at 13 ksi (90 MPa).

In practice, the displacement needed to achieve the target stress range for Specimen GR1 was obtained by monitoring the stress range at a point 36 in. (914 mm) above the top of the base plate, at a point where the stresses in the post were likely not affected by the presence of the conduit hole and the gusset plates. At this location, the computed cyclic stress range was 10 ksi (69 MPa) and the mean (static) stress range was 11 ksi (76 MPa).

Accordingly, the target stresses for Specimen GRI ranged from 6 ksi (41 MPa) to 16 ksi (109 MPa) on the *tension* or conduit hole side (North side or side CD) of the post, and from -6 ksi (-41 MPa) to -16 ksi (-109 MPa) on the *compression* side (South side or side GH) of the post; all measured at 36 in. (914 mm) above the base plate.

4.6 Crack Detection and Propagation

The presence of the cracks was monitored by a combination of visual observation and liquid dye penetrant, and confirmed by real-time analysis of key strain gage data. The liquid penetrant and strain gage monitoring techniques proved to be most reliable in determining the presence and growth of cracks in Specimen GRI.

4.7 Instrumentation

The instrumentation for Specimen GRI consisted of the following: an LVDT mounted on the servo-actuator center-line measuring the imposed displacement at the tip of the post; a load cell in-line with the servo-actuator measuring the imposed force; thirty-six vertical uniaxial strain gages placed along the height of the post at strategic locations, either at the extreme fibers (with respect to the imposed loading) or on the bolt lines adjacent to the extreme fibers, measuring axial strains parallel to the vertical axis of the post; four strain gages placed at the corners of the conduit hole monitoring local stresses; nine pairs of uniaxial strain gages placed on opposite faces of gusset plates, with each pair of gages combined into a single data channel, used to identify the crack formation and estimate the stresses in the gusset plates; and four units of four uniaxial strain gages, attached to four anchor bolts, used to estimate the stresses in the anchor bolts, with each unit combined into a single data channel. The instrumentation list and a schematic diagram of the strain gage locations are shown in Table 4.1 and Figure 4.3, respectively.

4.8 Experimental Results

4.8.1 General

The total number of loading cycles for Specimen GRI slightly exceeded 1,000,000. A total of 221 individual tests, each of 16 minutes duration, were recorded. Table 4.2 summarizes the key observations; more information is presented below. Prior to testing, the specimen was accidentally subjected to a half-cycle of loading with a peak displacement of nearly twice the yield value.

Specimen GRI was assumed to have failed at approximately 800,000 cycles, when the resistance of the post at the target displacement dropped to less than 90 percent of its initial value. The specimen cracked substantially during the cyclic tests. In particular, two cracks formed and propagated in the post from the lower corners of the conduit hole. Cyclic testing was continued beyond 800,000 cycles to

determine the effectiveness of the gusset plates in arresting these cracks. The cracks propagated into the gusset-to-post welds and then into the gusset plates. The test was terminated after approximately 1,000,000 cycles.

4.8.2 Data Analysis Procedure

The computer program MATLAB (The Mathworks, 1997) was used to process the experimental data. The experimental data was reduced in three steps. In the first step, the raw data was read, the file header was removed, and a test log was created. Next, the peak-to-peak extreme values of response were extracted. Stress ranges were obtained by multiplying the peak-to-peak strains by Young's modulus for steel, assumed to be equal to 30,000 ksi (208 GPa). Response histories were plotted in the third step.

4.8.3 Cracks in the Test Specimen

Several cracks were identified during cyclic testing, including cracks in the gusset-to-base plate welded connections, the gusset-to-post welded connection, the gusset-to-base plate welded connections, the post-to-base plate welded connections, the gusset parent metal, and in the post initiating at the upper and lower corners of the conduit hole. Figures 4.4 and 4.5 identify the cracks observed at the gusset-to-base plate connection and at the conduit hole at the end of the testing.

Figure 4.6 shows the crack pattern around the conduit hole. In particular, two horizontal cracks initiating at the lower left (a1) and right (b1) corners of the conduit hole (designated as cracks A and B, respectively) propagated substantially as the cycles accumulated. These cracks reached the gusset-to-post welded connections (a2 and b2) at approximately 985,000 cycles.

Crack A, starting at the lower left corner of the conduit hole (a1), propagated horizontally toward the gusset-plate groove weld (a2), passed through this weld (a3) at 1,020,000 cycles, and then propagated into the gusset parent metal (a4) at 1,055,000 cycles. Crack B, starting at the lower right corner of the conduit hole (b1), propagated to the gusset-plate groove weld (b2), through the gusset plate-to-post weld (b3) at 1,020,000 cycles, and then into the gusset parent metal (b4) at 1,055,000 cycles. Both cracks continued to propagate into the gusset parent metal. In addition, due to the propagation of crack A to the right (a5) and crack B to the left (b5) at the conduit hole, these cracks met below the bottom edge of the conduit hole at approximately 860,000 cycles.

Figure 4.7 shows the locations of the cracks (solid heavy line) in, and adjacent to, the gusset plates at the conclusion of the cyclic test. Most of the cracks developed in the gusset plate-to-base plate welded connections. Cracks also developed at the gusset plate-to-post connection in gusset CD (tension side) below the conduit hole.

4.8.4 Typical Test Data

Typical test data is shown in Figure 4.8. The data in these plots were collected at a cycle count of 10,000 cycles and are representative of the response of Specimen GR1 prior to substantial cracking. The stresses were obtained by multiplying the strain gage values by Young's modulus for steel, assumed to be 30,000 ksi (207 GPa). The plots show the response histories of the actuator force and displacement, the post stresses 3.6 in. (914 mm) above the base plate (sg2), the stresses at the lower left corner of the conduit hole (sg39), the stresses at the gusset plate CD (sg43), and the stresses at the anchor bolts in the tension side (sg52).

4.8.5 Response Maxima

The minimum and maximum responses were computed for each data channel and for all 212 tests. Figure 4.9 shows the response maxima of the actuator force history, the stress range at the lower corner of the conduit hole (sg 39), and the stress range in the post at 1.25 in. (32 mm) above the base plate on the tension side (sg33). The actuator force is relatively constant up to approximately 800,000 cycles, and starts to decrease noticeably thereafter. A similar trend is noted for the post stresses 1.25 in. (32 mm) above the base plate. The post stresses at the lower end of the conduit hole increase substantially after approximately 300,000 cycles due to stress redistribution in the post following cracking adjacent to the conduit hole. After approximately 700,000 cycles, cracks propagated to the gage, and the strain readings dropped to zero.

4.8.6 Strain Gage Histories

Figure 4.10 shows the average stress (strain) response, near the lower corner of the conduit hole, at 200,000 cycle increments of loading. The data shown was corrected to remove the drift in the transducer response history. Up to 600,000 cycles, the data is essentially symmetric and sinusoidal. At 800,000 cycles, the stress response has lost both its symmetry and its sinusoidal shape, and the stresses are significantly smaller indicating the presence of adjacent cracks. At 1,000,000 cycles, the stresses are negligible due to cracking at the sensor location.

4.8.7 Stress Profiles

Figure 4.11 shows the stress profile on the tension and compression faces of the post. The stresses are plotted for every 200,000 cycles. The stress distribution on the compression side does not change with the number of test cycles. However, on the tension side, the stress distribution varies with the number of cycles. Up to 600,000 cycles, the stress distribution is stable, but varies thereafter as the cracks around the conduit hole grow substantially. The highest stresses in the tension side occur 27 in. (686 mm) above the base and above the gusset plate. Below this height, the stresses in the post are dramatically reduced due to

the increase in section modulus resulting from the addition of gusset plates.

4.9 Analysis of Test Specimen

4.9.1 General

An elastic analysis was performed to estimate the response of Specimen GRI and to identify the regions of likely stress concentration in the specimen. The computer program SADSAP (Wilson, 1992) was used to perform the analysis. The program MATLAB (The Mathworks, 1997) was used to post-process the analysis data. The influence of residual stresses, weld profile, gusset plate copes (see Figure 4.1), and cracking were not considered.

4.9.2 Modeling

A finite element mesh consisting of three-dimensional quadrilateral shell elements (available in the SADSAP library) was used to model the cantilever post, the gusset plates, and the base plate. The shell element has six degrees-of-freedom per node (three translation and three rotation) and accounts for membrane and bending effects. A fine mesh was used to model the lower portion of the post, and a mesh of larger elements was used near the top of the post. Each gusset was modeled using 64 quadrilateral shell elements of variable size. The base plate was modeled using 128 quadrilateral shell elements. The post-to-base plate connections were assumed to be rigid. Equivalent springs were used to model the vertical axial stiffness of the anchor bolts connecting the base plate to the foundation. A load acting in the direction parallel to bolt lines AB and EF was applied at the top of the post; the load was distributed among all the nodes at the top of the post to avoid undesirable local deformations associated with concentrated loads. Figure 4.12 presents information on the modeling of Specimen GRI.

4.9.3 Stiffness of Specimen GRI

The deformation of the gusset-retrofitted post is similar to that of a cantilever structure; due to the flexural rotation at the base of the post, the specimen is more flexible than that calculated assuming a fixed base. The application of a horizontal of 1 kip at the cantilever tip results in a tip displacement of 0.0625 in. (1.6 mm) and a lateral stiffness (of the retrofitted post) of 16 kips/in. (2.8 MN/m). This stiffness value is close to the experimentally calculated value of 15 kips/in. (2.6 MN/m). Analysis of the Specimen GRI without the gusset plates results in a tip displacement of 0.078 in. (2 mm) and a lateral stiffness of 12.8 kips/in. (2.2 MN/m). The gusset plates increased the lateral stiffness of the post tested at EERC by about 25 percent. The deformed configuration of the post is shown in Figure 4.13. Note that such a percentage increase will not be realized in the field because the test specimens represent only a segment of a CMS structure.

4.9.4 Stress Distribution

The distribution of longitudinal stresses along the height of the post is shown in Figure 4.14. These values closely approximate the experimental stress values. The stresses on the post vary linearly along the height, from the top of the post up to the top of the gusset plates, and below the top of the gussets the stresses decrease nonlinearly due to the presence of the gusset plates. The conduit hole produces a stress concentration factor of approximately two and a half, that is comparable to the experimental value of two. Figure 4.14 also shows the stress contour at the tension gusset CD and at the compression gusset GH. High stresses are developed at the bottom of the gusset, where it connects with the base plate.

4.10 Summary

Specimen GRI was tested to approximately 1,000,000 cycles of loading. Significant cracking was detected at approximately 600,000 cycles. At approximately 800,000 cycles, the resistance of the post had dropped by 10 percent.

Although it is difficult to draw conclusions regarding the general performance of this type of retrofit detail from only one test, the following general observations are made.

1. *Effectiveness of gusset plates.* As expected, the gusset plates reduced the stresses in the post-to-base plate groove welded connections by increasing the section modulus of the post.
2. *Stress Concentration.* The addition of the gusset plates produced local stress concentrations in the post, with large increases recorded in the vicinity of the conduit hole.

Although the gusset-retrofitted post failed after only 1,000,000 cycles of loading at a stress range of 10 ksi (69 MPa), further studies are warranted. Substantially improved fatigue life will likely be achieved if a) the conduit hole is relocated to an elevation one post diameter or more above the top of the gusset plates, and b) weld flaws are eliminated for all welded connections prior to field installation. Testing of two or more additional gusset-retrofitted post specimens is recommended.

Table 4.1: Instrumentation for Specimen GR1

Ch. No.	Inst. ID.	Instrument	Location
Global transducers			
1	load	load cell	actuator center line; top of the post
2	displacement	lvdt	actuator center line; top of the post
Longitudinal strain gages placed on the post			
3	sg1	strain gage	above bolt-line C; 36" above base plate
4	sg2	strain gage	between bolt-lines C & D; 36" above base plate
5	sg3	strain gage	above bolt-line D; 36" above base plate
6	sg4	strain gage	above bolt-line G; 36" above base plate
7	sg5	strain gage	between bolt-lines G & H; 36" above base plate
8	sg6	strain gage	above bolt-line H; 36" above base plate
9	sg7	strain gage	above bolt-line C; 27" above base plate
10	sg8	strain gage	between bolt-lines C & D; 27" above base plate
11	sg9	strain gage	above bolt-line D; 27" above base plate
12	sg10	strain gage	above bolt-line G; 27" above base plate
13	sg11	strain gage	between bolt-lines G & H; 27" above base plate
14	sg12	strain gage	above bolt-line H; 27" above base plate
15	not used		
16	not used		
17	sg15	strain gage	above bolt-line G; 12" above base plate
18	sg16	strain gage	above bolt-line H; 12" above base plate
19	sg17	strain gage	above bolt-line C; 6" above base plate
20	sg18	strain gage	above bolt-line D; 6" above base plate
21	sg19	strain gage	above bolt-line G; 6" above base plate
22	sg20	strain gage	above bolt-line H; 6" above base plate
23	sg21	strain gage	above bolt-line C; 3.5" above base plate
24	sg22	strain gage	above bolt-line D; 3.5" above base plate
25	sg23	strain gage	above bolt-line G; 3.5" above base plate
26	sg24	strain gage	above bolt-line H; 3.5" above base plate
27	sg25	strain gage	above bolt-line C; 2.75" above base plate
28	sg26	strain gage	above bolt-line D; 2.75" above base plate
29	sg27	strain gage	above bolt-line G; 2.75" above base plate
30	sg28	strain gage	above bolt-line H; 2.75" above base plate

Table 4.1: Instrumentation for Specimen GTI

Ch. No.	Inst. ID.	Instrument	Location
31	sg29	strain gage	above bolt-line C; 2" above base plate
32	sg30	strain gage	above bolt-line D; 2" above base plate
33	sg31	strain gage	above bolt-line G; 2" above base plate
34	sg32	strain gage	above bolt-line H; 2" above base plate
35	sg33	strain gage	above bolt-line C; 1.25" above base plate
36	sg34	strain gage	above bolt-line D; 1.25" above base plate
37	sg35	strain gage	above bolt-line G; 1.25" above base plate
38	sg36	strain gage	above bolt-line H; 1.25" above base plate
39	sg37	strain gage	above bolt-line C; top corner of conduit hole
40	sg38	strain gage	above bolt-line D; top corner of conduit hole
41	sg39	strain gage	above bolt-line C; bottom corner of conduit hole
42	sg40	strain gage	above bolt-line D; bottom corner of conduit hole
Strain gage pairs placed on the opposite faces of gussets ¹			
43	sg41	strain gage	gusset 'GH'; 24" above base plate
44	sg42	strain gage	gusset 'BC'; 12" above base plate
45	sg43	strain gage	gusset 'CD'; 12" above base plate
46	sg44	strain gage	gusset 'DE'; 12" above base plate
47	sg45	strain gage	gusset 'FG'; 12" above base plate
48	sg46	strain gage	gusset 'GH'; 12" above base plate
49	sg47	strain gage	gusset 'HA'; 12" above base plate
50	sg48	strain gage	gusset 'CD'; 1.25" above base plate
51	sg49	strain gage	gusset 'GH'; 1.25" above base plate
Strain gage quadruplets placed at the opposite faces on the anchor bolt faces			
52	sg50	strain gage	bolt 'C'; 2" below foundation surface
53	sg51	strain gage	bolt 'D'; 2" below foundation surface
54	sg52	strain gage	bolt 'G'; 2" below foundation surface
55	sg53	strain gage	bolt 'H'; 2" below foundation surface

1. Gusset $\alpha\beta$ denotes the gusset plate located between bolts α and β (see Figure 4.2). For example, gusset GH is located between anchor bolts G and H.

Table 4.2: Test summary for Specimen GR1

Cycle count	Event
0	Start of cyclic testing.
60,000	Two parallel cracks appeared at the lower right corner of the conduit hole. A crack appeared at the flange-to-post welded connection on the gusset CD.
260,000	Two parallel cracks formed in the lower left corner of the post-to-stiffening tube weld at the conduit hole.
300,000	A crack formed at the bottom of gusset CD; the crack initiated on the gusset center-line. Two cracks appeared at the compression gusset FG, at the gusset-to-base plate connection. Two new cracks appeared at the gusset HG, one at the bottom of the gusset at the other at the gusset-to-plate connection, between the weld and the gusset. Cracks developed at gusset HA at the top of the weld between the gusset plate and the base plate.
340,000	Two new cracks developed on the gusset HG on the G face near the base plate.
370,000	The crack on the tension gusset CD had propagated all the way across the width of the gusset.
390,000	New parallel cracks on the G face of gusset HG developed.
420,000	The crack on the lower left corner of the conduit hole propagated from the weld into the column, parallel to the base plate.
440,000	A new crack appeared on gusset BC on the top of the weld between the base plate weld and the gusset. Two new cracks appeared on gusset DE between the base plate and the weld.
1,000,000	Test terminated.

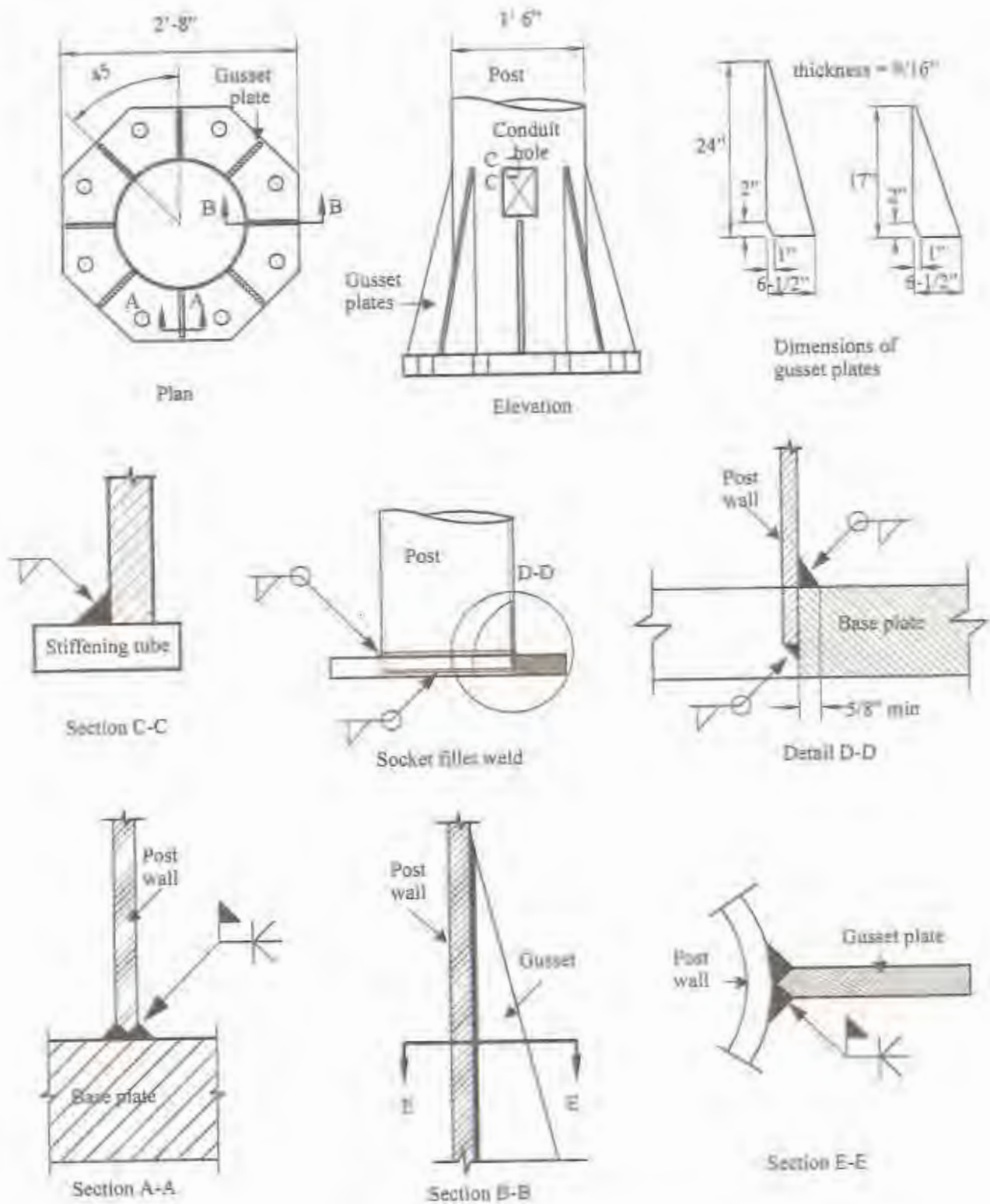
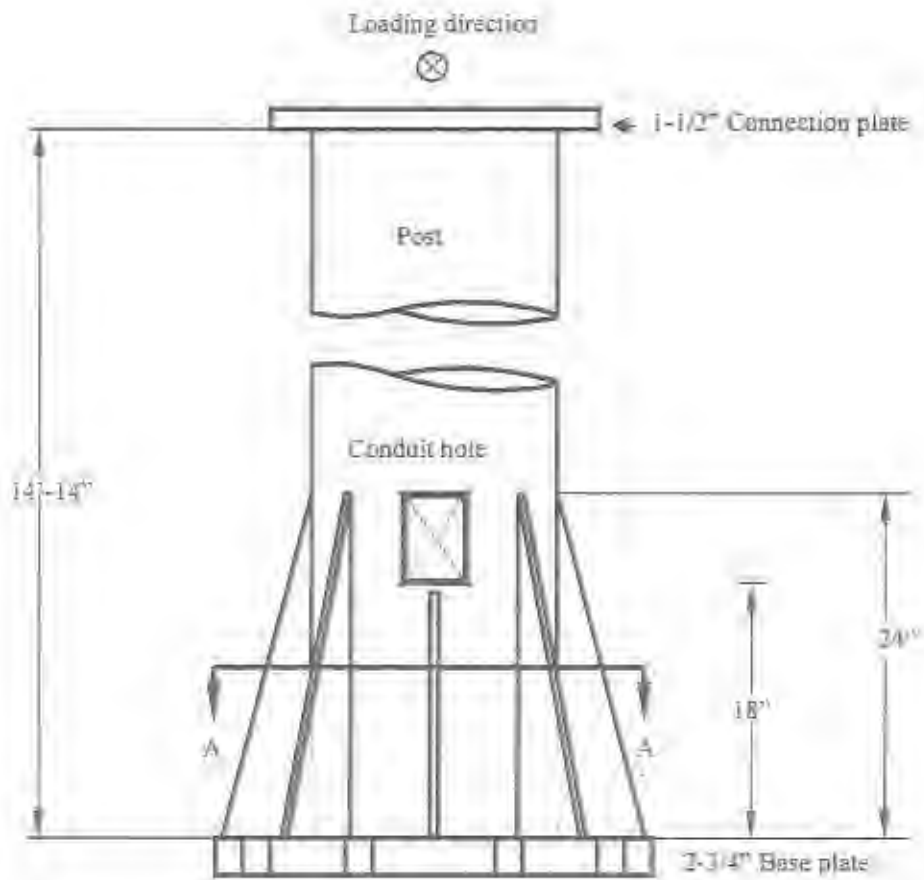
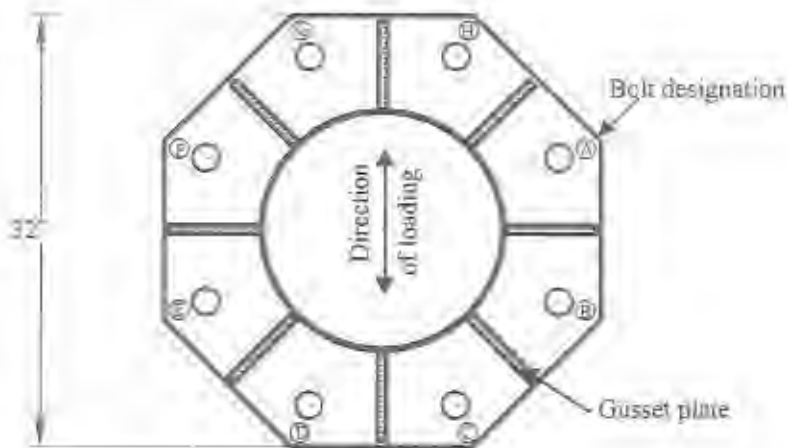


Figure 4.1: Dimensions and connection details for gusset-retrofit Specimen GR1



(a) Elevation



(b) Section A-A (Plan)

Figure 4.2: Schematics of setup for Specimen GR1

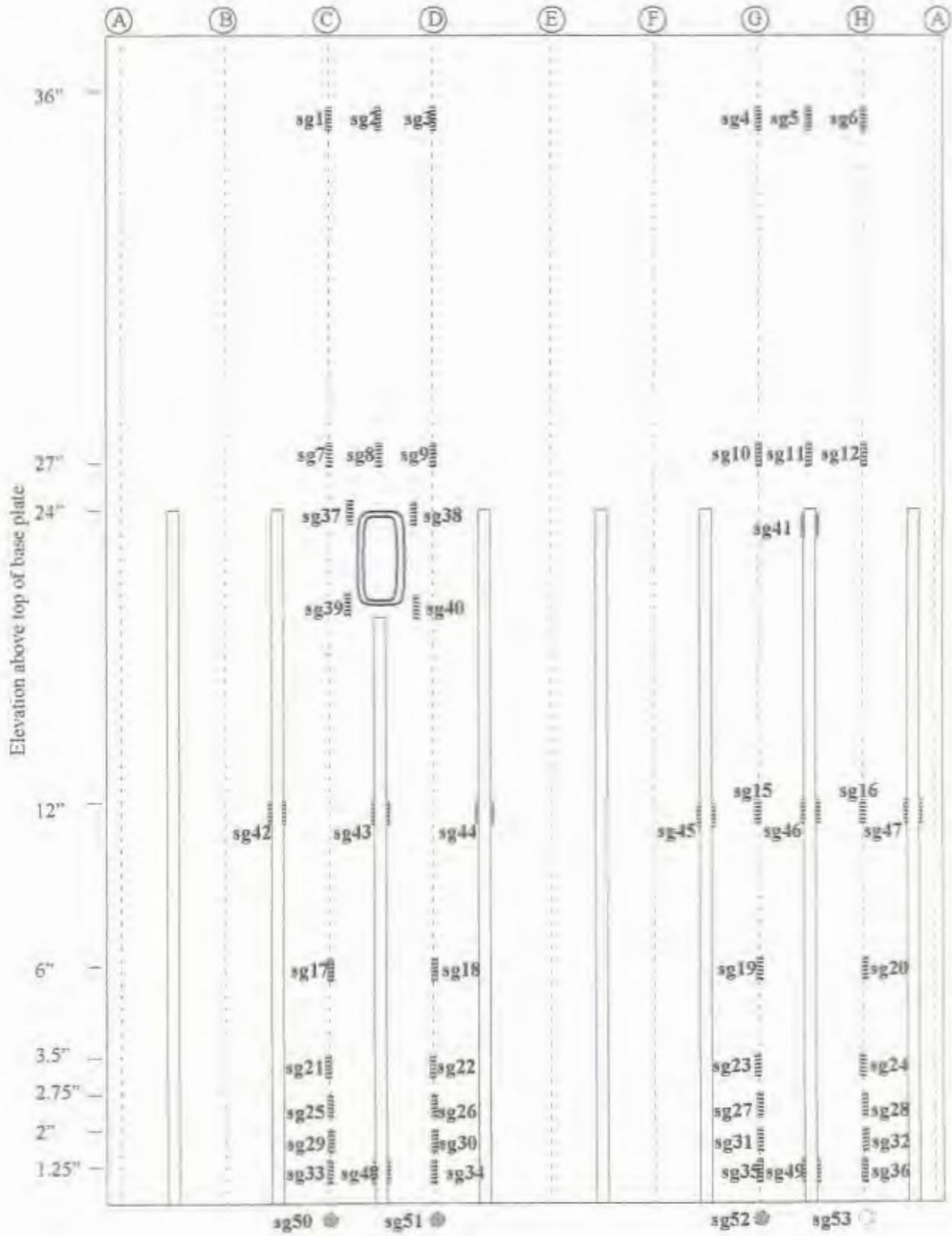


Figure 4.3: Instrumentation for Specimen GR1



Figure 4.4: Cracking of gusset-to-base plate weld for Specimen GR1



Figure 4.5: Crack propagation at the conduit hole for Specimen GR1

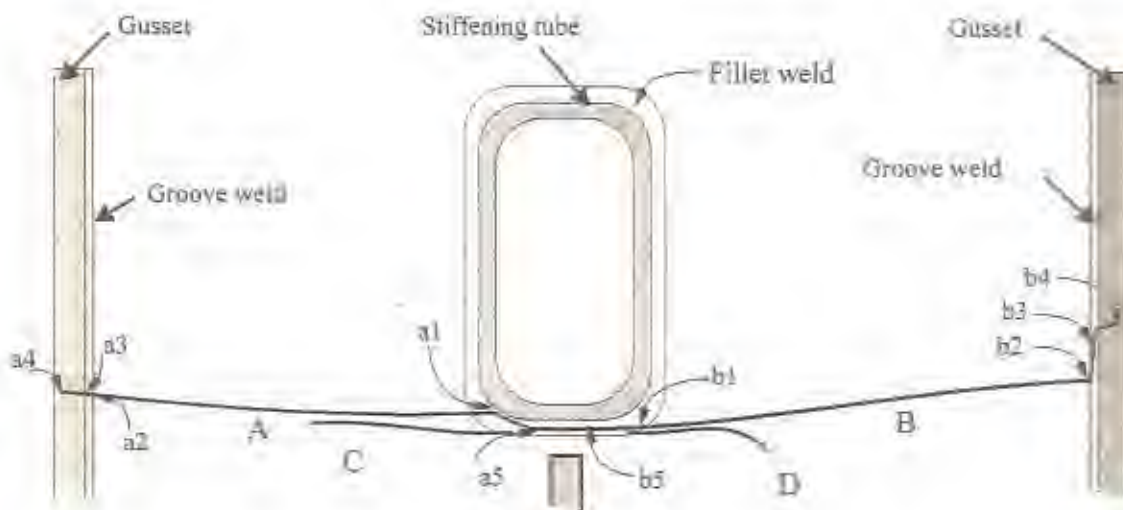


Figure 4.6: Crack pattern around the conduit hole for Specimen GR1

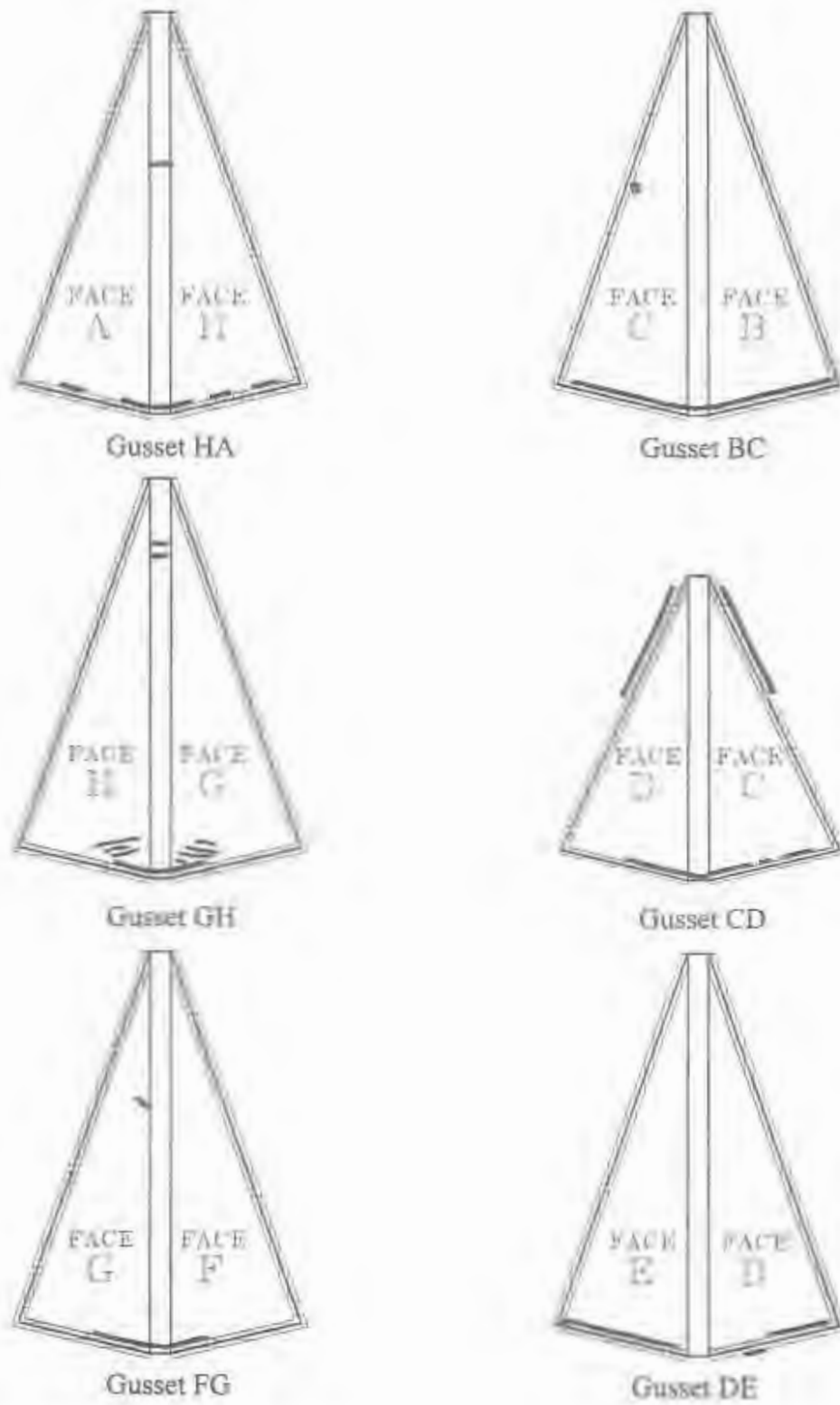


Figure 4.7: Cracking (solid heavy line) in the gusset plates (shown in exploded view) of Specimen GR1

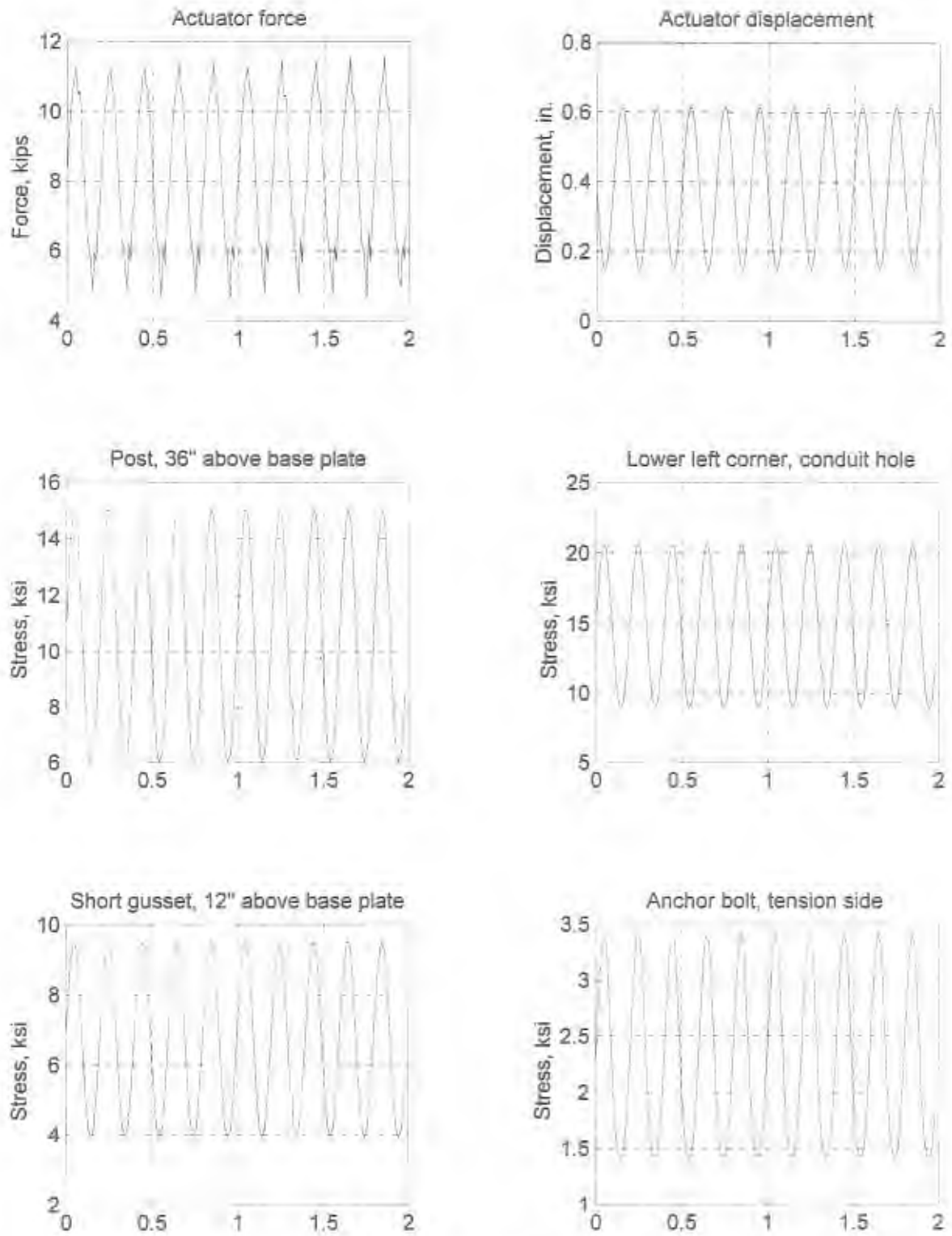


Figure 4.8: Typical response histories for Specimen GR1

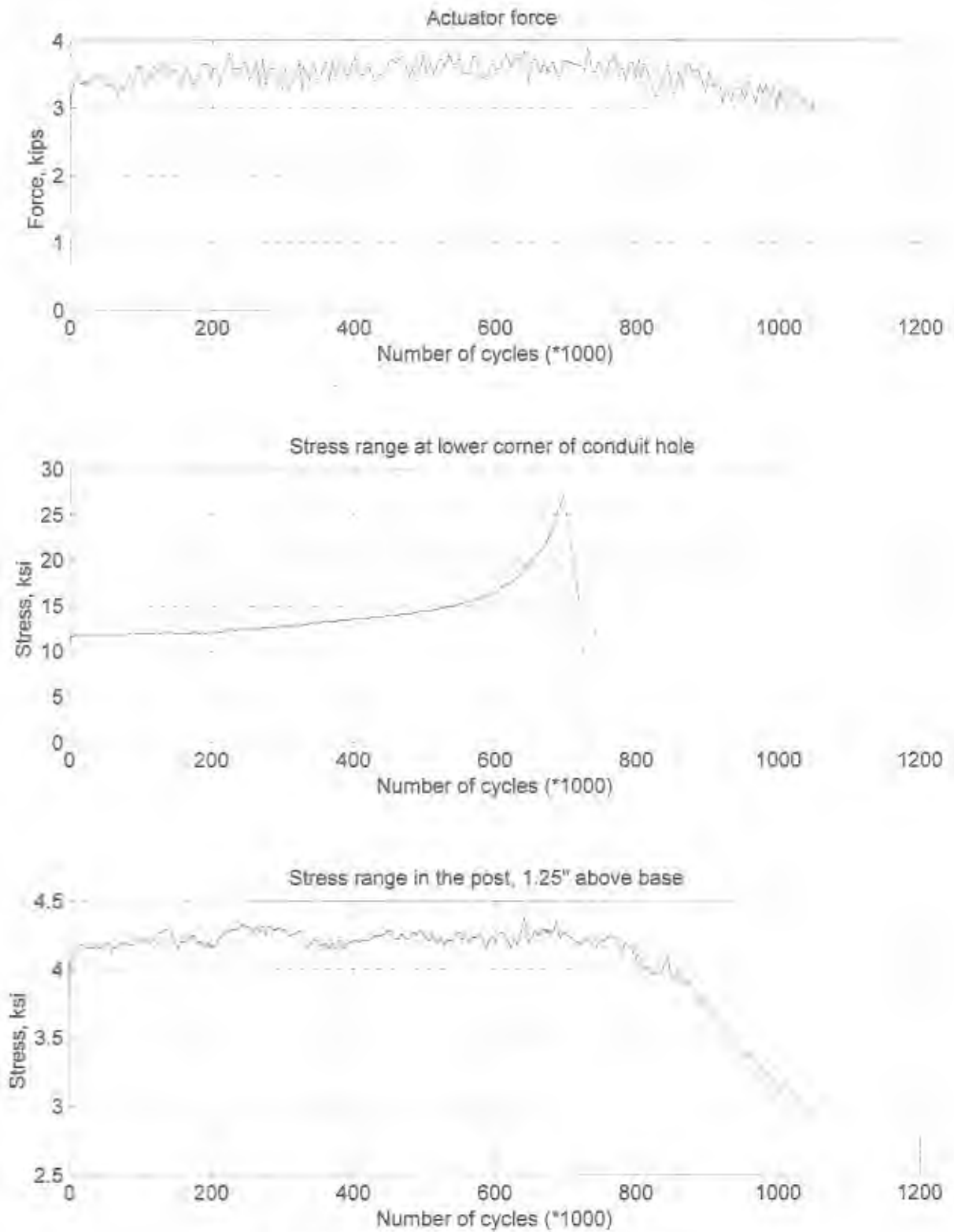


Figure 4.9: Response maxima for Specimen GR I

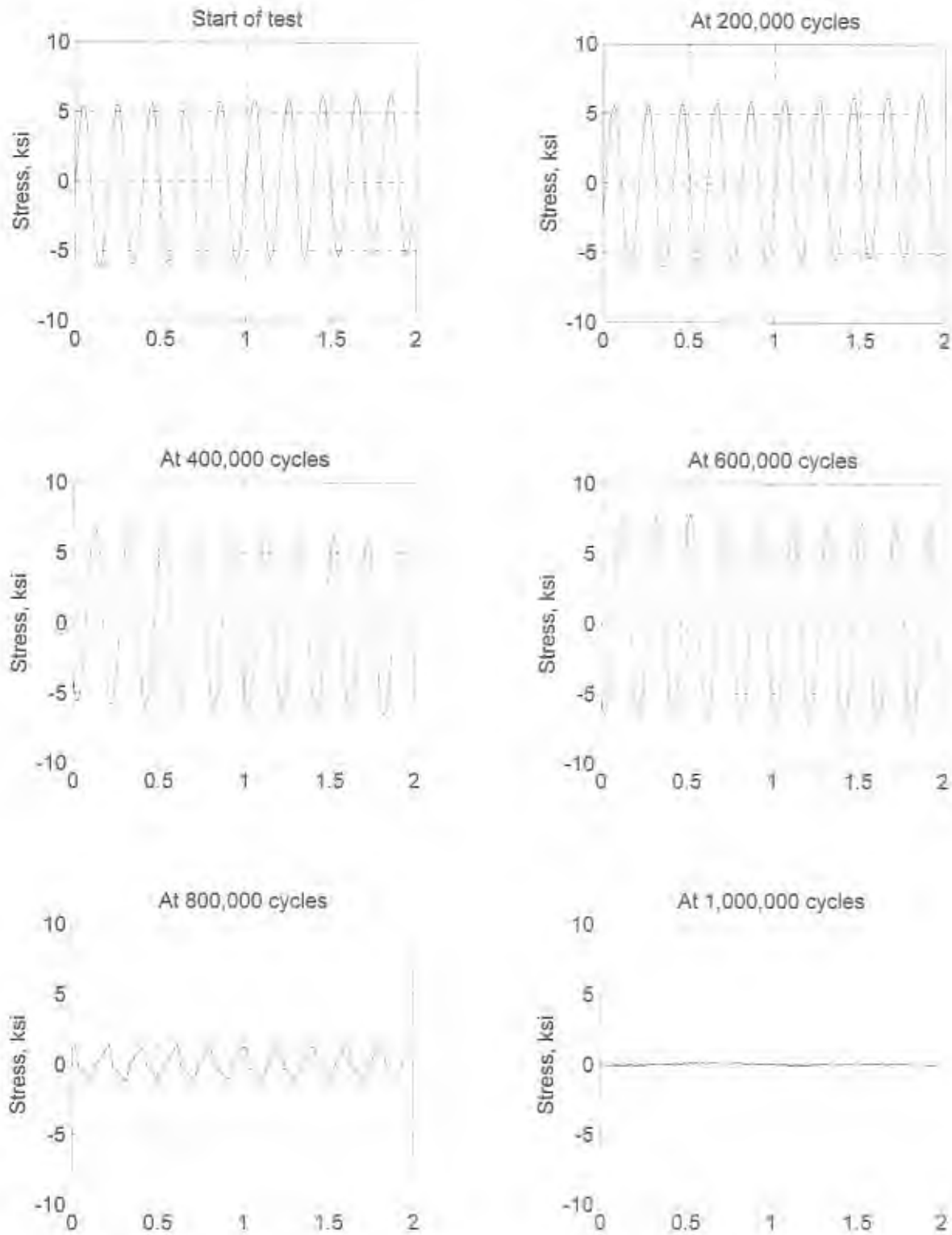


Figure 4.10: Response history (mean value removed) at the bottom left corner of conduit hole for Specimen GR1

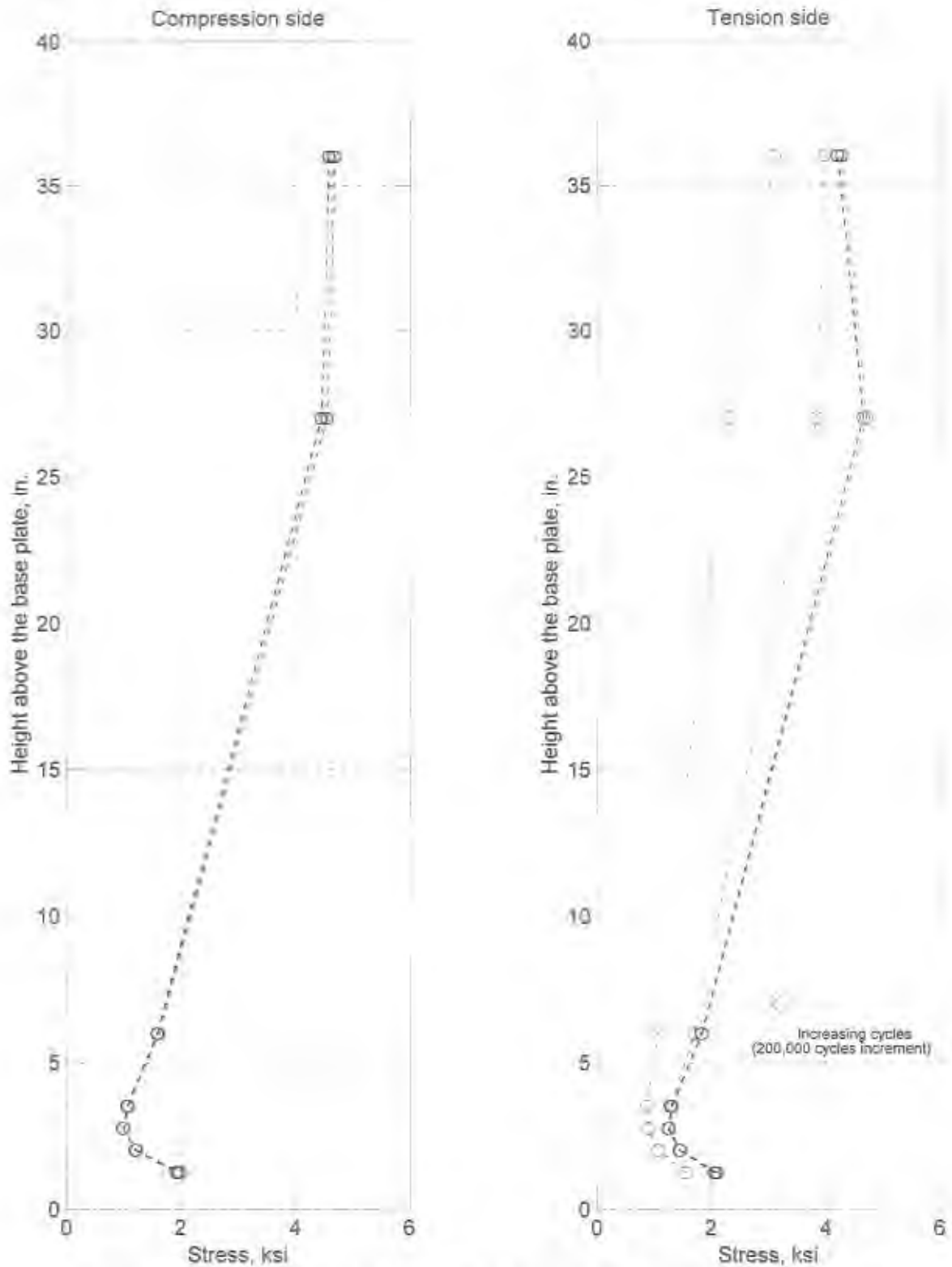
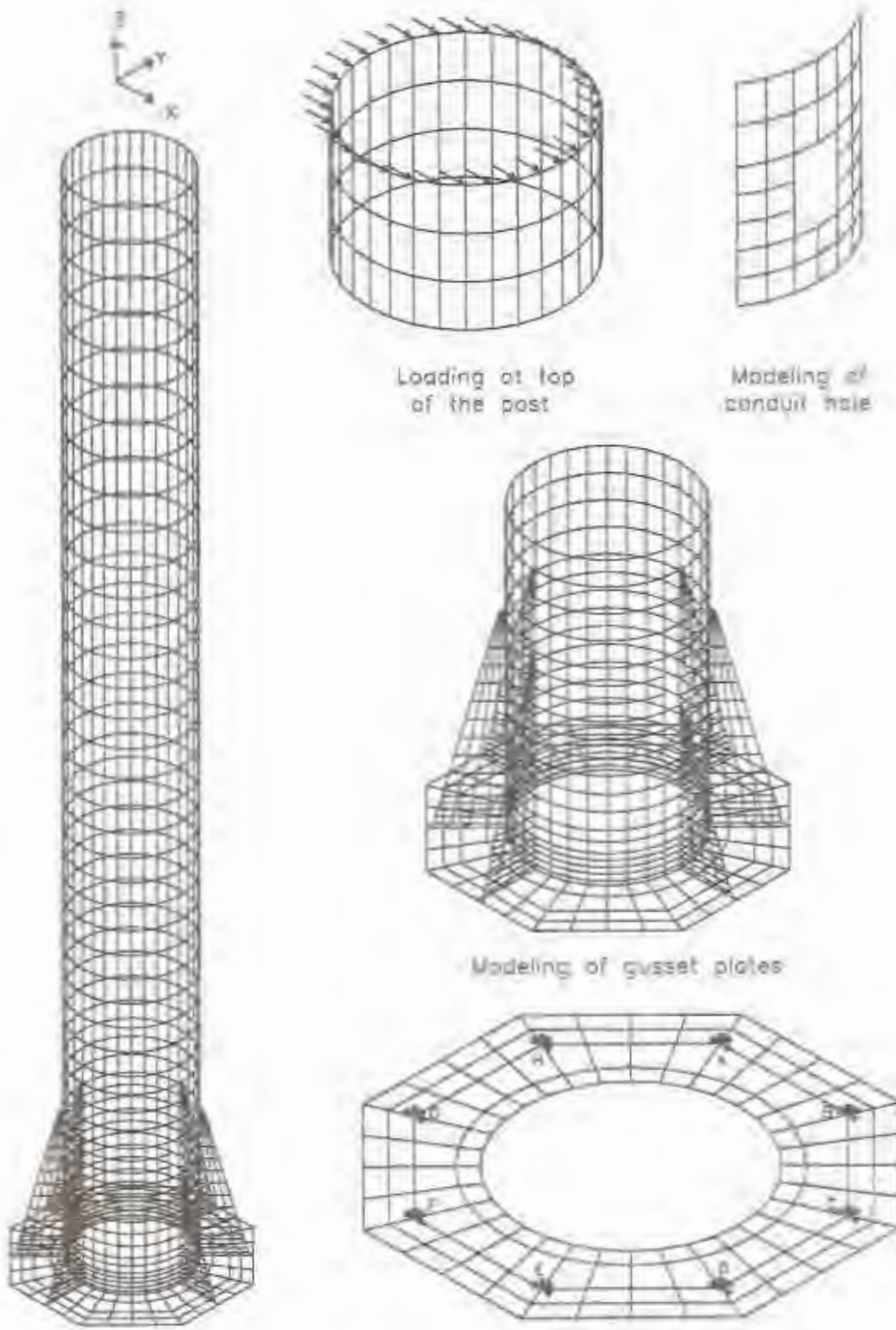


Figure 4.11: Stress distribution (mean value removed) along the post for Specimen GR1



Specimen GR1

Restraints at the base:

Figure 4.12: Analytical model of Specimen GR1



Post without gusset plates



Post with gusset plates

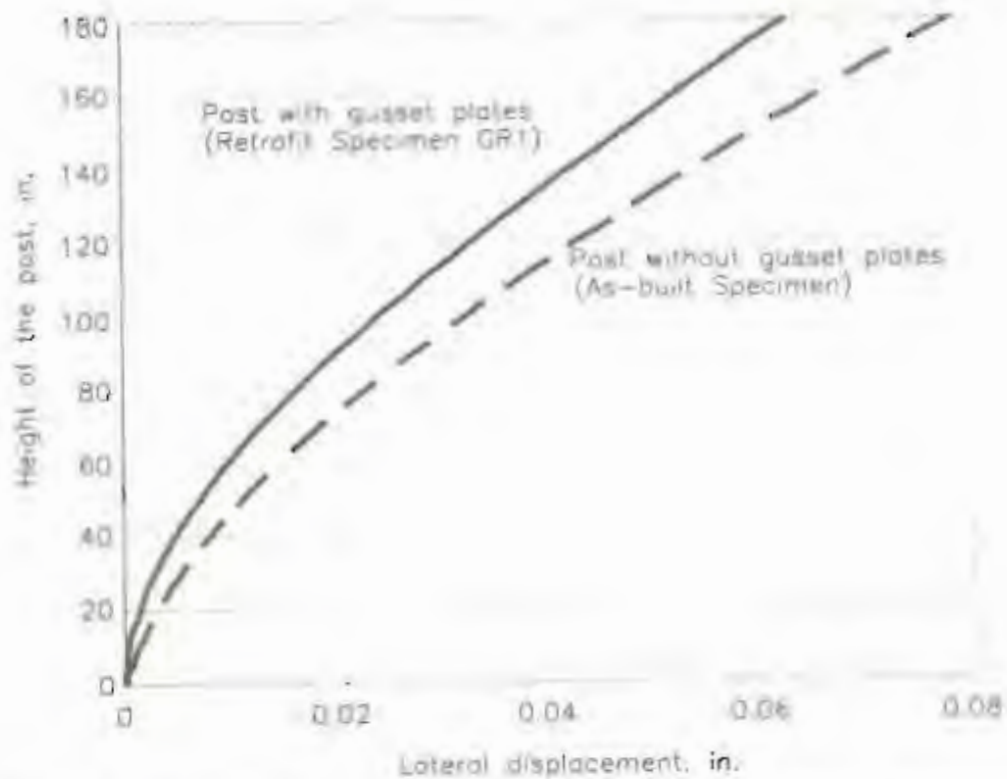


Figure 4.13: Deformed configuration due to a unit load applied at the top of Specimen GR1

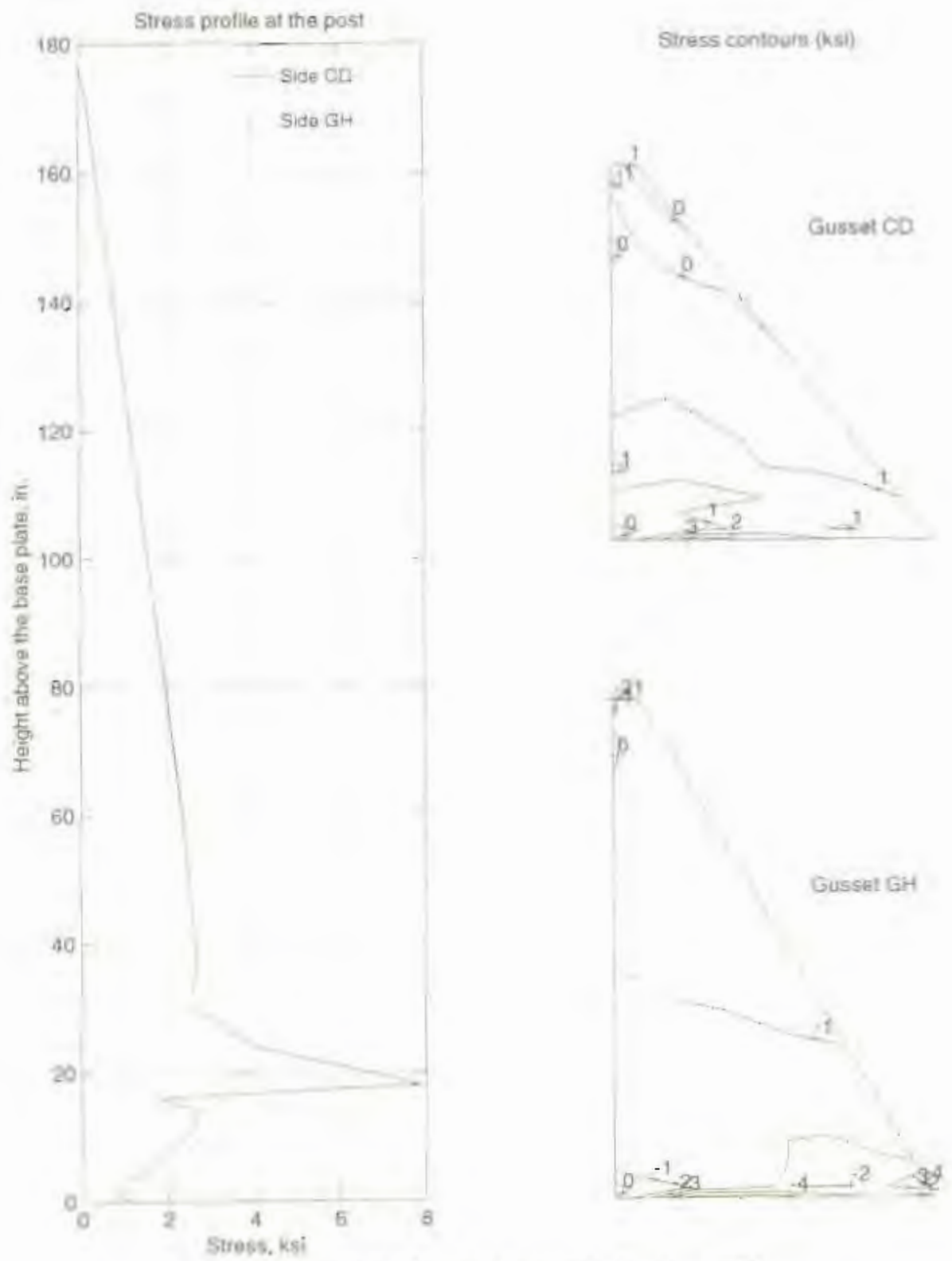


Figure 4.14: Computed stresses for Specimen GR1

CHAPTER 5: RESPONSE OF SPECIMEN CIP1

5.1 General

This chapter presents the results of the experimental studies on the response of a retrofitted cantilever post portion of a CMS structure. The post was extracted from a CMS structure that was initially designated for field installation. As such, the quality of the test specimen is likely representative of those CMS posts currently in service.

The steel post was fabricated from 18 in. (457 mm) diameter pipe with a wall thickness of 1/2 in. (13 mm). The post-to-base plate connection consisted of a full-penetration groove weld. The backup ring was left in place. Figure 5.1 shows the connection detail for the steel post. The 2-3/4 in. (70 mm) base plate was attached to the foundation using 8 No. 2-1/4 in. (57 mm) anchor bolts. The drainage hole shown in Figure 5.1(a) was flame-cut in the groove-welded connection to facilitate the galvanizing process. A special pedestal foundation was cast for Specimen CIP1 to replicate field conditions.

5.2 Retrofit Strategy

Examination by Gilani, et al. (1997) of results from the laboratory testing of the components of CMS specimens identified two locations in a steel CMS post that are susceptible to fatigue failure: the post-to-base plate groove-welded connection, and the region around the conduit hole. To assess the viability of a proposed retrofit scheme, a steel post from a CMS structure was retrofitted to details developed by Caltrans following the exact sequence of the events which have been proposed for the field work. The retrofit consisted of casting a concrete jacket around the lower portion of the post specimen. The objectives of this retrofit scheme were fourfold: 1) increase the section modulus near the post-to-base plate connection to reduce the cyclic stress range at the base of the post; 2) increase the overall stiffness of the CMS structure; and 3) increase the mechanical damping of the system. Figure 5.2 presents information on the retrofit scheme.

5.3 Test Configuration

The test specimen was fabricated by cutting a CMS post to a length of 14 ft. 4 in. (4.4 m) to accommodate the framework built to test post and mast-arm specimens (see Gilani, et al., 1997 for details). The post was connected to the foundation using eight 2-1/4 in. (57 mm) diameter anchor bolts. The top nuts were first snug tightened, then further tightened by the turn-of-the-nut method (AISC, 1995).

The retrofit work included: 1) removing the cover concrete to expose the foundation top

reinforcement (Figure 5.3); 2) drilling 16 No. 1-3/8 in. (35 mm) holes, two on each face of the octagonal plate, in the existing foundation (Figure 5.4); 3) placing #7 longitudinal reinforcement in the drilled holes; 4) bonding the reinforcement to the existing foundation using SET-45 chemical action concrete (Figure 5.5); 5) placing #4 hoops at 4 in. (102 mm) spacing around the longitudinal reinforcement (Figure 5.6); 6) reinforcing the opening around the conduit hole; 7) placing a steel jacket to serve as formwork (Figure 5.7); and 8) pouring a Caltrans-approved concrete mix around the post (Figure 5.8). Figure 5.9 shows the test setup for Specimen CIP1.

5.4 Material Properties, Welding Procedures, and Inspections

The test specimen was a component of one of three CMS structures fabricated from Grade A53 steel (API, 1995; ASTM, 1991) by a Caltrans-approved vendor. These CMS structures were inspected by Caltrans prior to shipment to a local Caltrans-approved fabricator for modifications to suit the testing setup at EBRC.

Ultrasonic testing (UT) was used to establish the integrity of the welded post-to-base plate connections for all three CMS posts. All three posts had rejectable flaws. The post with the greatest number of defects was selected for Specimen CIP1 to provide a measure of the effectiveness of the proposed retrofit technique. Figure 5.10 shows some of the flaws at the post-to-base plate welded connection for this specimen.

5.5 Specimen Testing

5.5.1 Cyclic Tests

Specimen CIP1 was tested with zero mean stress (i.e., no dead-load stress). Cyclic testing was carried out symmetrically with respect to the zero mean stress. During the casting of the concrete jacket, the specimen was subjected to cyclic loading at a stress range of 1.5 ksi (10 MPa) at the base of the post, about a zero mean stress, at a frequency of 1 Hz. The cyclic loading was intended to simulate the wind-induced vibration of the post (at its natural frequency) likely to be present during the field installation of a concrete jacket. As a result of the low-amplitude vibrations, a small oval-shaped gap was introduced at the top of the jacket.

The testing protocol for Specimen CIP1 is presented in Table 5.1. The nominal stress range was measured using the strain gage placed on the post immediately above the concrete jacket on the face of the post opposite the rectangular conduit hole. For a 14 ft 4 in. (4.4 m) post without the concrete jacket, the nominal stress range immediately above the jacket (6 feet [1.8 m] above the base plate) is 60 percent of the nominal stress range at the base of the post. For Specimen CIP1, the same ratio for the nominal stress

ranges between the above mentioned elevations was assumed.

5.5.2 Pull-back Tests

Pull-back, free-vibration tests were undertaken to assess the effectiveness of the concrete jacket in adding damping and stiffness to the steel post. Such tests were undertaken over the course of the testing program. The specific objectives of the pull-back tests were to compute the vibration frequency, modal damping, and lateral stiffness of the test specimen. The tests were carried out prior to the placement of the concrete jacket, after the low-amplitude vibration tests, at each change in the stress range, and at the conclusion of the cyclic tests; see Table 5.2 for details.

The pull-back and quick-release tests were carried out by connecting the top of the specimen to the reaction frame using the loading linkage shown in Figure 5.11. The linkage consisted of steel chains, a turnbuckle, a specially machined bolt (see Figure 5.12), and a load cell, all in series. The components in the linkage were connected in series using steel shackles. Using a turnbuckle, a static load of approximately 4 kips (18 kN) was induced in the linkage. The applied load was removed by cutting the machined bolt. The instrumentation for the pull-back free vibration tests consisted of accelerometers mounted on top of the specimen, a displacement transducer mounted parallel to the linkage, and the load cell.

5.5.3 Push-over Test

At the conclusion of the cyclic testing, a static-test-to-failure was undertaken. The specimen was pulled back (such that the face of the post containing the conduit hole was in compression) in increments of 0.25 in. to a final displacement of 10 in. (the stroke limit of the actuator). At the end of each loading step, the displacement was maintained, and cracks in the specimen, pedestal, and footing were documented.

5.6 Crack Detection and Propagation

Shrinkage cracks in the concrete jacket were marked prior to the start of cyclic testing. Flexural cracks were monitored and marked on the specimen over the course of the testing program. Real-time analysis of strain gage data was used to monitor the response of the jacket reinforcement and the steel post.

5.7 Instrumentation

The instrumentation for Specimen CIP1 consisted of an LVDT on the servo-actuator center line measuring the applied displacement; a load cell in-line with the servo-actuator measuring the actuator force; two displacement transducers measuring the relative motion between the bottom of the jacket and the pedestal and between the bottom of the pedestal and the foundation; twenty two strain gages distributed along the height of the steel post (on the compression and tension faces); four strain gages placed on the

post at the four corners of the conduit hole; eighteen strain gages distributed along the height of the longitudinal reinforcement adjacent to the tension and compression faces of the post; six strain gages placed on three transverse hoops at locations adjacent to the tension and compression face, and two strain gages (one vertical and one horizontal) placed on the supplemental reinforcement around the conduit hole.

The stress range was monitored by sg9 placed on the compression side of the post (opposite the conduit hole) immediately above the top of the concrete jacket. The instrumentation list for Specimen CIP1 is presented in Table 5.3. Figure 5.13 presents a schematic view of the longitudinal strain gages placed on the steel post and the jacket reinforcement.

5.8 Experimental Results: Cyclic Tests

5.8.1 General

Figure 5.14 shows Specimen CIP1 prior to cyclic testing. Figure 5.15 shows the specimen at the conclusion of the cyclic testing. A total of 913 individual tests, each of 16-minutes duration, were recorded. Table 5.4 summarizes the key observations; more information is presented in the following sections. The total number of loading cycles for Specimen CIP1 exceeded 4,500,000.

5.8.2 Data Analysis Procedures

The computer program MATLAB (The Mathworks, 1997) and its signal processing toolbox were used to process the experimental data. The experimental data were reduced in three steps. In the first step, the raw data was read, the file header was removed, and a test log was created. Next, the drift in the data was removed and the peak-to-peak extreme values of response were extracted. Stress ranges were obtained by multiplying the peak-to-peak strains by the Young's modulus for steel, assumed to be equal to 30,000 ksi (208 GPa). Response histories were plotted in the third step.

5.8.3 Cracks in the Test Specimen

The flexural cracks that formed in the reinforced concrete jacket at the start of cyclic testing propagated slowly over the course of the testing program. The strain gage maxima remained relatively constant for the 4,000,000 loading cycles at the stress range of 20 ksi (135 MPa). This observation indicates that no substantial cracks formed in the steel post.

5.8.4 Typical Test Data

To provide the reader with information on the type of data collected throughout the testing program, selected force, displacement, and stress histories after approximately 300,000 cycles of loading are shown in Figure 5.16. Summary information on the response of the specimen follows.

5.8.5 Response Maxima

The maximum peak-to-peak response for each data channel was obtained for each individual test. Figure 5.17 shows the lateral stiffness history of the specimen; the stiffness was calculated by dividing the actuator force by the displacement at the tip of the post. Due to flexural cracking in the concrete jacket the lateral stiffness of the specimen reduced gradually. At the conclusion of the cyclic testing, the lateral stiffness of the specimen was approximately 80 percent of its initial value. Figure 5.18 shows the response maxima histories for the actuator force and displacement and selected gages. The maxima histories for force, displacement, and post strains are approximately constant throughout the test; the reinforcement strains increase slightly during the test. The abrupt jumps in the response at 2,000,000 and 4,000,000 cycles are a direct result of the change in the stress range (see Table 5.1).

5.8.6 Strain Gage Histories

Selected stress-range data were used to study the change in the response of the specimen as a function of the number of accumulated cycles. To account for drifting in the transducers, the data was adjusted by removing the error, which was assumed to be linearly increasing (from zero) over the course of an individual test. To best illustrate the changes in the stress range in the post and in the vertical reinforcement, the corrected data are presented. Figure 5.19 shows the stress-response history (sg3) at 3 in. (76 mm) above the base plate on the compression side of the steel post, and Figure 5.20 shows the stress-response history (sg32) at 3 in. (76 mm) above the base plate on the vertical reinforcement placed on the compression side of the specimen.

5.8.7 Stress Profiles

Figure 5.21 shows the stress profile for the steel post and the reinforcement in the reinforced concrete jacket. The top of the reinforced concrete jacket, the underside of the base plate, and the top of foundation are identified in this figure. The data correspond to the compression face of the specimen and are plotted following 1,000,000, 2,000,000, 3,000,000, and 4,000,000 cycles of loading. The stress profile in the steel post is essentially unchanged for the 4,000,000 loading cycles. Along the post elevation, above the concrete jacket, the stresses decrease linearly in proportion to the bending moment in the post. The stresses decrease substantially below the top of the reinforced concrete jacket where the section modulus of the test specimen is increased due to the presence of the jacket. Above the foundation, the stress profile for the reinforcement shifts during the cyclic testing due to concrete cracking.

5.9 Experimental Results: Pull-back Tests

5.9.1 General

Typical free vibration test data recorded for i) the steel post alone, ii) Specimen CIP1 prior to cyclic testing, iii) Specimen CIP1 after 2,500,000 cycles of loading, and iv) Specimen CIP1 at the conclusion of the cyclic testing, were selected for further analysis. Figure 5.22 shows the acceleration histories recorded at the top of the specimen during the free vibration tests:

5.9.2 Analysis of Experimental Data

The data processing package MATLAB and its signal processing toolbox were used to process the experimental acceleration response-history data. For each test, Fourier spectra were generated using Hanning windows of 2048 data points. Samples had a duration of 10.24 seconds for the test of the steel post and 4.1 seconds for the subsequent tests. For all Fourier analyses, the windows were overlapped by 200 points. The frequency resolution was approximately 0.24 Hz and 0.098 Hz for the steel post tests scanned at 200 Hz and for subsequent tests scanned at 500 Hz, respectively. Figure 5.23 shows the Fourier power spectra for the acceleration records.

5.9.3 Modal Properties

Modal properties of Specimen CIP1 at different cycle counts can be computed from either the history plots (Figure 5.22) or the frequency domain plots (Figure 5.23). Modal frequencies were estimated using the peaks of the Fourier spectra. Since the response is primarily a SDOF response, both the half-power and the log-decrement methods (Clough and Penzien, 1993) can be used to estimate modal damping. In the half-power method, the modal damping ratio, ξ_n , is estimated from:

$$\xi_n = \frac{(\omega_2 - \omega_1)}{2\omega_n} \quad (5.1)$$

where ω_n is the modal frequency and ω_2 and ω_1 are the half-power frequencies. In the log-decrement method, an analytical function of the form:

$$y = A \sin(\omega t + \phi) e^{-\omega \xi t} \quad (5.2)$$

is fitted to the response-history data, and the damping ratio is computed from the log decrement equation:

$$\xi = \frac{1}{2\pi(N)} \ln\left(\frac{y_2}{y_1}\right) \quad (5.3)$$

where N is the number of cycles between the two amplitude readings and y_2 and y_1 are the amplitudes of the analytic function. Table 5.5 summarizes the modal properties of Specimen CIP1.

5.10 Experimental Results: Push-over Tests

Figure 5.25 shows the push-over response of Specimen CIP1. At the end of each step in the static loading cycle, the displacement was held constant and the cracks were documented. This procedure led to load relaxation in the specimen as indicated. Shown in Figure 5.25 are: i) the force-displacement response; ii) the stress in the post just above the concrete jacket; iii) the stress in the longitudinal rebar at 3 in. (76 mm) above the base plate; iv) the hoop stress in a lateral reinforcement.

The maximum lateral resistance of the specimen was approximately 55 kips (245 kN). The resistance reduced at large displacements due to cracking of the concrete and possible fracture of reinforcement in the footing. At the conclusion of the test, the residual displacement at the top of the specimen was approximately 5.5 in. (140 mm). The maximum stress in the post was 60 ksi (420 MPa) and close to the yield stress of the steel post (see Chapter 3). The photographs in Figure 5.25 show damage to the specimen following the push-over test.

5.11 Summary

A concrete-jacket retrofitted post was subjected to 4,500,000 cycles of loading. Although it is difficult to draw conclusions regarding the general performance of this type of retrofit detail from only one test, the following general observations are made.

1. *Increased damping and stiffness.* The addition of the reinforced concrete jacket substantially increased the stiffness and the damping ratio of the post (by factors exceeding 2.5 and 5, respectively) for the test specimen.
2. *Effect of flaws in the weldment.* The groove-welded post-to-base plate connection in Specimen CIP1 included a number of rejectable flaws. The addition of the reinforced concrete jacket substantially reduced the stresses in the post-to-base plate connection and thus reduced the likelihood of fatigue failure.
3. *Application to field CMS structures.* The beneficial effects of adding the reinforced concrete jacket to the steel post, which included increased strength and damping, are not expected to be matched in their entirety in the field specimens. The test specimen was less than 15 ft (4.6 m) tall, and the jacket extended for 6 ft (1.8 m), of its length. In the field, the linear length of the CMS (post plus mast arm) exceeds 54 ft (16.5 m) and the jacket will only cover a small percentage of this total length. As such, the large increases in damping and stiffness measured in the laboratory will not be replicated in the field.

Table 5.1: Stress range for the cyclic tests of Specimen CIP1

Cycle count	Test stress range (72 in. above base)	Target stress range (base)	Test frequency
0-20,000	1 ksi (7 MPa)	1.5 ksi (10 MPa)	1 Hz
0-2,000,000	12 ksi (81 MPa)	20 ksi (135 MPa)	5 Hz
2,000,000-2,500,000	15 ksi (101 MPa)	25 ksi (169 MPa)	5 Hz
2,500,000-4,000,000	12 ksi (81 MPa)	20 ksi (135 MPa)	5 Hz
4,000,000-4,500,000	24 ksi (162 MPa)	40 ksi (270 MPa)	5 Hz

Table 5.2: Sequence of pull-back tests

Pull-back test number	Cycle count	Scan frequency (Hz)	Comments
1	0	200	Steel post only
2	0	500	After placement of concrete jacket
3	2,000,000	250	Prior to increase in stress amplitude
4	2,500,000	500	Prior to decrease in stress amplitude
5	4,000,000	500	After four million cycles
6	4,500,000	500	Termination of cyclic tests

Table 5.3: Instrumentation for Specimen CIP1

Ch. No.	Inst. ID.	Instrument	Location
Global sensors			
1	load	load cell	actuator center line; top of the post
2	displacement	lvdt	actuator center line; top of the post
Strain gages placed on the steel post			
3	sg1	strain gage	compression side of the post; just above the base plate
4	sg2	strain gage	compression side of the post; 1.25" above the base plate
5	sg3	strain gage	compression side of the post; 3" above the base plate
6	sg4	strain gage	compression side of the post; 6" above the base plate
7	sg5	strain gage	compression side of the post; 12" above the base plate
8	sg6	strain gage	compression side of the post; 27" above the base plate
9	sg7	strain gage	compression side of the post; 36" above the base plate
10	sg8	strain gage	compression side of the post; 72" above the base plate (below jacket)
11	sg9	strain gage	compression side of the post; 72" above the base plate (above jacket)
12	sg10	strain gage	compression side of the post; 90" above the base plate
13	sg11	strain gage	compression side of the post; 108" above the base plate
14	not used		
15	dcdt2	dcdt	compression side; between the pedestal and the footing
16	sg14	strain gage	tension side of the post; 3" above the base plate
17	sg15	strain gage	tension side of the post; 6" above the base plate
18	sg16	strain gage	tension side of the post; 12" above the base plate
19	not used		
20	sg18	strain gage	tension side of the post; 36" above the base plate
21	sg19	strain gage	tension side of the post; 72" above the base plate (below jacket)
22	dcdt1	dcdt	compression side; between the pedestal and the jacket
23	sg21	strain gage	tension side of the post; 90" above the base plate
24	sg22	strain gage	tension side of the post; 108" above the base plate
25	sg23	strain gage	neutral axis side of the post; just above the base plate
26	sg24	strain gage	tension side of the post; NW corner conduit hole
27	sg25	strain gage	tension side of the post; NE corner conduit hole

Table 3.3: Instrumentation for Specimen CIP1

28	sg26	strain gage	tension side of the post; SW corner conduit hole
29	sg27	strain gage	tension side of the post; SE corner conduit hole
30	sg12	strain gage	tension side of the post; just above the base plate
31	sg17	strain gage	tension side of the post; 27" above the base plate
strain gages placed on the concrete-jacket vertical reinforcement			
32	sg28	strain gage	compression side reinforcement; 3" below foundation
33	sg29	strain gage	compression side reinforcement; just below foundation
34	sg30	strain gage	compression side reinforcement; just above foundation
35	sg31	strain gage	compression side reinforcement; just below base plate
36	sg32	strain gage	compression side reinforcement; just above base plate
37	sg33	strain gage	compression side reinforcement; 3" above base plate
38	sg34	strain gage	compression side reinforcement; 12" above base plate
39	sg35	strain gage	compression side reinforcement; 36" above base plate
40	sg36	strain gage	compression side reinforcement; 72" above base plate (below jacket)
41	sg37	strain gage	tension side reinforcement; 3" below foundation
42	sg38	strain gage	tension side reinforcement; just below foundation
43	sg39	strain gage	tension side reinforcement; just above foundation
44	sg40	strain gage	tension side reinforcement; just below base plate
45	sg41	strain gage	tension side reinforcement; just above base plate
46	sg42	strain gage	tension side reinforcement; 3" above base plate
47	sg43	strain gage	tension side reinforcement; 12" above base plate
48	sg44	strain gage	tension side reinforcement; 36" above base plate
49	sg45	strain gage	tension side reinforcement; 72" above base plate (below jacket)
Strain gages placed on the concrete jacket transverse reinforcement			
50	sg46	strain gage	compression side of the bottom hoop
51	sg47	strain gage	tension side of the bottom hoop
52	not used		
53	sg48	strain gage	compression side of the third hoop from the bottom
54	sg49	strain gage	tension side of the third hoop from the bottom
55	sg50	strain gage	compression side of the top hoop
56	sg51	strain gage	tension side of the top hoop

Table 5.3: Instrumentation for Specimen CIP1

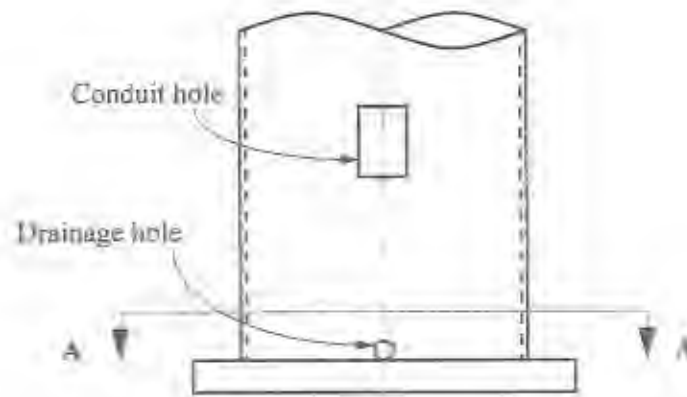
strain gages placed on the supplementary reinforcement around the conduit hole			
57	sg52	strain gage	vertical face of reinforcement, nearest to the steel post
58			not used
59			not used
60			not used
61			data acquisition counter
62			data acquisition timer
63	sg53	strain gage	horizontal face of reinforcement, nearest to the steel post

Table 5.4: Test summary for Specimen CIP1

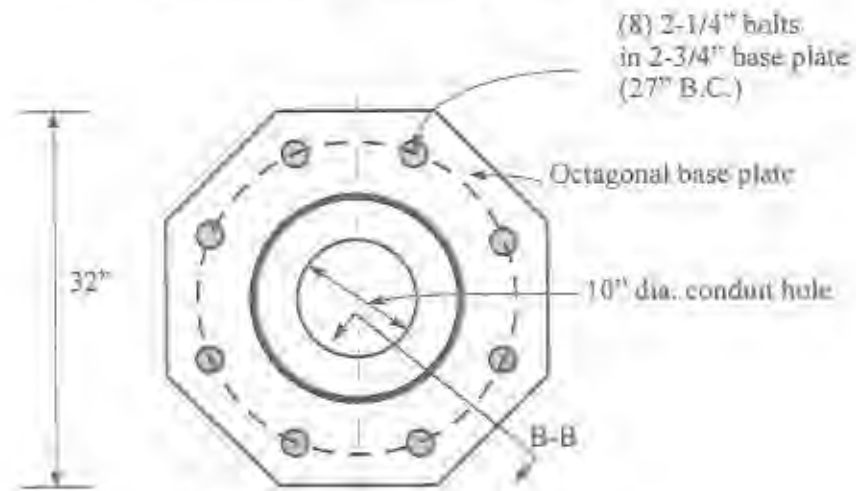
Cycle count (millions)	Event
0	Start of test.
0	Shrinkage cracks in the concrete jacket marked.
0.1	Cracks at the jacket-to-pedestal and pedestal-to-foundation interface observed.
4.0	Completion of tests at 20 ksi nominal stress range, no evidence of failure.
4.5	Completion of tests at 40 ksi nominal stress range, no evidence of failure.
4.5+	Substantial cracking of the foundation during the push-over tests. No evidence of failure in the test specimen.

Table 5.5: Modal properties of the test specimen

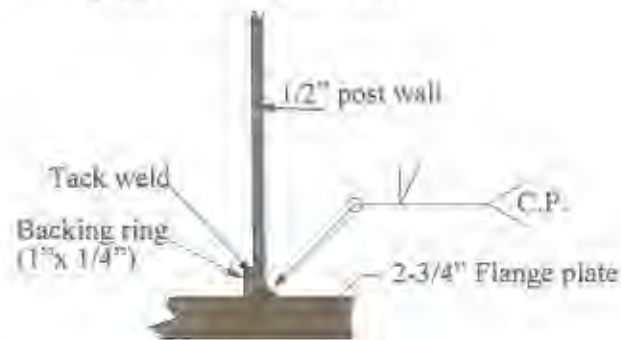
Pull-back test number	Cycle count	Frequency (Hz)	Damping (% critical)	Comments
1	0	13.1	0.3	Steel post alone
2	0	23.4	1.5	CIP1, prior to cyclic testing
4	2,500,000	21.5	1.6	CIP1, midway through the cyclic testing
6	4,500,000	20.0	1.8	CIP1, at the end of the cyclic testing



(a) Elevation at base of steel specimen



(b) Section A-A (plan view)



(c) Section B-B (connection details)

Figure 5.1: Connection details for the steel post of Specimen CIP1

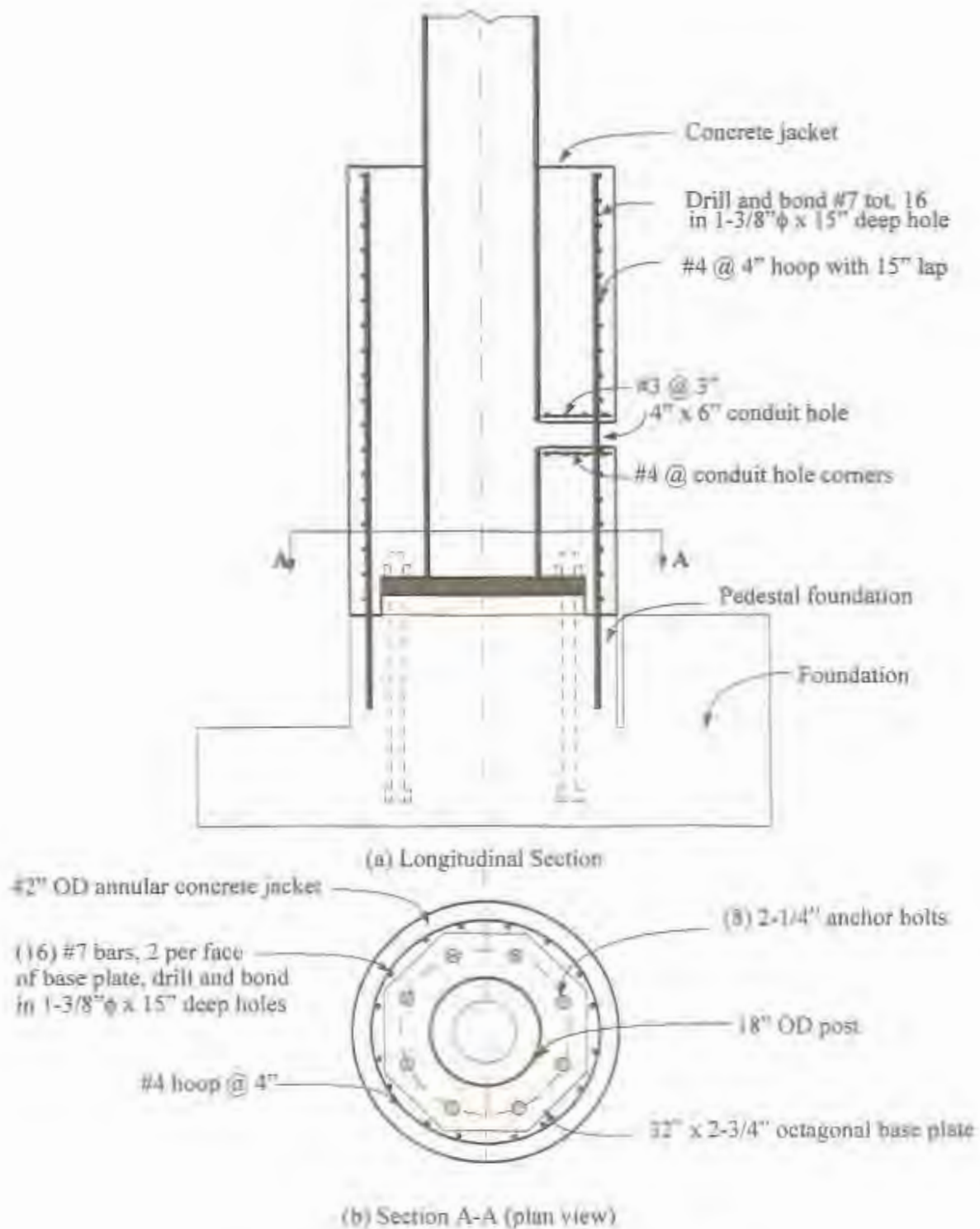


Figure 5.2: Retrofit details for Specimen CIP1



Figure 5.3: Removing the cover concrete and exposing top reinforcement



Figure 5.4: Drilling the existing foundation



Figure 5.5: Grouting the longitudinal reinforcement



Figure 5.6: Placing the transverse hoops



Figure 5.7: Placing the steel formwork



Figure 5.8: Casting the concrete jacket

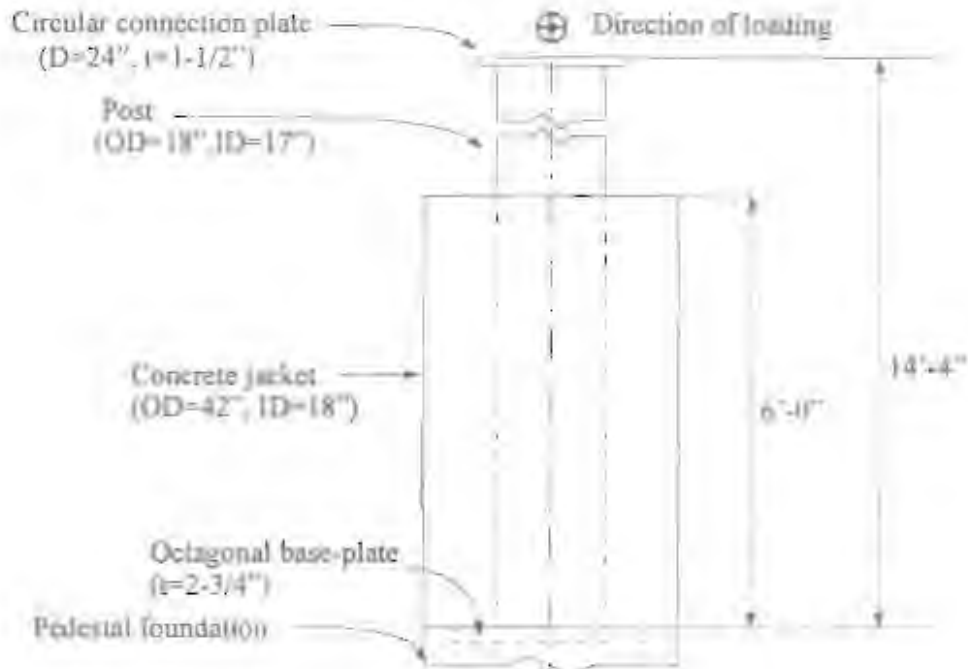


Figure 5.9: Test setup for Specimen CIP1



Figure 5.10: Location of flaws on the tension side of the post detected by ultrasonic testing



Figure 5.11: Test setup for the pull-back tests

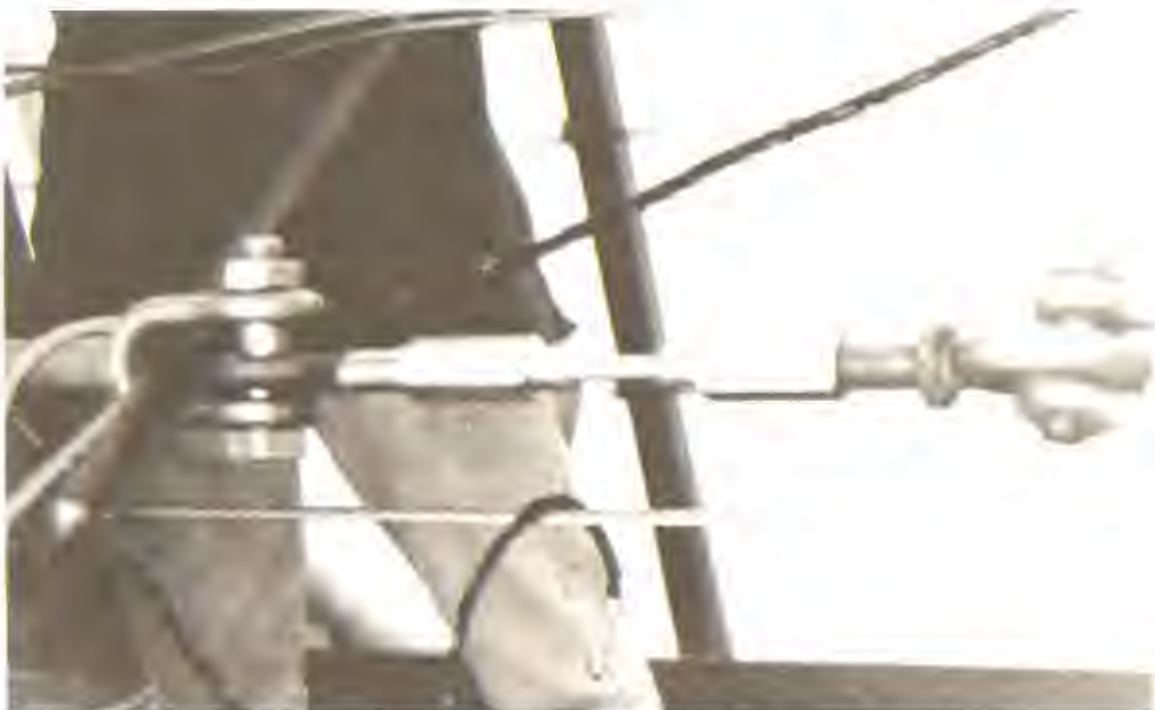


Figure 5.12: Machined bolt used for the sudden release of applied load

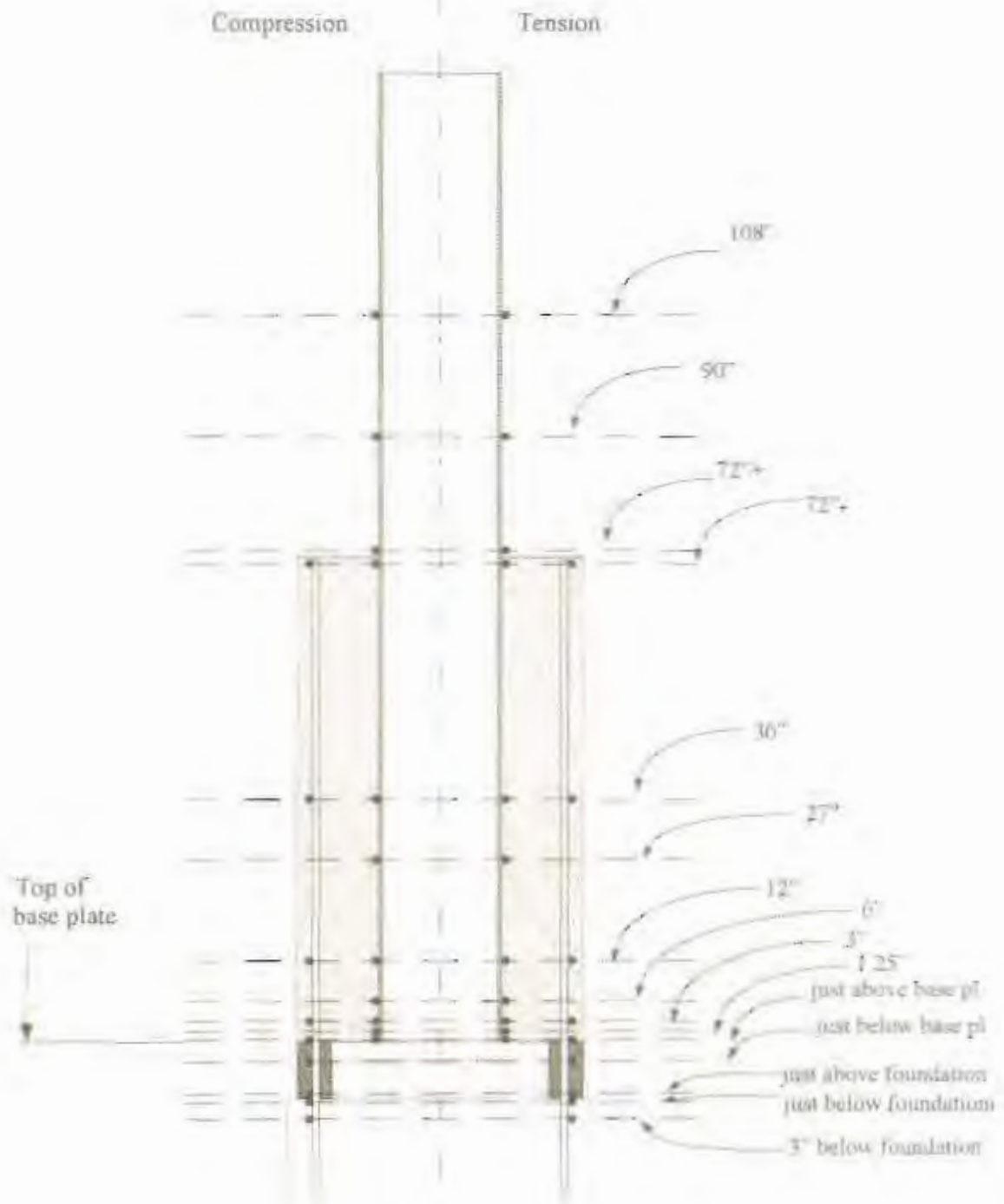


Figure 5.13. Schematic view of longitudinal strain gages on the post and jacket reinforcement.



Figure 5.14: Photograph of Specimen CIP1 prior to cyclic testing



Figure 5.15: Photograph of Specimen CIP1 at the conclusion of the cyclic testing

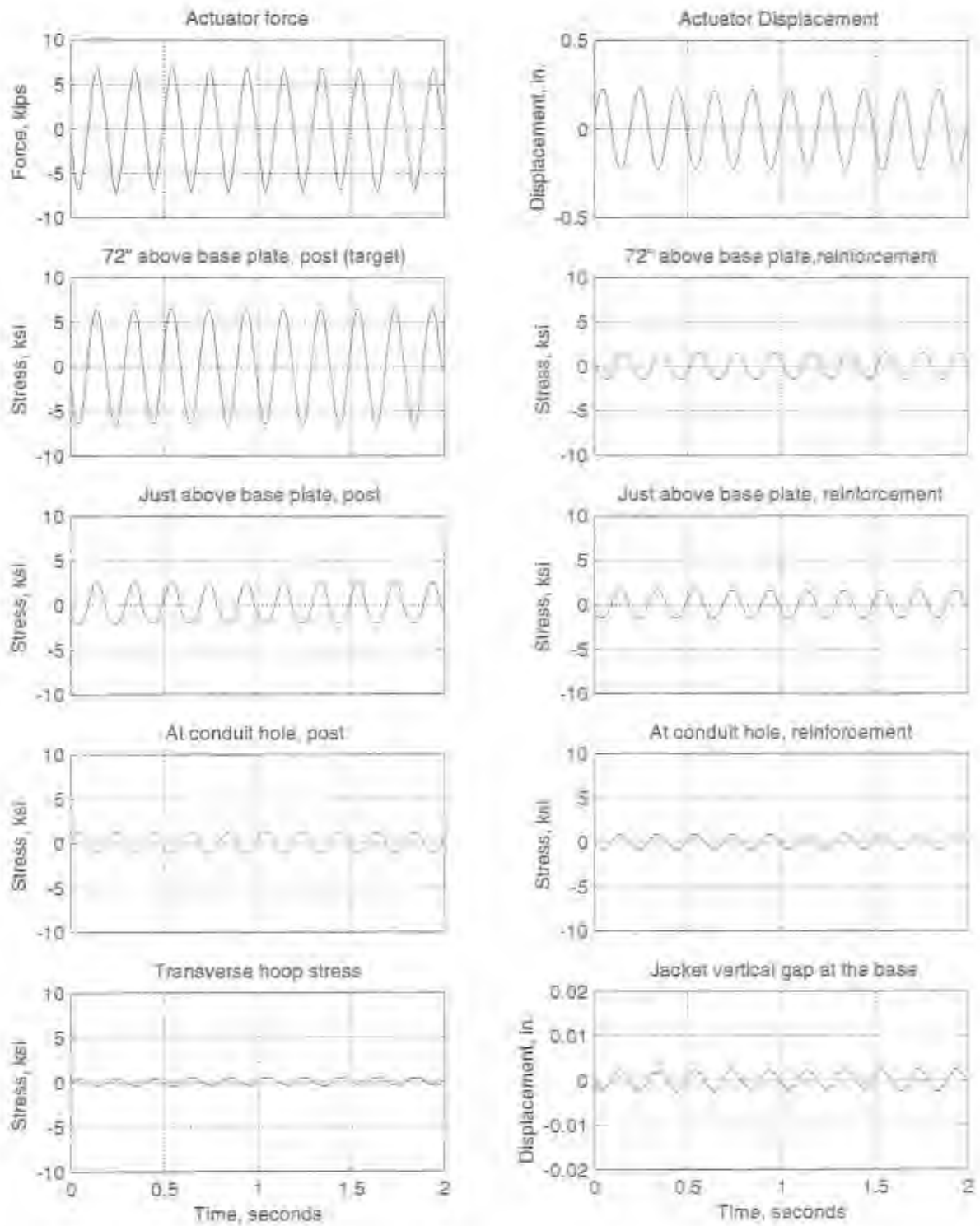


Figure 5.16: Typical response histories for Specimen CIP1

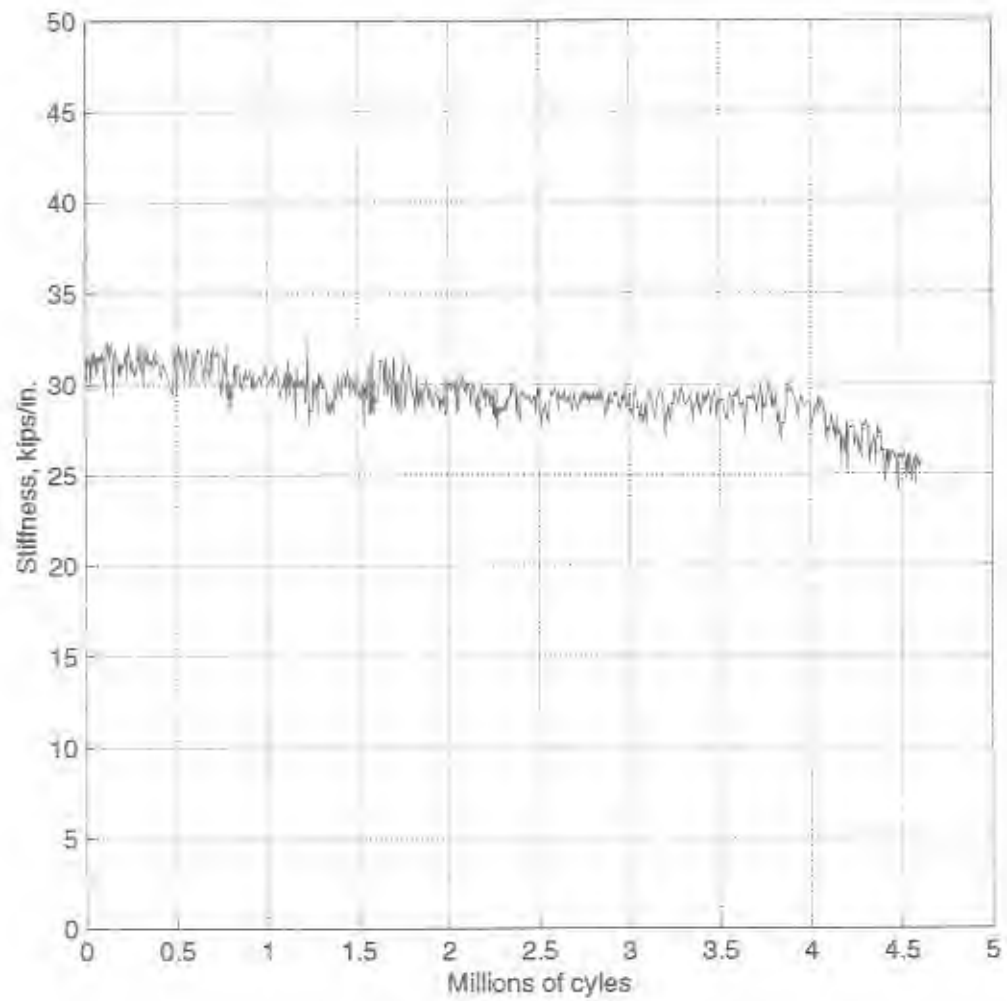


Figure 5.17: Lateral stiffness history for Specimen CIP1

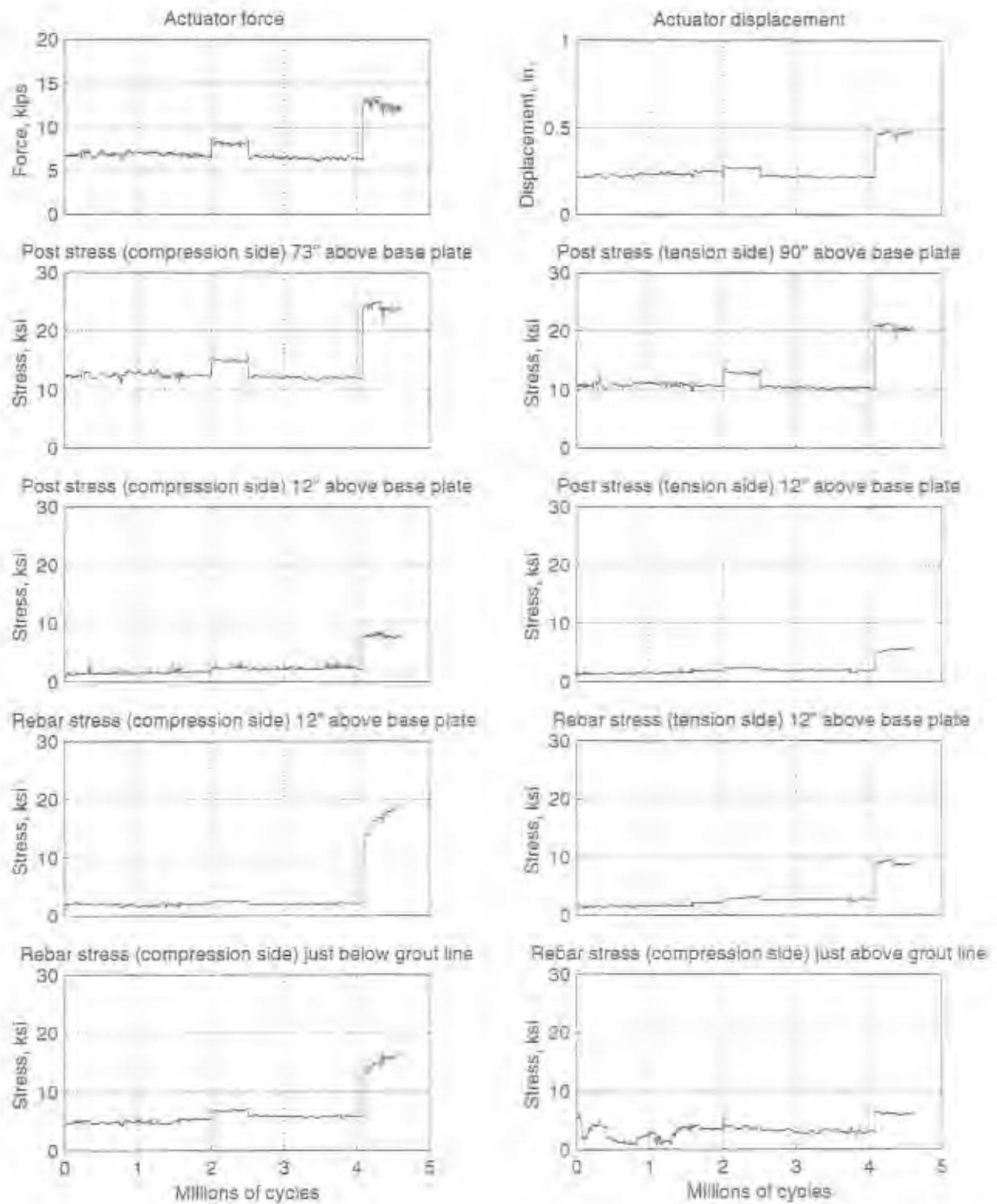


Figure 5.18: Response maxima for Specimen CIP1

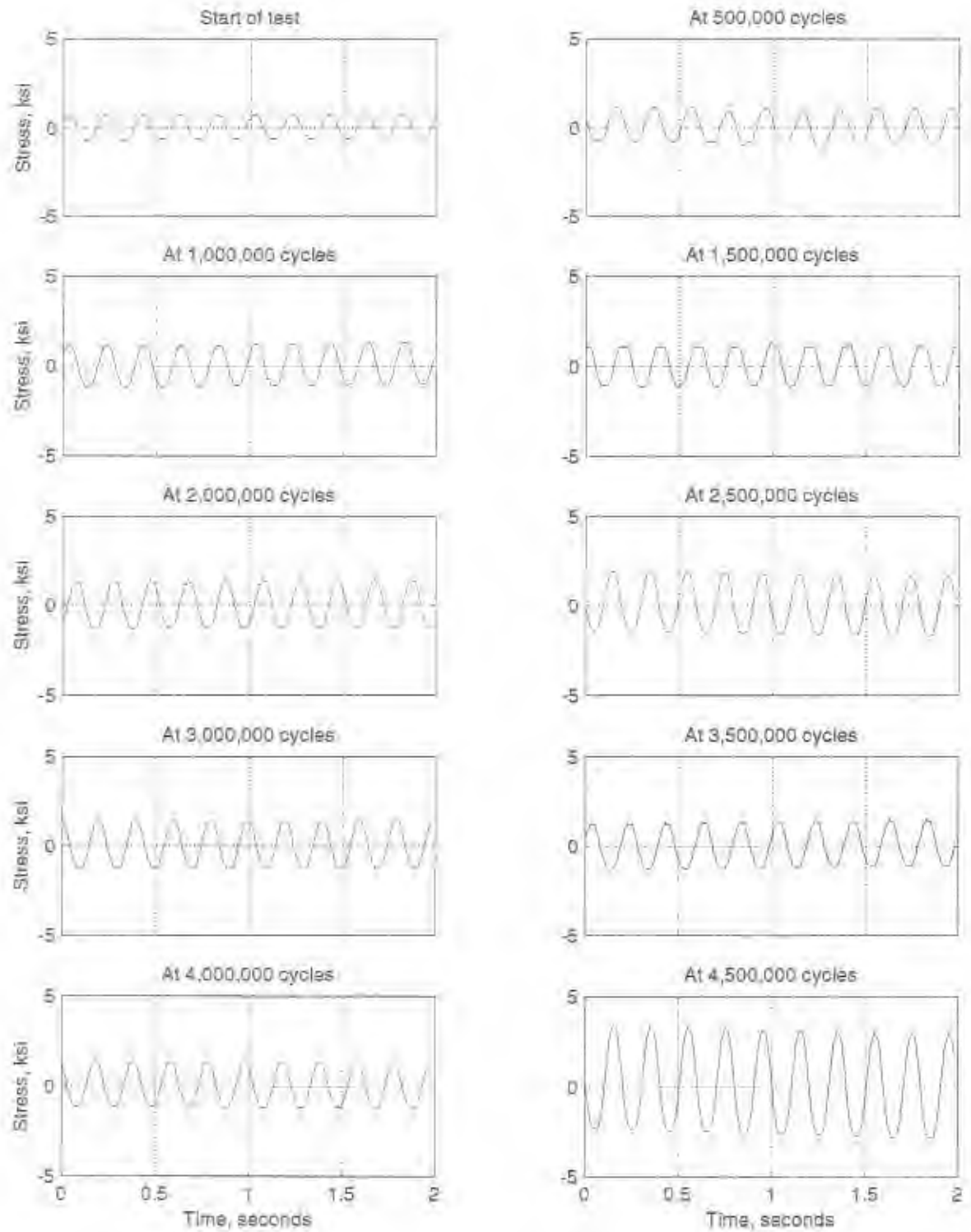


Figure 5.19: Post stress history at 3 in. above the base plate (sg3) for Specimen CIP1

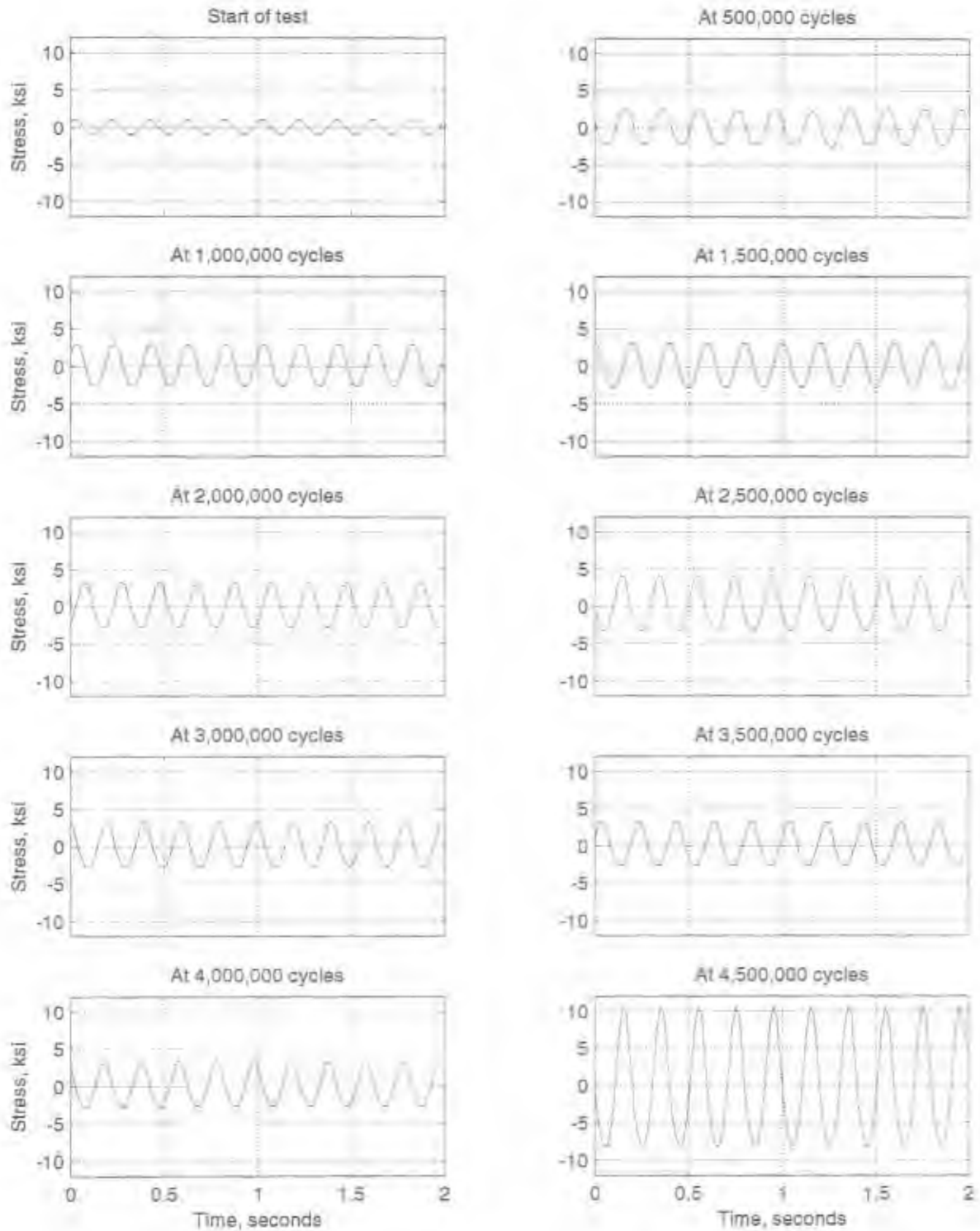


Figure 5.20: Reinforcement stress history at 3 in. above the base plate (sg33) for Specimen CIP1

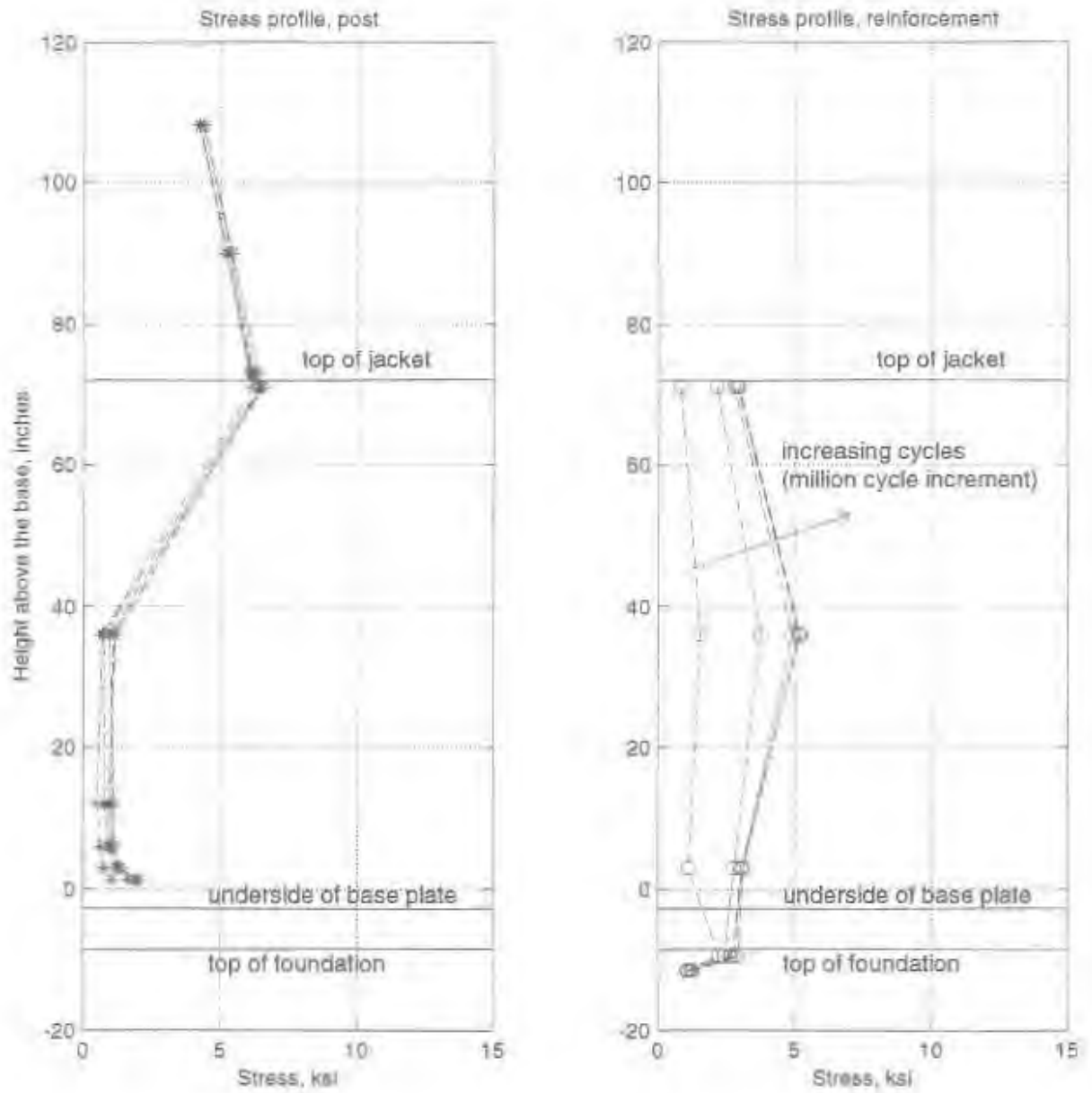


Figure 5.21: Stress profiles for Specimen CIP1

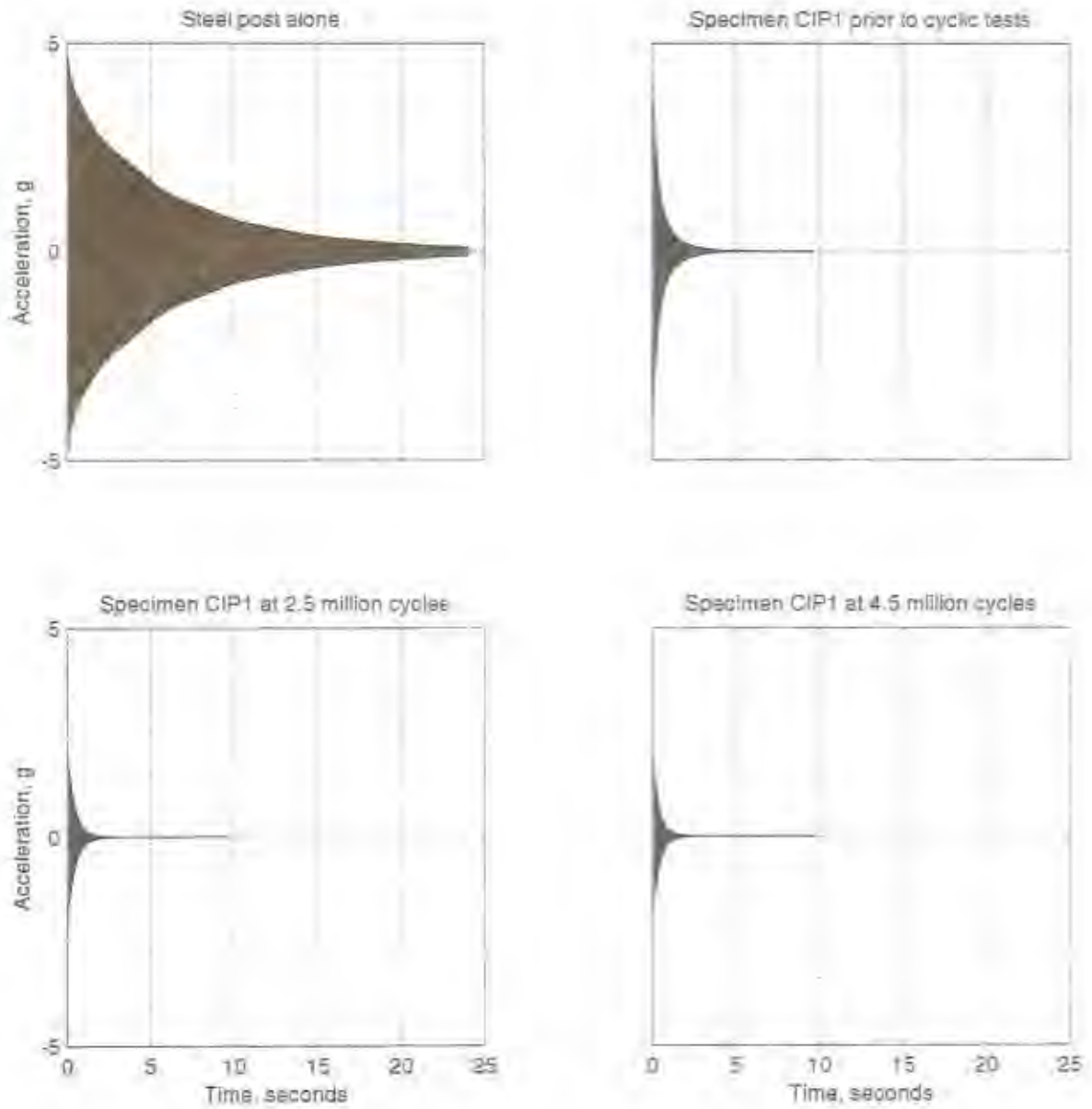


Figure 5.22: Free vibration acceleration response for Specimen CIP1

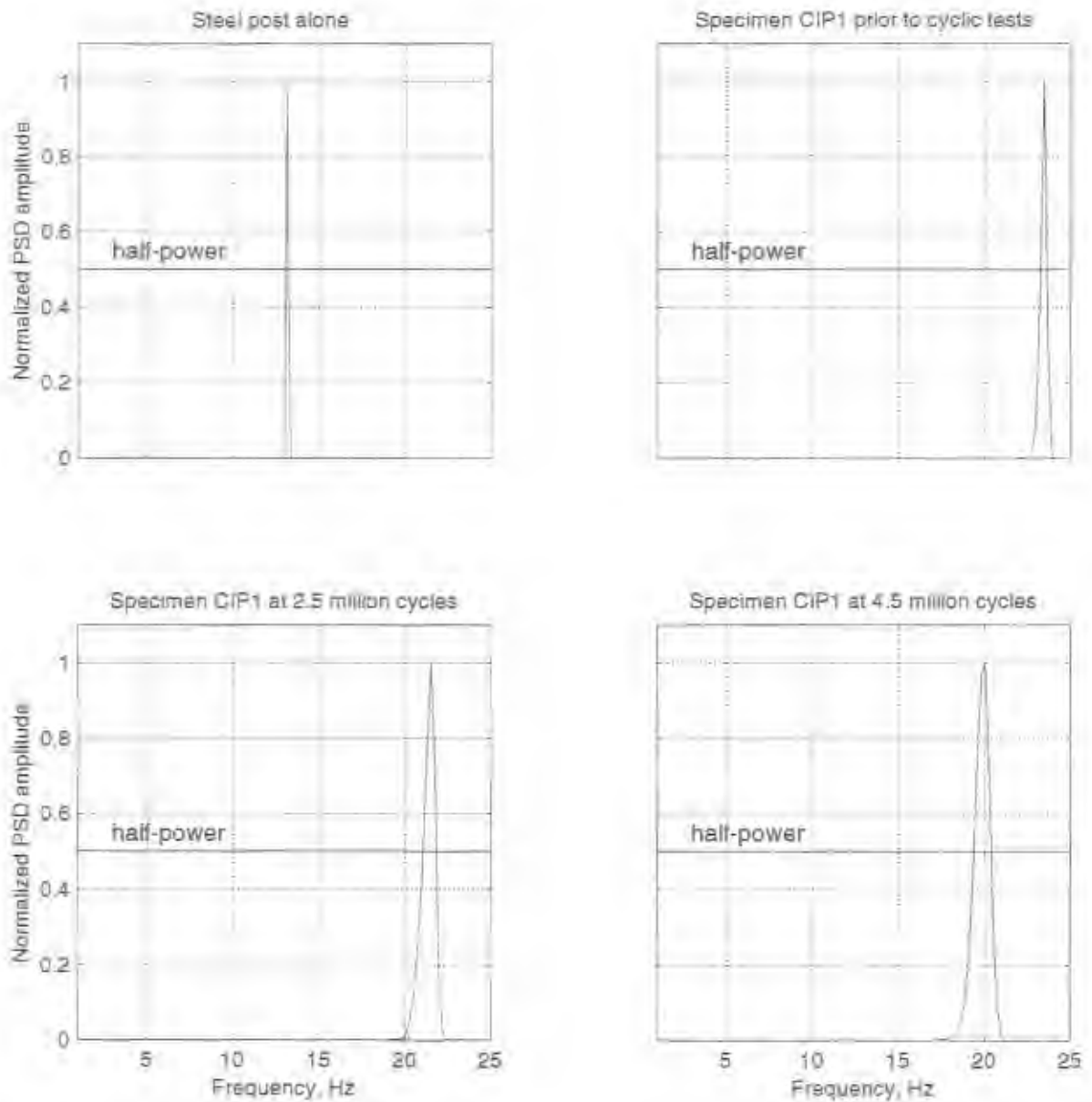


Figure 5.23: Acceleration frequency response for Specimen CIP1

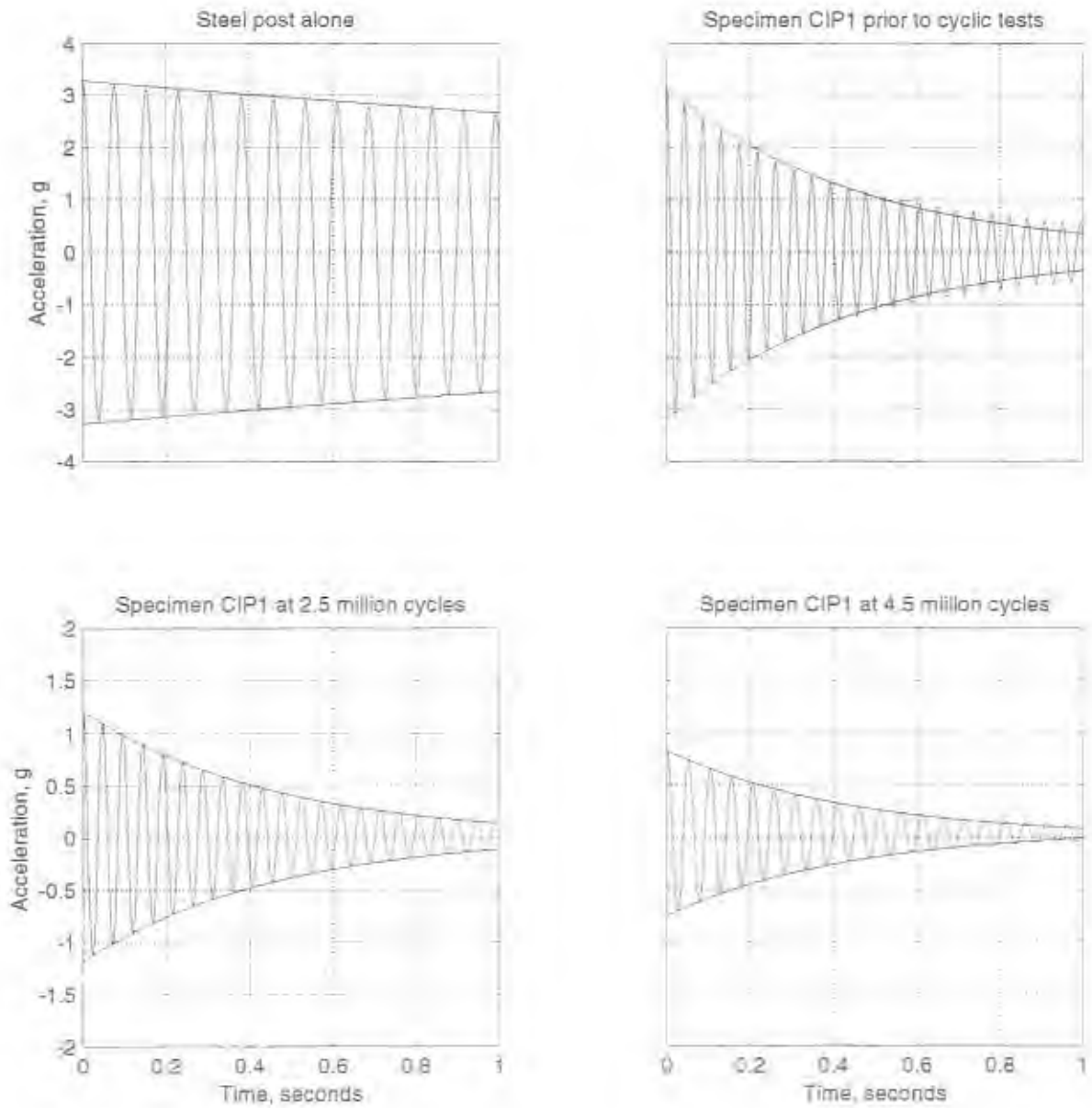


Figure 5.24: Analytical acceleration curve fitting for Specimen CIP1

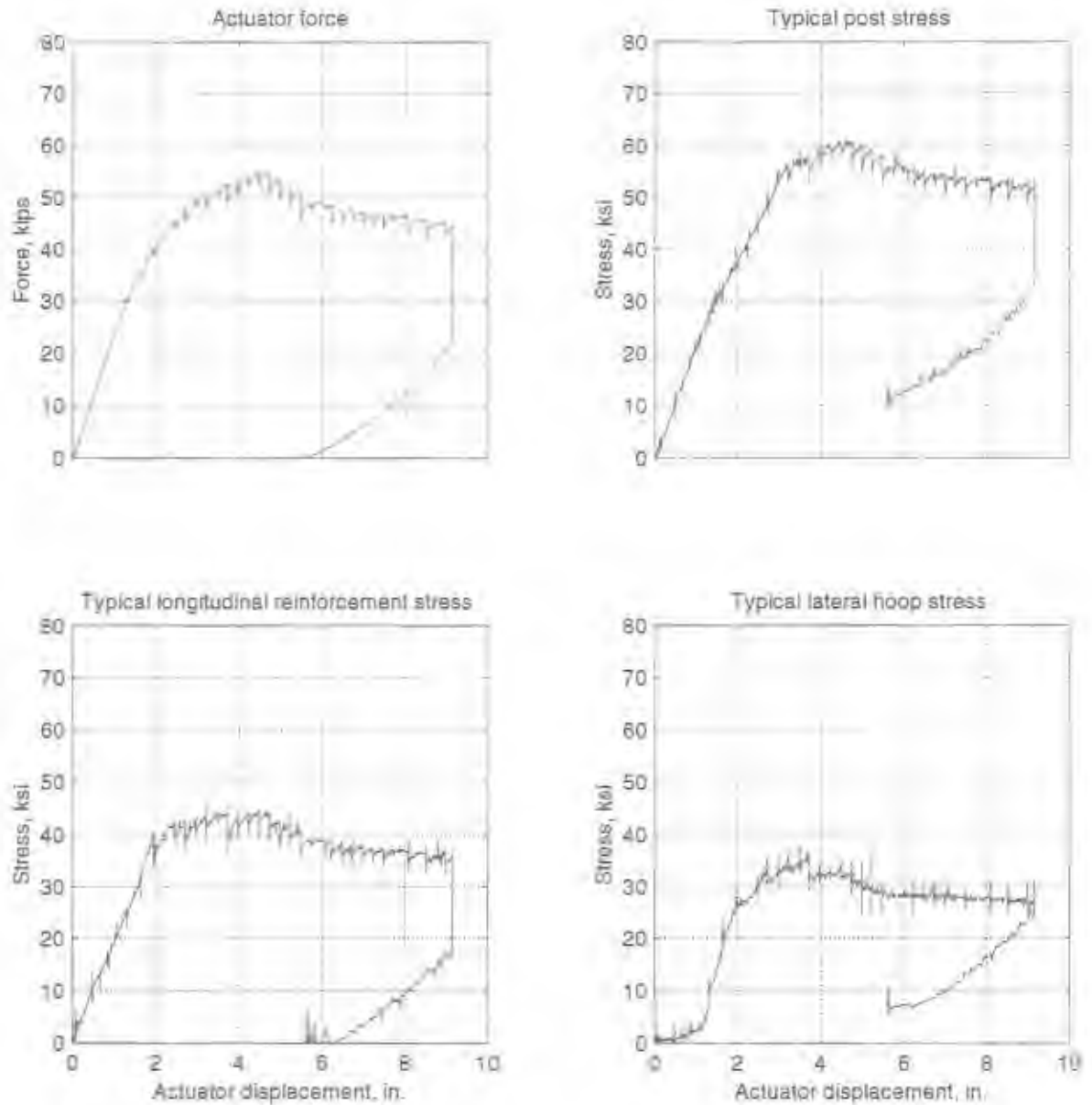
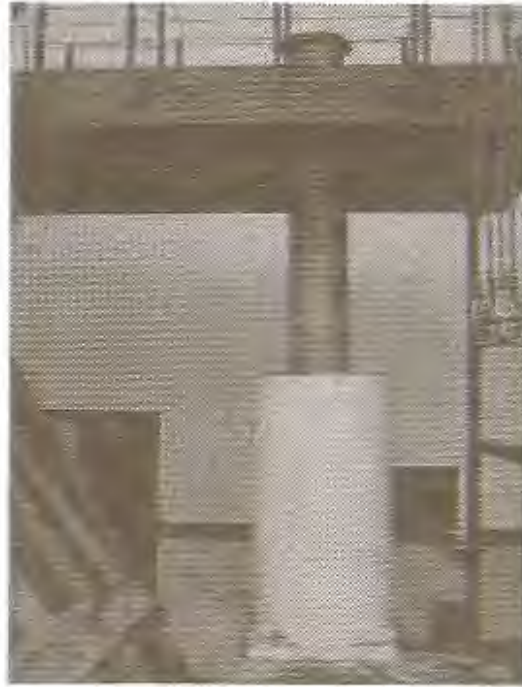


Figure 5.25: Push-over response for Specimen CIP1



(a) Deformed configuration



(b) Cracks in the footing

Figure 5.26: Photos of Specimen CIP1 at the conclusion of push-over tests

CHAPTER 6: SUMMARY, CONCLUSIONS, AND RECOMMENDATIONS

6.1 Summary

6.1.1 Introduction

Changeable Message Sign (CMS) structures are widely used in California by the California Department of Transportation (Caltrans) to deliver information to freeway motorists regarding road and weather conditions. These structures are inverted L-shaped cantilever structures composed of a vertical post and a horizontal mast arm. Both the post and the mast arm are fabricated from steel pipe sections. The top of the post is bent 90° to make the connection to the mast arm. The mast arm is connected to the post by a flanged connection; annular plates are groove-welded to the post and the mast arm, and the flange plates are bolted together with 26 No. 3/4-in. (19 mm) diameter high-strength bolts. The steel post is welded to a 2-3/4 in. (70 mm) thick base plate, which in turn is anchored to a concrete foundation (typically a CIDH pile) by 8 No. 2-1/4 in. (57 mm) diameter anchor bolts. In all CMS structures built prior to 1997, a 4 in. by 6 in. (101 mm by 152 mm) rectangular hole is flame-cut in the post, approximately 18 in. (457 mm) above the base plate, to provide access to electrical wiring in the post. In some CMS structures, a small hole is flame cut in the welded post-to-base plate connection to facilitate the galvanizing process.

The failure of a post-to-base plate welded connection in a CMS structure in Southern California prompted Caltrans to undertake widespread field investigations of CMS structures in California. Several CMS structures were instrumented to characterize their dynamic response. The field data indicated that a) the welded connections in the CMS structures are subjected to stress levels that substantially exceed the allowable stress levels recommended by the AASHTO specifications (AASHTO, 1994), and b) CMS structures are relatively flexible with little structural damping (Winter, 1996).

As a result of these findings, Caltrans identified three topical areas for investigation:

1. Full-scale laboratory experimental studies to develop an understanding of the fatigue life of components of CMS structures.
2. Full-scale laboratory tests of proposed schemes for retrofitting CMS structures if deemed necessary by the results of 1.
3. The use of energy dissipation devices to mitigate wind-induced vibrations in CMS structures.

Caltrans contracted with the University of California at Berkeley to study the first two topical areas. This report addresses the second topical area, namely, the response of retrofitted CMS structures.

The reader is referred to Gilani, et al. (1997) for results of the studies on the response of components of existing CMS structures.

6.1.2 Retrofit Schemes

Examination by the authors of the results of the laboratory testing of components of CMS structures identified two locations in the steel post that were susceptible to fatigue failure: the post-to-base plate groove-welded connection, and the region around the conduit hole. Two retrofit schemes were developed by Caltrans: a steel gusset-plate retrofit, and a cast-in-place concrete-jacket retrofit. Both schemes sought to reduce the stresses in the post at the two critical locations identified above.

The steel gusset-plate retrofit scheme consisted of welding eight gusset plates of 9/16 in. (14 mm) thick A36 steel to the post-to-base plate connection. The triangular gusset plates were welded to the post and the base plate using full-penetration groove welds. The gussets were centered between the base plate anchor bolts. The gusset coinciding with the conduit hole on the tension face of the post was 17 in. (432 mm) tall and was terminated approximately 1 in. (25 mm) below the underside of the conduit hole; the other seven gussets were 24 in. (610 mm) tall. All eight gussets were 6.5 in. (165 mm) wide at their base.

The concrete-jacket retrofit scheme consisted of adding a reinforced concrete shell to the steel post. The jacket had a outside diameter of 42 in. (1.1 m) and was 6 ft (1.8 m) tall. The jacket was attached to a foundation by drilling and bonding a total of 16 #7 vertical reinforcement bars. The transverse reinforcement in the jacket consisted of #4 hoops, with a 15 in. (381 mm) lap, placed at 4 in. (102 mm) spacing. Trim reinforcement was added around the conduit hole.

6.1.3 Summary of Laboratory Experimental Data

A customized reaction frame was designed and built to facilitate high-cycle fatigue testing of components of CMS structures. Each test specimen was loaded at its free end by a fatigue-rated servo-actuator. The responses of the two retrofitted test specimens are summarized in Table 6.1 below.

Table 6.1: Summary data for retrofitted specimens

Retrofit scheme	EERC designation	Maximum cycles	Comments
steel-gusset	GR1	1,000,000	Specimen failed at 800,000 cycles
concrete-jacket	CIP1	4,500,000	

The testing of Specimen GR1 was halted after approximately 1,000,000 cycles following 1) the propagation of large fatigue-induced cracks, which had formed at the lower corners of the rectangular conduit hole, into the gusset-to-post welds and the gusset parent material, and 2) the growth of fatigue

cracks in the post-to-base plate welded connection.

The response of Specimen CIP1 was relatively stable for 4,500,000 cycles of loading; no significant change in the strength or stiffness of the specimen was observed.

6.1.4 Modeling of CMS Structures

The gusset-retrofitted post was modeled as a cantilever structure, using the computer code SADSAP, to provide information on the stress distributions in the post around the conduit hole, adjacent to the post-to-base plate connection, and in the steel gusset plates. Quadrilateral shell elements were used to model the post, the gusset plates, and the base plate. Spring elements were used to model the axial stiffness of the 2-1/4 in. (57 mm) diameter anchor bolts.

The analysis predicted that the local stresses in the post were increased by a factor of 2.5 around the conduit hole. This value is consistent with experimental data.

6.2 Conclusions and Recommendations

6.2.1 Fatigue Life of Retrofitted CMS Posts

Specimen GR1 was tested to approximately 1,000,000 cycles of loading. However, significant cracks formed after approximately 600,000 cycles and propagated thereafter. Although the gusset plates were effective in increasing the section modulus of the post and decreasing the flexural stresses at the base of the post, the retrofit scheme was unable to prevent, and likely contributed to, substantial cracking around the conduit hole. On the basis of the laboratory tests, this scheme is not recommended for the retrofit of existing CMS structures.

Specimen CIP1 was subjected to 4,500,000 cycles of loading. The addition of the reinforced concrete jacket substantially increased the stiffness and the damping ratio of the post (by factors exceeding 2.5 and 5, respectively, for the test specimen), and substantially reduced the stresses in the post below the top of the concrete jacket, thus reducing the likelihood of fatigue failure.

Of the two retrofit schemes studied by the authors, the concrete-jacket retrofit outperformed the steel gusset-plate retrofit. The concrete-jacket retrofit detail served to reduce the stresses in the lower six feet of the post, whereas the gusset plate retrofit only reduced the flexural stresses near the post-to-base plate connection. As such, the response of the two retrofitted specimens should not be directly compared.

An *improved* steel gusset plate retrofit scheme would involve: a) reconfiguring the gusset plates to clear the conduit hole by at least six inches (152 mm), and b) removing and replacing all flawed weldments in the post-to-base plate connection (only possible for the full-penetration welded connection) using an

approved WPS (see Section 6.2.2). The proposed retrofit detail should be tested in the laboratory prior to field installation.

If the construction details are replicated in their entirety in the field, the concrete-jacket retrofit scheme will likely substantially increase the fatigue life of existing CMS structures with flawed welded connections.

6.2.2 Recommendations for Improving the Fatigue Life of New CMS Structures

On the basis of the experimental studies conducted at EERC, recommendations can be made regarding how Caltrans could improve the fatigue life of components of CMS structures. These recommendations are listed below; some of these recommendations are repeated from the Volume I report (Gilani, et al., 1997).

1. *Relocate and reconfigure the conduit hole in the post.* The conduit hole should be moved at least one post diameter from either the base plate or the top of any gusset plates. The rectangular conduit hole in the post should be replaced by a circular conduit hole to reduce the stress concentrations around the hole. The conduit hole should be drilled rather than flame cut to minimize residual strains. If stiffening rings are to be welded into the conduit hole, AWS-conforming seal welds should be used.
2. *Develop prequalified Welding Procedure Specifications (WPS) for groove-welded connections.* Standardized WPSs are commonly used for joining steel components in the building, bridge, and offshore oil industries. In the past, it has been the contractors' responsibility to develop and implement a WPS (Shepard, 1997) for Caltrans sign structures. To maintain high standards of construction, Caltrans should prepare a WPS for groove-welded post-to-base plate, mast arm-to-flange plate, gusset plate-to-post (mast arm), and gusset plate-to base (flange) plate connections. A WPS for the subject connections should include, but not be limited to, information on welding type (i.e., shielded metal arc welding, flux core-arc welding), end preparation, fit-up and root opening, maximum electrode diameter, electrode type, maximum current, maximum root-pass thickness, and pre-heat and cool-down requirements. The use of toughness-rated weld filler metal is recommended. Improved weld profiles, such as those shown in Figure 3.10 of AWS D1.1 (AWS, 1997), should be investigated. It is recommended that a welding consultant be engaged by Caltrans to develop the WPS.
3. *Develop improved quality control and inspection (quality assurance) procedures.* Current Caltrans standards for quality control and inspection of welded components should be reviewed. Minimum standards for quality control should be developed by Caltrans and imposed on all contractors fabricating components for CMS structures. Visual inspection alone of non-redundant welded connections is likely inappropriate. As a minimum, all groove-welded connections should be

ultrasonically tested (UT) by an approved testing agency as part of the quality control program. Good quality control and inspection are key to high-quality construction. All weld defects identified by UT should be gouged out and replaced prior to shipment of the post to the field. Standard procedures for repairing such defects must be developed. A Caltrans inspector should be present during the fit-up and welding of all connections to ensure that the WPS is followed exactly. It is recommended that a welding consultant be engaged by Caltrans to develop new quality control and inspection procedures.

6.3 Recommendations for Future Studies

The work described in this report and the companion Volume I report (Gilani, et al., 1997) has focused on evaluating the fatigue life of existing and retrofitted components of CMS structures. This work addresses one-half of the problem, namely, characterizing the fatigue life of key components at specified stress ranges. To complete the research program in a comprehensive manner, the following studies are recommended:

1. *Continue laboratory testing of components of CMS structures.* New guidelines for the design of CMS structures should not be prepared using a limited number of data points. Additional high-cycle fatigue testing of components of CMS structures at different stress levels is needed to provide the requisite information.
2. *Undertake additional field testing of CMS structures.* Field testing of CMS structures in high-wind areas could provide, at a substantially reduced cost with respect to wind-tunnel testing, valuable new data relating wind speed and direction to both pressures on components of CMS structures and design forces on these components. This work would address the other half of the problem, namely, do the AASHTO procedures accurately predict, in an engineering sense, the loads that act on a CMS structure? Without such information, a comprehensive solution to the problem is not possible.
3. *Develop and test vibration mitigation strategies.* Stresses in components of CMS structures can be reduced by either increasing the size and configuration of the structural components (e.g., increasing the diameter of the post, by adding gussets or jackets) or by reducing the effects of the dynamic component of the wind loads using damping technologies. Although attention to date has focused on increasing the section modulus of the post and mast arm, it may be more cost-effective to reduce the wind-load demands than to increase the strength of components of a CMS structure. It is likely that existing vibration mitigation strategies developed for wind and oil pipeline applications could be readily adapted to reduce the effects of wind loads on CMS structures. Such solutions should be implemented into field, the response monitored, and the efficacy of the solution verified before widespread implementation is undertaken.

CHAPTER 7 : REFERENCES

- AASHTO (1992). *Standard Specifications for Highway Bridges*, American Association of State Highway and Transportation Officials, AASHTO, 15th Edition, Washington D. C.
- AASHTO (1994). *Standard Specifications for Structural Supports for Highway Signs, Luminaries and Traffic Signals*, American Association of State Highway and Transportation Officials, AASHTO, Washington, D. C.
- ACI (1974). "Considerations for Design of Concrete Structures Subjected to Fatigue Loading," *American Concrete Institute Journal Proceedings*, Vol. 71, No. 3, Detroit, Michigan.
- AISC (1995). *Load and Resistance Factor Design Specifications*, American Institute of Steel Construction, 2nd Edition, Chicago, Illinois.
- API (1995). *Specifications for Line Pipe*, American Petroleum Institute, 41st Edition, Washington D. C.
- ASTM (1991). *Standard Specifications for Pipe, Steel, Black and Hot-Dipped, Zinc-Coated Welded and Seamless*, American Society of Testing Materials, ASTM Standards in Building and Codes, 28th Edition, Vol. 1, A1-B 210M, Philadelphia, Pennsylvania.
- AWS (1996). *Structural Welding Code*, American Welding Society, AWS D1.1, 15th Edition, Miami, Florida.
- Benner, E. W. and Muir, S. E. (1967). "Some Fatigue Tests on High Strength Concrete in Axial Compression," *Mag. of Conc. Res.*, Vol. 19, No. 59.
- Bury, M. R. C. and Domone, P. L. (1974). "The Role of Research in the Design of Concrete Offshore Structures," *Offshore Technology Conference Proceedings*, Dallas, Texas.
- Cough, R. W. and Penzien, J. (1993). *Dynamics of Structures*, McGraw-Hill, Inc., 2nd Edition, New York, New York.
- Daniels, J. H. and Herbein, W. C. (1980). *Fatigue of Curved Steel Bridge Elements - Fatigue Testing of Curved Plate Girder Assemblies*, Report FHWA-RD-79-133, Federal Highway Administration, Virginia.
- Fisher, J. A., Albrecht, P. A., Yen, B. T., Klingerman, D. J. and McNamee, B. M. (1974). *Fatigue Strength of Steel Beams with Divided Stiffeners and Anchorage*, NCHRP Report 147, Transportation Research Board, Washington, D. C.

- Fischer, J. W., Hausammann, H., Sullivan, M. D. and Pense, A. W. (1979). *Detection and Repair of Fatigue Damage in Welded Highway Bridges*. NCHRP Report 206, Transportation Research Board, Washington, D. C.
- Gilani, A. S., Chavez, J. W., Whittaker, A. S. (1997). *Fatigue Life Evaluation of Changeable Sign Structures. Volume 1: As-Built Specimens*. Report No. UCB/EERC-97/10, Earthquake Engineering Research Center, University of California at Berkeley, Berkeley, California
- Gugino, A. and Woody, J. (1996). *Private Communication*. California Department of Transportation, Caltrans Sacramento, California
- Kaczinski, M. R., Dexter, R. J. and Van Dien, J. P. (1996). *Fatigue-Resistant Design of Cantilevered Signal, Sign, and Light Supports*. Report to NCHRP, ATLSS Engineering Research Center, Lehigh University, Bethlehem, Pennsylvania
- Matlab (1997). *The Language of Technical Computing*. The Mathworks, Inc., Natick, Massachusetts
- Miner, M. A. (1945). "Cumulative Damage in Fatigue." *Journal of Applied Mechanics*, ASME, Vol. 67, pp. 159-164, New York, New York.
- Schilling, C. G., Klippstein, K. H., Barsom, J. M. and Blake, G. T. (1978) *Fatigue of Welded Steel Bridge Members Under Variable Amplitude Loadings*. NCHRP Report 188, Transportation Research Board, Washington, D. C.
- Shepard, R. (1997). *Private Communication*. California Department of Transportation, Caltrans Sacramento, California
- Whittaker, A. S., Bertero, V.V., and Gilani, A. S. (1997) *Full-Scale Seismic Testing of Beam-Column Assemblies*. Report to the SAC Joint Venture, Earthquake Engineering Research Center, University of California at Berkeley, Berkeley, California.
- Wilson, E. L. (1992). *SADSDAP, Static and Dynamic Structural Analysis Program*. Structural Analysis Programs, Inc. Berkeley, California
- Winter, W. (1996). "Instrumentation Activity Report." California Department of Transportation, Caltrans Sacramento, California

EERC REPORTS

EERC reports are available from the National Information Service for Earthquake Engineering (NISEE) and from the National Technical Information Service (NTIS). To order EERC Reports, please contact the Earthquake Engineering Research Center, 1301 S. 46th Street, Richmond, California 94804-4698, ph 510-231-9468.

- UCB/EERC-97/13: Fatigue Life Evaluation of Changeable Message Sign Structures – Volume 2: Retrofitted Specimens, by Chavez, J.W., Gilani, A.S., and Whittaker, A.S., December, 1998. \$20
- UCB/EERC-97/12: New Design and Analysis Procedures for Intermediate Hinges in Multiple-Frame Bridges, by DesRoches, R. and Fenves, G. L., December, 1997. \$26
- UCB/EERC-97/11: Viscous Heating of Fluid Dampers During Seismic and Wind Excitations – Analytical Solutions and Design Formulae, by Makris, N., Roussos, Y., Whittaker, A.S., and Kelly, J.M., November, 1997. \$15
- UCB/EERC-97/10: Fatigue Life Evaluation of Changeable Message Sign Structures – Volume 1: As-Built Specimens, by Gilani, A.S., Chavez, J.W., and Whittaker, A.S., November, 1997. \$20
- UCB/EERC-97/09: Second U.S.-Japan Workshop on Seismic Retrofit of Bridges, edited by K. Kawashima and S.A. Mahin, September, 1997. \$57
- UCB/EERC-97/08: Implications of the Landers and Big Bear Earthquakes on Earthquake Resistant Design of Structures, by Anderson, J.C. and Bertero, V.V., July 1997. \$20
- UCB/EERC-97/07: Analysis of the Nonlinear Response of Structures Supported on Pile Foundations, by Badoni, D. and Makris, N., July 1997. \$20
- UCB/EERC-97/06: Executive Summary on: Phase 3: Evaluation and Retrofitting of Multilevel and Multiple-Column Structures – An Analytical, Experimental, and Conceptual Study of Retrofitting Needs and Methods, by Mahin, S.A., Fenves, G.L., Filippou, F.C., Moehle, J.P., Thewall, C.R., May, 1997. \$20
- UCB/EERC-97/05: The EERC-CUREe Symposium to Honor Vitelmo V. Bertero, February 1997. \$26
- UCB/EERC-97/04: Design and Evaluation of Reinforced Concrete Bridges for Seismic Resistance, by Aschheim, M., Moehle, J.P. and Mahin, S.A., March 1997. \$26
- UCB/EERC-97/03: U.S.-Japan Workshop on Cooperative Research for Mitigation of Urban Earthquake Disasters: Learning from Kobe and Northridge – Recommendations and Resolutions, by Mahin, S., Okada, T., Shinozuka, M. and Toki, K., February 1997. \$15
- UCB/EERC-97/02: Multiple Support Response Spectrum Analysis of Bridges Including the Site-Response Effect & MSRS Code, by Der Kiureghian, A., Keshishian, P. and Hakobian, A., February 1997. \$20
- UCB/EERC-97/01: Analysis of Soil-Structure Interaction Effects on Building Response from Earthquake Strong Motion Recordings at 58 Sites, by Stewart, J.P. and Stewart, A.F., February 1997. \$57
- UCB/EERC-96/05: Application of Dog Bones for Improvement of Seismic Behavior of Steel Connections, by Popov, E.P., Elondet, M. and Stepanov, L., June 1996. \$13
- UCB/EERC-96/04: Experimental and Analytical Studies of Base Isolation Applications for Low-Cost Housing, by Tantiwangsa, W. and Kelly, J.M., July 1996. \$20
- UCB/EERC-96/03: Experimental and Analytical Evaluation of a Retrofit Double-Deck Viaduct Structure: Part I of II, by Zayati, F., Mahin, S. A. and Moehle, J. P., June 1996. \$33
- UCB/EERC-96/02: Field Testing of Bridge Design and Retrofit Concepts. Part 2 of 2: Experimental and Analytical Studies of the Mt. Diablo Blvd. Bridge, by Gilani, A.S., Chavez, J.W. and Fenves, G.L., June 1996. \$20
- UCB/EERC-96/01: Earthquake Engineering Research at Berkeley – 1996: Papers Presented at the 11th World Conference on Earthquake Engineering, by EERC, May 1996. \$26

- UCB/EERC-95/14: Field Testing of Bridge Design and Retrofit Concepts. Part 1 of 2: Field Testing and Dynamic Analysis of a Four-Span Seismically Isolated Viaduct in Walnut Creek, California, by Gilani, A.S., Mahin, S.A., Fenves, G.L., Aiken, I.D. and Chavez, J.W., December 1995. \$26
- UCB/EERC-95/13: Experimental and Analytical Studies of Steel Connections and Energy Dissipators, by Yang, T.-S. and Popov, E.P., December 1995. \$26
- UCB/EERC-95/12: Natural Rubber Isolation Systems for Earthquake Protection of Low-Cost Buildings, by Taniwangsa, W., Clark, P. and Kelly, J.M., June 1996. \$20
- UCB/EERC-95/11: Studies in Steel Moment Resisting Beam-to-Column Connections for Seismic-Resistant Design, by Blackman, B. and Popov, E.P., October 1995, PB96-143243. \$20
- UCB/EERC-95/10: Seismological and Engineering Aspects of the 1995 Hyogoken-Nanbu (Kobe) Earthquake, by EERC, November 1995. \$26
- UCB/EERC-95/09: Seismic Behavior and Retrofit of Older Reinforced Concrete Bridge T-Joints, by Lowes, L.N. and Moehle, J.P., September 1995, PB96-159850. \$20
- UCB/EERC-95/08: Behavior of Pre-Northridge Moment Resisting Steel Connections, by Yang, T.-S. and Popov, E.P., August 1995, PB96-143177. \$15
- UCB/EERC-95/07: Earthquake Analysis and Response of Concrete Arch Dams, by Tan, H. and Chopra, A.K., August 1995, PB96-143185. \$20
- UCB/EERC-95/06: Seismic Rehabilitation of Framed Buildings Infilled with Unreinforced Masonry Walls Using Post-Tensioned Steel Braces, by Teran-Gilmore, A., Bertero, V.V. and Youssef, N., June 1995, PB96-143136. \$26
- UCB/EERC-95/05: Final Report on the International Workshop on the Use of Rubber-Based Bearings for the Earthquake Protection of Buildings, by Kelly, J.M., May 1995. \$20
- UCB/EERC-95/04: Earthquake Hazard Reduction in Historical Buildings Using Seismic Isolation, by Garevski, M., June 1995. \$15
- UCB/EERC-95/03: Upgrading Bridge Outrigger Knee Joint Systems, by Stojadinovic, B. and Thewalt, C.R., June 1995, PB95-269338. \$20
- UCB/EERC-95/02: The Attenuation of Strong Ground Motion Displacements, by Gregor, N.J., June 1995, PB95-269346. \$26
- UCB/EERC-95/01: Geotechnical Reconnaissance of the Effects of the January 17, 1995, Hyogoken-Nanbu Earthquake, Japan, August 1995, PB96-143300. \$26
- UCB/EERC-94/12: Response of the Northwest Connector in the Landers and Big Bear Earthquakes, by Fenves, G.L. and Desroches, R., December 1994. \$20
- UCB/EERC-94/11: Earthquake Analysis and Response of Two-Level Viaducts, by Singh, S.P. and Fenves, G.L., October 1994, PB96-133756 (A09). \$20
- UCB/EERC-94/10: Manual for Menshin Design of Highway Bridges: Ministry of Construction, Japan, by Sugita, H. and Mahin, S., August 1994, PB95-192100(A08). \$20
- UCB/EERC-94/09: Performance of Steel Building Structures During the Northridge Earthquake, by Bertero, V.V., Anderson, J.C. and Krawinkler, H., August 1994, PB95-112025(A10). \$26
- UCB/EERC-94/08: Preliminary Report on the Principal Geotechnical Aspects of the January 17, 1994 Northridge Earthquake, by Stewart, J.P., Bray, J.D., Seed, R.B. and Sitar, N., June 1994, PB94203635(A12). \$26
- UCB/EERC-94/07: Accidental and Natural Torsion in Earthquake Response and Design of Buildings, by De la Llera, J.C. and Chopra, A.K., June 1994, PB94-203627(A14). \$33
- UCB/EERC-94/05: Seismic Response of Steep Natural Slopes, by Sitar, N. and Ashford, S.A., May 1994, PB94-203643(A10). \$26
- UCB/EERC-94/04: Insitu Test Results from Four Loma Prieta Earthquake Liquefaction Sites: SPT, CPT, DMT and Shear Wave Velocity, by Mitchell, J.K., Lodge, A.L., Coutinho, R.Q., Kayen, R.E., Seed, R.B., Nishio, S. and Stokoe II, K.H., April 1994, PB94-190089(A09). \$20
- UCB/EERC-94/03: The Influence of Plate Flexibility on the Buckling Load of Elastomeric Isolators, by

- Kelly, J.M., March 1994, PB95-192134(A04). \$15
- UCB/EERC-94/02: Energy Dissipation with Slotted Bolted Connections, by Grigorian, C.E. and Popov, E.P., February 1994, PB94-164605. \$26
- UCB/EERC-94/01: Preliminary Report on the Seismological and Engineering Aspects of the January 17, 1994 Northridge Earthquake, by EERC, January 1994, (PB94 157 666/AS)A05. \$15
- UCB/EERC-93/13: On the Analysis of Structures with Energy Dissipating Restraints, by Inaudi, J.A., Nitta, D.K. and Kelly, J.M., December 1993, PB94-203619(A07). \$20
- UCB/EERC-93/12: Synthesized Strong Ground Motions for the Seismic Condition Assessment of the Eastern Portion of the San Francisco Bay Bridge, by Bolt, B.A. and Gregor, N.J., December 1993, PB94-165842(A10). \$26
- UCB/EERC-93/11: Nonlinear Homogeneous Dynamical Systems, by Inaudi, J.A. and Kelly, J.M., October 1995. \$20
- UCB/EERC-93/09: A Methodology for Design of Viscoelastic Dampers in Earthquake-Resistant Structures, by Abbas, H. and Kelly, J.M., November 1993, PB94-190071(A10). \$26
- UCB/EERC-93/08: Model for Anchored Reinforcing Bars under Seismic Excitations, by Monti, G., Spacone, E. and Filippou, F.C., December 1993, PB95-192183(A05). \$15
- UCB/EERC-93/07: Earthquake Analysis and Response of Concrete Gravity Dams Including Base Sliding, by Chavez, J.W. and Fenves, G.L., December 1993, (PB94 157 658/AS)A10. \$26
- UCB/EERC-93/06: On the Analysis of Structures with Viscoelastic Dampers, by Inaudi, J.A., Zantirios, A. and Kelly, J.M., August 1993, PB94-165867(A06). \$20
- UCB/EERC-93/05: Multiple-Support Response Spectrum Analysis of the Golden Gate Bridge, by Nakamura, Y., Der Kiureghian, A. and Liu, D., May 1993, (PB93 221 752)A05. \$15
- UCB/EERC-93/04: Seismic Performance of a 30-Story Building Located on Soft Soil and Designed According to UBC 1991, by Teran-Gilmore, A. and Bertero, V.V., 1993, (PB93 221 703)A17. \$33
- UCB/EERC-93/03: An Experimental Study of Flat-Plate Structures under Vertical and Lateral Loads, by Hwang, S.-H. and Moshle, J.P., February 1993, (PB94 157 690/AS)A13. \$26
- UCB/EERC-93/02: Evaluation of an Active Variable-Damping-Structure, by Polak, E., Meeker, G., Yamada, K. and Kurata, N., 1993, (PB93 221 711)A05. \$15
- UCB/EERC-92/18: Dynamic Analysis of Nonlinear Structures using State-Space Formulation and Partitioned Integration Schemes, by Inaudi, J.A. and De la Llera, J.C., December 1992, (PB94 117 702/AS)A05. \$15
- UCB/EERC-92/17: Performance of Tall Buildings During the 1985 Mexico Earthquakes, by Teran-Gilmore, A. and Bertero, V.V., December 1992, (PB93 221 737)A11. \$26
- UCB/EERC-92/16: Tall Reinforced Concrete Buildings: Conceptual Earthquake-Resistant Design Methodology, by Bertero, R.D. and Bertero, V.V., December 1992, (PB93 221 695)A12. \$26
- UCB/EERC-92/15: A Friction Mass Damper for Vibration Control, by Inaudi, J.A. and Kelly, J.M., October 1992, (PB93 221 745)A04. \$15
- UCB/EERC-92/14: Earthquake Risk and Insurance, by Brillinger, D.R., October 1992, (PB93 223 352)A03
- UCB/EERC-92/13: Earthquake Engineering Research at Berkeley - 1992, by EERC, October 1992, PB93-223709(A10). \$13
- UCB/EERC-92/12: Application of a Mass Damping System to Bridge Structures, by Hasegawa, K. and Kelly, J.M., August 1992, (PB93 221 786)A06. \$26
- UCB/EERC-92/11: Mechanical Characteristics of Neoprene Isolation Bearings, by Kelly, J.M. and Quiroz, E., August 1992, (PB93 221 729)A07. \$20
- UCB/EERC-92/10: Slotted Bolted Connection Energy Dissipators, by Grigorian, C.E., Yang, T.-S. and Popov, E.P., July 1992, (PB92 120 285)A03. \$20
- UCB/EERC-92/09: Evaluation of Code Accidental-Torsion Provisions Using Earthquake Records from Three Nominally Symmetric-Plan Buildings, by De la Llera, J.C. and Chopra, A.K., September 1992, (PB94 117 611)A08. \$13

- UCB/EERC-92/08: Nonlinear Static and Dynamic Analysis of Reinforced Concrete Subassemblages, by Filippou, F.C., D'Ambrosi, A. and Issa, A., August 1992, \$20
- UCB/EERC-92/07: A Beam Element for Seismic Damage Analysis, by Spacone, E., Ciampi, V. and Filippou, F.C., August 1992, (PB95-192126)A06. \$20
- UCB/EERC-92/06: Seismic Behavior and Design of Semi-Rigid Steel Frames, by Nader, M.N. and Astaneh-Asl, A., May 1992, PB93-221760(A17). \$33
- UCB/EERC-92/05: Parameter Study of Joint Opening Effects on Earthquake Response of Arch Dams, by Fenves, G.L., Mojtahedi, S. and Reimer, R.B., April 1992, (PB93 120 301)A04. \$15
- UCB/EERC-92/04: Shear Strength and Deformability of RC Bridge Columns Subjected to Inelastic Cyclic Displacements, by Aschheim, M. and Moehle, J.P., March 1992, (PB93 120 327)A06. \$20
- UCB/EERC-92/03: Models for Nonlinear Earthquake Analysis of Brick Masonry Buildings, by Mengi, Y., McNiven, H.D. and Tanrikulu, A.K., March 1992, (PB93 120 293)A08. \$20
- UCB/EERC-92/02: Response of the Dumbarton Bridge in the Loma Prieta Earthquake, by Fenves, G.L., Filippou, F.C. and Ste, D.T., January 1992, (PB93 120 319)A09. \$20
- UCB/EERC-92/01: Studies of a 49-Story Instrumented Steel Structure Shaken During the Loma Prieta Earthquake, by Chen, C.-C., Bonowitz, D. and Astaneh-Asl, A., February 1992, (PB93 221 778)A08. \$20
- UCB/EERC-91/18: Investigation of the Seismic Response of a Lightly-Damped Torsionally-Coupled Building, by Boroschek, R. and Mahin, S.A., December 1991, (PB93 120 335)A13. \$26
- UCB/EERC-91/17: A Fiber Beam-Column Element for Seismic Response Analysis of Reinforced Concrete Structures, by Taucer, F., Spacone, E. and Filippou, F.C., December 1991, (PB94 117 629AS)A07. \$20
- UCB/EERC-91/16: Evaluation of the Seismic Performance of a Thirty-Story RC Building, by Anderson, J.C., Miranda, E., Bertero, V.V. and The Kajima Project Research Team, July 1991, (PB93 114 841)A12. \$26
- UCB/EERC-91/15: Design Guidelines for Ductility and Drift Limits: Review of State-of-the-Practice and State-of-the-Art in Ductility and Drift-Based Earthquake-Resistant Design of Buildings, by Bertero, V.V., Anderson, J.C., Krawinkler, H., Miranda, E. and The CUREe and The Kajima Research Teams, July 1991, (PB93 120 269)A08. \$20
- UCB/EERC-91/14: Cyclic Response of RC Beam-Column Knee Joints: Test and Retrofit, by Mazzoni, S., Moehle, J.P. and Thewalt, C.R., October 1991, (PB93 120 277)A03. \$13
- UCB/EERC-91/13: Shaking Table - Structure Interaction, by Rinawi, A.M. and Clough, R.W., October 1991, (PB93 114 917)A13. \$26
- UCB/EERC-91/12: Performance of Improved Ground During the Loma Prieta Earthquake, by Mitchell, J.K. and Wentz, Jr., F.J., October 1991, (PB93 114 791)A06. \$20
- UCB/EERC-91/11: Seismic Performance of an Instrumented Six-Story Steel Building, by Anderson, J.C. and Bertero, V.V., November 1991, (PB93 114 809)A07. \$20
- UCB/EERC-91/10: Evaluation of Seismic Performance of a Ten-Story RC Building During the Whittier Narrows Earthquake, by Miranda, E. and Bertero, V.V., October 1991, (PB93 114 783)A06. \$20
- UCB/EERC-91/09: A Preliminary Study on Energy Dissipating Cladding-to-Frame Connections, by Cohen, J.M. and Powell, G.H., September 1991, (PB93 114 510)A05. \$15
- UCB/EERC-91/08: A Response Spectrum Method for Multiple-Support Seismic Excitations, by Der Kiureghian, A. and Neuenhofer, A., August 1991, (PB93 114 536)A04. \$15
- UCB/EERC-91/07: Estimation of Seismic Source Processes Using Strong Motion Array Data, by Chiou, S.-J., July 1991, (PB93 114 551/AS)A08. \$20
- UCB/EERC-91/06: Computation of Spatially Varying Ground Motion and Foundation-Rock Impedance Matrices for Seismic Analysis of Arch Dams, by Zhang, L. and Chopra, A.K., May 1991, (PB93 114 825)A07. \$20
- UCB/EERC-91/05: Base Sliding Response of Concrete Gravity Dams to Earthquakes, by Chopra, A.K. and

- Zhang, L., May 1991, (PB93 114 544/AS)A05. \$15
- UCB/EERC-91/04: Dynamic and Failure Characteristics of Bridgestone Isolation Bearings, by Kelly, J.M., April 1991, (PB93 114 528)A05. \$15
- UCB/EERC-91/03: A Long-Period Isolation System Using Low-Modulus High-Damping Isolators for Nuclear Facilities at Soft-Soil Sites, by Kelly, J.M., March 1991, (PB93 114 577/AS)A10. \$26
- UCB/EERC-91/02: Displacement Design Approach for Reinforced Concrete Structures Subjected to Earthquakes, by Qi, X. and Moehle, J.P., January 1991, (PB93 114 569/AS)A09. \$20
- UCB/EERC-90/21: Observations and Implications of Tests on the Cypress Street Viaduct Test Structure, by Bollo, M., Mahin, S.A., Moehle, J.P., Stephen, R.M. and Qi, X., December 1990, (PB93 114 775)A13. \$26
- UCB/EERC-90/20: Seismic Response Evaluation of an Instrumented Six Story Steel Building, by Shen, J.-H. and Astaneh-Asl, A., December 1990, (PB91 229 294/AS)A04. \$15
- UCB/EERC-90/19: Cyclic Behavior of Steel Top-and-Bottom Plate Moment Connections, by Harriott, J.D. and Astaneh-Asl, A., August 1990, (PB91 229 260/AS)A05. \$15
- UCB/EERC-90/18: Material Characterization of Elastomers used in Earthquake Base Isolation, by Papoulias, K.D. and Kelly, J.M., 1990, PB94-190063(A08). \$15
- UCB/EERC-90/17: Behavior of Peak Values and Spectral Ordinates of Near-Source Strong Ground-Motion over a Dense Array, by Niazi, M., June 1990, (PB93 114 833)A07. \$20
- UCB/EERC-90/14: Inelastic Seismic Response of One-Story, Asymmetric-Plan Systems, by Goel, R.K. and Chopra, A.K., October 1990, (PB93 114 767)A11. \$26
- UCB/EERC-90/13: The Effects of Tectonic Movements on Stresses and Deformations in Earth Embankments, by Bray, J. D., Seed, R. B. and Seed, H. B., September 1989, PB92-192996(A18). \$39
- UCB/EERC-90/12: Effects of Torsion on the Linear and Nonlinear Seismic Response of Structures, by Sedarat, H. and Bertero, V.V., September 1989, (PB92 193 002/AS)A15. \$33
- UCB/EERC-90/11: Seismic Hazard Analysis: Improved Models, Uncertainties and Sensitivities, by Araya, R. and Der Kiureghian, A., March 1988, PB92-193010(A08). \$20
- UCB/EERC-90/10: Experimental Testing of the Resilient-Friction Base Isolation System, by Clark, P.W. and Kelly, J.M., July 1990, (PB92 143 072)A08. \$20
- UCB/EERC-90/09: Influence of the Earthquake Ground Motion Process and Structural Properties on Response Characteristics of Simple Structures, by Come, J.P., Pister, K.S. and Mahin, S.A., July 1990, (PB92 143 064)A15. \$33
- UCB/EERC-90/08: Soil Conditions and Earthquake Hazard Mitigation in the Marina District of San Francisco, by Mitchell, J.K., Masood, T., Kayen, R.E. and Seed, R.B., May 1990, (PB 193 267/AS)A04. \$15
- UCB/EERC-90/07: A Unified Earthquake-Resistant Design Method for Steel Frames Using ARMA Models, by Takewaki, I., Conte, J.P., Mahin, S.A. and Pister, K.S., June 1990, PB92-192947(A05). \$15
- UCB/EERC-90/05: Preliminary Report on the Principal Geotechnical Aspects of the October 17, 1989 Loma Prieta Earthquake, by Seed, R.B., Dickenson, S.E., Riemer, M.F., Bray, J.D., Sitar, N., Mitchell, J.K., Idriss, I.M., Kayen, R.E., Kropp, A., Harder, L.F., Jr. and Power, M.S., April 1990, (PB 192 970)A08. \$20
- UCB/EERC-90/03: Earthquake Simulator Testing and Analytical Studies of Two Energy-Absorbing Systems for Multistory Structures, by Aiken, I.D. and Kelly, J.M., October 1990, (PB92 192 988)A13. \$26
- UCB/EERC-90/02: Javid's Paradox: The Influence of Preform on the Modes of Vibrating Beams, by Kelly, J.M., Sackman, J.L. and Javid, A., May 1990, (PB91 217 943/AS)A03. \$15
- UCB/EERC-89/16: Collapse of the Cypress Street Viaduct as a Result of the Loma Prieta Earthquake, by Nims, D.K., Miranda, E., Aiken, I.D., Whittaker, A.S. and Bertero, V.V., November 1989, (PB91 217 935/AS)A05. \$15

- UCB/EERC-89/15: Experimental Studies of a Single Story Steel Structure Tested with Fixed, Semi-Rigid and Flexible Connections, by Nader, M.N. and Astanek-Asl, A., August 1989, (PB91 229 211/AS)A10. \$26
- UCB/EERC-89/14: Preliminary Report on the Seismological and Engineering Aspects of the October 17, 1989 Santa Cruz (Loma Prieta) Earthquake, by EERC, October 1989, (PB92 139 682/AS)A04. \$15
- UCB/EERC-89/13: Mechanics of Low Shape Factor Elastomeric Seismic Isolation Bearings, by Aiken, I.D., Kelly, J.M. and Tajirian, P.F., November 1989, (PB92 139 732/AS)A09. \$20
- UCB/EERC-89/12: ADAP-88: A Computer Program for Nonlinear Earthquake Analysis of Concrete Arch Dams, by Fenves, G.L., Mojtahedi, S. and Reimer, R.B., September 1989, (PB92 139 674/AS)A07. \$20
- UCB/EERC-89/11: Static Tilt Behavior of Unanchored Cylindrical Tanks, by Lau, D.T. and Clough, R.W., September 1989, (PB92 143 049)A10. \$26
- UCB/EERC-89/10: Measurement and Elimination of Membrane Compliance Effects in Undrained Triaxial Testing, by Nicholson, P.G., Seed, R.B. and Anwar, H., September 1989, (PB92 139 641/AS)A13. \$26
- UCB/EERC-89/09: Feasibility and Performance Studies on Improving the Earthquake Resistance of New and Existing Buildings Using the Friction Pendulum System, by Zayas, V., Low, S., Mahin, S.A. and Bozzo, L., July 1989, (PB92 143 064)A14. \$33
- UCB/EERC-89/08: Seismic Performance of Steel Moment Frames Plastically Designed by Least Squares Stress Fields, by Ohji, K. and Mahin, S.A., August 1989, (PB91 212 597)A05. \$15
- UCB/EERC-89/07: EADAP - Enhanced Arch Dam Analysis Program: Users's Manual, by Ghansat, Y. and Clough, R.W., August 1989, (PB91 212 522)A06. \$20
- UCB/EERC-89/06: Effects of Spatial Variation of Ground Motions on Large Multiply-Supported Structures, by Hao, H., July 1989, (PB91 229 161/AS)A08. \$20
- UCB/EERC-89/05: The 1985 Chile Earthquake: An Evaluation of Structural Requirements for Bearing Wall Buildings, by Wallace, J.W. and Moehle, J.P., July 1989, (PB91 218 008/AS)A13. \$26
- UCB/EERC-89/04: Earthquake Analysis and Response of Intake-Outlet Towers, by Goyal, A. and Chopra, A.K., July 1989, (PB91 229 286/AS)A19. \$39
- UCB/EERC-89/03: Implications of Site Effects in the Mexico City Earthquake of Sept. 19, 1985 for Earthquake-Resistant Design Criteria in the San Francisco Bay Area of California, by Seed, H.B. and Sun, J.I., March 1989, (PB91 229 369/AS)A07. \$20
- UCB/EERC-89/02: Earthquake Simulator Testing of Steel Plate Added Damping and Stiffness Elements, by Whittaker, A., Bertero, V.V., Alonso, J. and Thompson, C., January 1989, (PB91 229 252/AS)A10. \$26
- UCB/EERC-89/01: Behavior of Long Links in Eccentrically Braced Frames, by Engelhardt, M.D. and Popov, E.P., January 1989, (PB92 143 056)A18. \$39
- UCB/EERC-88/20: Base Isolation in Japan, 1988, by Kelly, J.M., December 1988, (PB91 212 449)A05. \$15
- UCB/EERC-88/19: Steel Beam-Column Joints in Seismic Moment Resisting Frames, by Tsai, K.-C. and Popov, E.P., November 1988, (PB91 217 984/AS)A20. \$39
- UCB/EERC-88/18: Use of Energy as a Design Criterion in Earthquake-Resistant Design, by Uang, C.-M. and Bertero, V.V., November 1988, (PB91 210 906/AS)A04. \$15
- UCB/EERC-88/17: Earthquake Engineering Research at Berkeley - 1988, by EERC, November 1988, (PB91 210 864)A10. \$26
- UCB/EERC-88/16: Reinforced Concrete Flat Plates Under Lateral Load: An Experimental Study Including Biaxial Effects, by Pan, A. and Moehle, J.P., October 1988, (PB91 210 856)A13. \$26
- UCB/EERC-88/15: Dynamic Moduli and Damping Ratios for Cohesive Soils, by Sun, J.I., Golezorkhi, R. and Seed, H.B., August 1988, (PB91 210 922)A04. \$15
- UCB/EERC-88/14: An Experimental Study of the Behavior of Dual Steel Systems, by Whittaker, A.S., Uang, C.-M. and Bertero, V.V., September 1988, (PB91 212 712)A16. \$33
- UCB/EERC-88/13: Implications of Recorded Earthquake Ground Motions on Seismic Design of Building

- Structures, by Uang, C.-M. and Bertero, V.V., November 1988, (PB91 212 548)A06, \$20
- UCB/EERC-88/12: Nonlinear Analysis of Reinforced Concrete Frames Under Cyclic Load Reversals, by Filippou, F.C. and Issa, A., September 1988, (PB91 212 589)A07, \$20
- UCB/EERC-88/11: Liquefaction Potential of Sand Deposits Under Low Levels of Excitation, by Carter, D.P. and Seed, H.B., August 1988, (PB91 210 880)A15, \$33
- UCB/EERC-88/10: The Landslide at the Port of Nice on October 16, 1979, by Seed, H.B., Seed, R.B., Schiesser, F., Biondeau, F. and Juran, I., June 1988, (PB91 210 914)A05, \$15
- UCB/EERC-88/09: Alternatives to Standard Mode Superposition for Analysis of Non-Classically Damped Systems, by Kusanov, A.A. and Clough, R.W., June 1988, (PB91 217 992/AS)A04, \$15
- UCB/EERC-88/08: Analysis of Near-Source Waves: Separation of Wave Types Using Strong Motion Array Recordings, by Darragh, R.B., June 1988, (PB91 212 621)A08, \$20
- UCB/EERC-88/07: Theoretical and Experimental Studies of Cylindrical Water Tanks in Base-Isolated Structures, by Chalhoub, M.S. and Kelly, J.M., April 1988, (PB91 217 976/AS)A05, \$15
- UCB/EERC-88/06: DRAIN-2DX User Guide, by Allahbadi, R. and Powell, G.H., March 1988, (PB91 212 530)A12, \$26
- UCB/EERC-88/05: Experimental Evaluation of Seismic Isolation of a Nine-Story Braced Steel Frame Subject to Uplift, by Griffith, M.C., Kelly, J.M. and Aiken, I.D., May 1988, (PB91 217 968/AS)A07, \$20
- UCB/EERC-88/04: Re-evaluation of the Slide in the Lower San Fernando Dam in the Earthquake of Feb. 9, 1971, by Seed, H.B., Seed, R.B., Harder, L.F. and Jong, H.-L., April 1988, (PB91 212 456/AS)A07, \$20
- UCB/EERC-88/03: Cyclic Behavior of Steel Double Angle Connections, by Astaneh-Asl, A. and Nader, M.N., January 1988, (PB91 210 872)A05, \$15
- UCB/EERC-88/02: Experimental Evaluation of Seismic Isolation of Medium-Rise Structures Subject to Uplift, by Griffith, M.C., Kelly, J.M., Coveney, V.A. and Koh, C.G., January 1988, (PB91 217 950/AS)A09, \$20
- UCB/EERC-88/01: Seismic Behavior of Concentrically Braced Steel Frames, by Kharib, I., Mahin, S.A. and Pister, K.S., January 1988, (PB91 210 898/AS)A11, \$26

